2015-07-30

Host-Guest Binding Interactions Influenced by Electrochemical Reactions

Beijun Cheng
University of Miami, beijuncheng@gmail.com

UNIVERSITY OF MIAMI

HOST-GUEST BINDING INTERACTIONS INFLUENCED BY ELECTROCHEMICAL REACTIONS

By

Beijun Cheng

A DISSERTATION

Submitted to the Faculty
of the University of Miami
in partial fulfillment of the requirements for
the degree of Doctor of Philosophy

Coral Gables, Florida

August 2015

UNIVERSITY OF MIAMI

A dissertation submitted in partial fulfillment of
the requirements for the degree of
Doctor of Philosophy

HOST-GUEST BINDING INTERACTIONS INFLUENCED BY ELECTROCHEMICAL REACTIONS

Beijun Cheng

Approved:

_____
Angel E. Kaifer, Ph.D.
Professor of Chemistry

_____
Françisco M. Raymo, Ph.D.
Professor of Chemistry

_____
James N. Wilson, Ph.D.
Professor of Chemistry

_____
Dean of the Graduate School

_____
Xiangyang Zhou, Ph.D.
Professor of Mechanical
and Aerospace Engineering

CHENG, BEIJUN (Ph.D., Chemistry)

Host-Guest Binding Interactions Influenced by Electrochemical Reactions (August 2015)

Abstract of a dissertation at the University of Miami.

Dissertation supervised by Professor Angel E. Kaifer.
No. of pages in text. (106)

Chapter 1 is an introduction about supramolecular chemistry and electrochemistry in supramolecular chemistry. First, there is a general introduction about the history of supramolecular chemistry and two important host molecules: cucurbit[n]uril and pillar[n]arene. Then a brief history of electrochemistry and several examples of electrochemistry in supramolecular chemistry are described.

Chapter 2 is the electrochemical studies of viologen dications in cholate media and competition between the cholate assemblies and the cucurbit[7]uril host. The electrochemical data reveals that the binding interations between viologens and cholate assemblies are mainly hydrophobic. Competition studies with cucurbit[7]uril indicates that the rigid host molecule (cucurbit[7]uril) has better binding ability towards viologens than the dynamic host system (cholate assemblies).

Chapter 3 describes the cathodic voltammetric behavior of pillar[5]quinone in dichloromethane solution. Our data show that the symmetry of the macrocycle has a pronounced effect on the electron uptake sequence. The uptake of the first

five electrons follows a 2-1-2 pattern and only a total of eight electrons could be injected into the macrocycle under our experimental conditions.

Chapter 4 is about the investigation of gel formation of PAMAM deidrimers with CO_2. CO_2 was used to crosslink adjancent dendrimers to form a three-dimensional structure, which is crucial for the formation of gel. In this investigation, we found that in H_2O, no matter how big the generation is, there is no gel formed. However, in methanol, generation 0.0 has no gelation; generation 1.0 did not gel, but has some precipitates; in generation 5.0, even with a concentration of 0.005M of the dendrimer, there was gel formed with CO_2 bubbled. We also converted the gel of generation 5.0 to its original PAMAM dendrimer structure by nitrogen bubbling.

Chapter 5 is about the synthesis of a tetra-cholic acid cavitand. Cholic acid has a hydrophobic convex face and a hydrophilic concave face. Cavitand is one of the earliest synthetic host molecules and its has a rigid cavity. We attached four cholic acids to the upper rim of a cavitand by click chemistry, hoping that it could form an amphiphilic host molecule.

Table of Contents

List of Figures vi

List of Schemes xvi

List of Tables xvii

List of Equations xviii

Chapter 1 : Introduction 1

1.1 Introduction to supramolecular chemistry 1

1.1.1 Introduction to cucurbit[n]urils 6

1.1.2 Pillar[n]arene in supramolecular chemistry 10

1.2 Introduction to electrochemistry in supramolecular chemistry 14

Chapter 2 : Electrochemistry of Viologen Dications in Cholate Media and Competition between the Cholate Assemblies and the Cucurbit[7]uril Host 18

2.1 Overview 18

2.1.1 Cholic acid and cholate 18

2.1.2 Bile salt aggregates 19

2.2 Results 22

2.3 Discussion 46

Chapter 3 :The Cathodic Voltammetric Behaviour of Pillar[5]quinone in Nonaqueous Media. Symmetry Effects on the Electron Uptake Sequence 49

3.1 Overview 49

3.2 Results 50

3.2.1 Studies of the electron uptake sequence 50

3.2.2 Binding interaction studies 58

3.3 Experimental section 61

3.3.1 Synthesis 61

3.3.2 Electrochemical experiments 62

3.3.3 NMR diffusion measurements 63

Chapter 4 : Investigation of Gel Formation of PAMAM Dendrimers with CO_2 65

4.1 Overview 65

4.2 Results and discussions 66

4.2.1 Gelation studies of PAMAM dendrimers in D_2O 72

4.2.2 Gelation of PAMAM dendrimer with CO_2 in CD_3OD 78

4.3 Conclusion 89

Chapter 5 : Synthesis of a Tetra-cholic Acid Cavitand 91

5.1 Overview 91

5.2 Results and discussions 94

5.2.1 Synthesis 94

5.2.2 Electrochemical studies 97

5.3 Experimental section 98

5.3.1 Synthesis of 3 98

5.3.2 Spectra 99

References 101

List of Figures

Figure 1-1. (A) Donald J. Cram; (B) Jean-Marie Lehn; (C) Charles Pedersen--Nobel Prize Laureates in Chemistry at 1987 1

Figure 1-2. (A) DNA assembly; (B) Protein assembly..... 2

Figure 1-3. (A) First Schiff's base macrocycle from acetone and ethylene diamine by Curtis;[1a] (B) Schiff's base macrocycle by Jager;[1b] (C) Schiff's base macrocycle by Busch.[1c] 4

Figure 1-4. (A) Pederson's Crown Ether;[2] (B) Lehn's Cryptand;[3] (C) Cram's Cavitand.[4] 4

Figure 1-5. (A) β-Cyclodextrin; (B) Calix[4]arene; (C) Cucurbit[7]uril, (D) Pillar[5]arene. (Red: Oxygen; Blue: Nitrogen; White: Hydrogen)..... 5

Figure 1-6. (A) Structure of Cucurbit[7]uril; (B) Comparison of the relative sizes of CB5, CB6, CB7, CB8 and CB10.[5] Taken from Isaacs, L. *Chem.Comm.* **2009,** 619. 6

Figure 1-7. (A) Side view of cucurbit[14]uril; (B) Top view of cucurbit[14]uril.[6] Taken from Cheng, X.-J.; Liang, L.-L.; Chen, K.; Ji, N.-N.; Xiao, X.; Zhang, J.-X.; Zhang, Y.-Q.; Xue, S.-F.; Zhu, Q.-J.; Ni, X.-L.; Tao, Z. *Angew. Chem. Int. Ed.* **2013,** *52*, 7252..... 7

Figure 1-8. Selected guest molecules which can bind with CB[5], CB[6], CB[7] and CB[8] respectively.[11] Taken from Lee, J. W.; Samal, S.; Selvapalam, N.; Kim, H.-J.; Kim, K. *Acc. Chem. Res.* **2003,** *36*, 621..... 8

Figure 1-9. Structure of Pillar[5]arene..... 10

Figure 1-10. Ring expansions from pillar[5]arene reported by Tomoki Ogoshi.[12] Taken from Ogoshi, T.; Ueshima, N.; Sakakibara, F.; Yamagishi, T.-A.; Haino, T. *Org. Lett.* **2014,** *16*, 2896..... 10

Figure 1-11. (1) Monophosphoryl copillar[5]arene; (2) 1,4-dimethoxyl pillar[5]arene; **BBO.** 1,4-butanediol; **BO.** 1-butanol.[15] Taken from Chen, Y.; He, M.; Li, B.; Wang, L.; Meier, H.; Cao, D. *RSC Adv.* **2013,** *3*, 21405. 11

Figure 1-12. (A) Benzo-18-crown-6 functionalized copillar[5]arene; (B) Guest molecules; (C) pH-responsive dynamic[1]catenane.[16] Taken from Yan, X.; Wei, P.; Li, Z.; Zheng, B.; Dong, S.; Huang, F.; Zhou, Q. *Chem. Comm.* **2013,** *49*, 2512. 12

Figure 1-13. (A) Structure of the amphiphilic pillar[5]arene by Feihe Huang; (B) Schematic illustration of the self-assembly process of amphiphilic pillar[5]arene 1 into microtubes.[17] Taken from Yao, Y.; Xue, M.; Chen, J.; Zhang, M.; Huang, F. *J. Am. Chem. Soc.* **2012,** *134*, 15712..... 13

Figure 1-14. Electrochemically switchable molecular shuttle.[18] Taken from Bissell, R. A.; Cordova, E.; Kaifer, A. E.; Stoddart, J. F. *Nature* **1994,** *369*, 133..... 15

Figure 1-15. Electrochemically driven formation of a molecular capsule around ferrocenium by six resorcinarene.[19] Taken from Philip, I. E.; Kaifer, A. E. *J. Am. Chem. Soc.* **2002,** *124*, 12678. 15

Figure 1-16. Electrochemical investigation of the binding interaction between cucurbit[7]uril and methyl viologen by Angel Kaifer and Kimoon Kim, respectively.[20] Taken from Kim, H.-J.; Jeon, W. S.; Ko, Y. H.; Kim, K. *Proc. Natl. Acad. Sci.* **2002,** *99*, 5007. 16

Figure 2-1. (A) Cholic acid; (B) Sodium Cholate..... 18

Figure 2-2. 3-D structure of cholic acid..... 19

Figure 2-3. (A) Methyl viologen dication; (B) Propyl viologen dication; (C) Butyl viologen dication; (D) Heptyl ethyl viologen dication..... 21

Figure 2-4. Cyclic voltammetric behavior on glass carbon (0.071 cm^2) of 1.0 mM MV^{2+} in 0.2 M NaCl containing variable concentrations of sodium cholate. Scan rate: 0.1 V s^{-1}..... 23

Figure 2-5. Square wave voltammetric behavior of 1.0 mM HEV^{2+} in 0.2 M NaCl and variable concentration of sodium cholate. 24

Figure 2-6. Square wave voltammetric behavior of 1.0 mM MV^{2+} NaCl and variable concentrations of sodium cholate..... 26

Figure 2-7. Cyclic voltammetric behavior on glassy carbon (0.071 cm^2) of 1.0 mM PV^{2+} in 0.2 M NaCl containing variable concentrations of sodium cholate. Scan rate: 0.1 V s^{-1}..... 26

Figure 2-8. Square wave voltammetric behavior of 1.0 mM PV^{2+} in 0.2 M NaCl and variable concentrations of sodium cholate..... 27

Figure 2-9. Cyclic voltammetric behavior on glassy carbon (0.071 cm^2) of 1.0 mM BV^{2+} in 0.2 M NaCl containing variable concentrations of sodium cholate. Scan rate: 0.1 V s^{-1}..... 27

Figure 2-10. Square wave voltammetric behavior of 1.0 mM BV^{2+} in 0.2 M NaCl and variable concentrations of sodium cholate..... 28

Figure 2-11. Cyclic voltammetric behavior on glassy carbon (0.071 cm^2) of 1.0 mM HEV^{2+} in 0.2 M NaCl containing variable concentrations of sodium cholate. Scan rate: 0.1 V s^{-1}. 28
Figure 2-12. Half-wave potentials measured in SWV experiments for the first one-electron reduction of the viologen probes in 0.2 M NaCl and variable concentrations of sodium cholate. 29
Figure 2-13. Half-wave potentials measured in CV experiments for the first one-electron reduction of the viologen probes in 0.2 M NaCl and variable concentrations of sodium cholate. 29
Figure 2-14. Electronic absorption spectra after exhaustive one–electron reduction of a solution containing 1.0 mM MV^{2+} and 200 mM NaCl in the absence (black) and in the presence (red) of 80 mM NaCh. 31
Figure 2-15. Electronic absorption spectra after exhaustive one–electron reduction of a solution containing 1.0 mM PV^{2+} and 200 mM NaCl in the absence (black) and in the presence (red) of 80 mM NaCh. 32
Figure 2-16. Electronic absorption spectra after exhaustive one–electron reduction of a solution containing 1.0 mM BV^{2+} and 200 mM NaCl in the absence (black) and in the presence (red) of 80 mM NaCh. 32
Figure 2-17. Electronic absorption spectra after exhaustive one–electron reduction of a solution containing 1.0 mM HEV^{2+} and 200 mM NaCl in the absence (black) and in the presence (red) of 80 mM NaCh. 33
Figure 2-18. ^1H NMR spectra (500 MHz, 0.2 M NaCl/D_2O) of (bottom) 1.0 mM CB7, (middle) 1.0 mM NaCh and (top) 1.0 mM NaCh + 1.0 mM CB7. 34

Figure 2-19. Square wave voltammetric behavior of 1.0 mM MV^{2+} in the presence of 1.0 equivalent CB7 in 0.2 M NaCl and variable concentrations of sodium cholate. 35
Figure 2-20. Half-wave potentials for the first reduction of methyl viologen (1.0 mM) in the absence and in the presence of 1.0 equiv of CB7 as a function of sodium cholate concentration. The experiments were run in 0.2 M NaCl supporting electrolyte. 35
Figure 2-21. Cyclic voltammetric behavior on glassy carbon (0.071 cm^2) of 1.0 mM MV^{2+} in the presence of 1.0 equivalent CB7 in 0.2 M NaCl containing variable concentrations of sodium cholate. Scan rate: 0.1 V s^{-1}. 36
Figure 2-22. Half-wave potentials measured in CV for the first reduction of methylviologen (1.0 mM) in the absence and in the presence of 1.0 equiv CB7 as a function of sodium cholate concentration. The experiments were run in 0.2 M NaCl supporting electrolyte. 36
Figure 2-23. Electronic absorption spectrum of 25.6 uM MV•Cl_2 in 280.0 mM NaCl/H_2O in the presence of increasing concentrations (0.0-102.3uM, in the direction of the arrow) of CB7. Insert shows the best fit of the experimental data to the 1:1 binding model. (CB7•MV^{2+}: λ_{max} = 253 nm, ε = 1.1 x 10^4 $M^{-1}cm^{-1}$ at 25 °C) 38
Figure 2-24. Absorbance versus CB7 concentration of aqueous solutions containing 25.6 μM methylviologen at 200.0 mM NaCl and 80.0 mM NaCh. The continuous lines show the best fit of the experimental data to 1:1 binding isotherms. 38

Figure 2-25. Absorbance versus CB7 concentration of aqueous solutions containing 25.6 μM methylviologen at 240.0 mM NaCl. The continuous lines show the best fit of the experimental data to 1:1 binding isotherms. 39
Figure 2-26. Absorbance versus CB7 concentration of aqueous solutions containing 25.6 μM methylviologen at 200.0 mM NaCl and 40.0 mM NaCh. The continuous lines show the best fit of the experimental data to 1:1 binding isotherms. 39
Figure 2-27. Absorbance versus CB7 concentration of aqueous solutions containing 25.6 μM methylviologen at 200.0 mM NaCl. The continuous lines show the best fit of the experimental data to 1:1 binding isotherms. 40
Figure 2-28. ^{1}H NMR spectra (500 MHz, 0.2 M NaCl/D_2O) of 1.0 mM HEV^{2+} (bottom) in the absence and (top) in the presence of 1.0 equiv of CB7. 42
Figure 2-29. Cyclic voltammetric behavior on glassy carbon (0.071 cm^2) of 1.0 mM BV^{2+} in the presence of 1.0 equivalent CB7 in 0.2 M NaCl containing variable concentrations of sodium cholate. Scan rate: 0.1 V s^{-1}. 43
Figure 2-30. Half-wave potentials measured in CV for the first reduction of BV^{2+} (1.0 mM) in the absence and in the presence of 1.0 equiv CB7 as a function of sodium cholate concentration. The experiments were run in 0.2 M NaCl supporting electrolyte. 44
Figure 2-31. Cyclic voltammetric behavior on glassy carbon (0.071 cm^2) of 1.0 mM HEV^{2+} in the presence of 1.0 equivalent CB7 in 0.2 M NaCl containing variable concentrations of sodium cholate. Scan rate: 0.1 V s^{-1}. 44

Figure 2-32. Half-wave potentials for the first reduction of HEV^{2+} (1.0 mM) in the absence and in the presence of 1.0 equiv of CB7 as a function of the sodium cholate concentration. The experiments were run in 0.2 mM NaCl supporting electrolyte. 45

Figure 3-1. (A) Structure of pillar[5]quinone (P5Q); (B) structure of the model quinone compound, *p*-xyloquinone(XQ). 50

Figure 3-2. Cathodic voltammetric behavior on glassy carbon (0.07 cm^2) of 1.0 mM XQ in CH_2Cl_2 solution also containing 0.1 M $TBAPF_6$ as the supporting electrolyte. (A) Square wave voltammetry. (B) Normal Pulse Voltammetry. 52

Figure 3-3. Cathodic voltammetric behavior on glassy carbon (0.07 cm^2) of 1.0 mM P5Q in CH_2Cl_2 solution also containing 0.1 M $TBAPF_6$ as the supporting electrolyte. (A) Square wave voltammetry. (B) Normal Pulse Voltammetry. 53

Figure 3-4. The guest molecule studies..... 59

Figure 3-5. (A) ^1H NMR spectrum of P5Q 1.0 mM in CD_2Cl_2; (B). ^1H NMR spectrum of the guest molecule (Figure 3-4) 1.0 mM in CD_2Cl_2; (C) ^1H NMR spectrum of P5Q and the guest molecule with a 1:1 ratio 59

Figure 3-6. **Black:** SWV of guest molecule **1** (1 mM) in the absence of P5Q; **Red:** SWV of guest molecule **1** (1 mM) in the presence of 1 mM P5Q..... 60

Figure 3-7. **Black:** SWV of P5Q (1 mM) in the absence of guest molecule **1**; **Red:** SWV of P5Q (1 mM) in the presence of 1 mM guest molecule **1**..... 61

Figure 3-8. Normalized signal decay as a function of gradient strength for P5Q in CD_2Cl_2. 64

Figure 3-9. Normalized signal decay as a function of gradient strength for XQ in CD_2Cl_2. 64

Figure 4-1. Structure of generation 2.0 PAMAM Dendrimer 65

Figure 4-2. (A) Structure of PAMAM dendrimer, ethylenediamine core, generation 0.0 (B) General structure of PAMAM dendrimer, generation *n*. 67

Figure 4-3. Schematic representation of PAMAM dendrimers, generation n, indicating the lettering scheme used to identify the methylene groups. (A) generation 0.0; (B) generation *n*. 69

Figure 4-4. ^1H NMR chemical assignment for PAMAM dendrimer, generation 0.0 in D_2O, 400 MHz NMR..... 70

Figure 4-5. ^1H NMR chemical assignment for PAMAM dendrimer, generation 1.0 in D_2O, 400 MHz NMR..... 70

Figure 4-6. ^1H NMR chemical assignment for PAMAM dendrimer, generation 3.0 in D_2O, 400 MHz NMR..... 71

Figure 4-7. ^1H NMR chemical assignment for PAMAM dendrimer, generation 5.0 in D_2O, 400 MHz NMR..... 71

Figure 4-8. ^1H NMR spectra of the bubbling of CO_2 into PAMAM dendrimer, generation 0.0. Down: no bubbling of CO_2. From down to up, the amount of CO_2 introduced increases. 73

Figure 4-9. ^1H NMR spectra of the bubbling of CO_2 into PAMAM dendrimer, generation 5.0. Down: no bubbling of CO_2. From down to up, the amount of CO_2 introduced increases. 73

Figure 4-10. Titration of PAMAM dendrimer, generation 5.0 with DCl in D_2O, 400 MHz NMR. 75
Figure 4-11. Titration of PAMAM dendrimer, generation 1.0 with $NaHCO_3$ in D_2O, 400 MHz NMR. 75
Figure 4-12. Titration of the solution already titrated with $NaHCO_3$ with DCl in D_2O, 400 MHz NMR. 76
Figure 4-13. Analysis of the reaction between CO_2 and PAMAM dendrimer, generation 0.0..... 77
Figure 4-14. Analysis of the reaction between CO_2 and PAMAM dendrimer, generation 5.0..... 77
Figure 4-15. ^1H NMR chemical assignment for PAMAM dendrimer, generation 0.0 in CD_3OD, 400 MHz NMR. 79
Figure 4-16. ^1H NMR chemical assignment for PAMAM dendrimer, generation 1.0 in CD_3OD, 400 MHz NMR. 79
Figure 4-17. ^1H NMR chemical assignment for PAMAM dendrimer, generation 5.0 in CD_3OD, 400 MHz NMR. 80
Figure 4-18. ^1H NMR analysis of PAMAM dendrimer, generation 0.0, 0.01 M titrated with CO_2 in CD_3OD, 400 MHz NMR. 80
Figure 4-19. ^1H NMR analysis of PAMAM dendrimer, generation 0.0, 0.16 M with CO_2 in CD_3OD, 400 MHz NMR..... 81
Figure 4-20. ^1H NMR analysis of PAMAM dendrimer, generation 0.0, 0.32 M with CO_2 in CD_3OD, 400 MHz NMR..... 81

Figure 4-21. ^{1}H NMR analysis of PAMAM dendrimer, generation 1.0, 0.01 M with CO_2 in CD_3OD, 400 MHz NMR. 83
Figure 4-22. ^{1}H NMR analysis of PAMAM dendrimer, generation 1.0, 0.08 M with CO_2 in CD_3OD, 400 MHz NMR. 83
Figure 4-23. ^{1}H NMR analysis of PAMAM dendrimer, generation 1.0, 0.16 M with CO_2 in CD_3OD, 400 MHz NMR. 84
Figure 4-24. ^{1}H NMR analysis of PAMAM dendrimer, generation 5.0, 0.005 M with CO_2 in CD_3OD, 400 MHz NMR. 85
Figure 4-25. ^{1}H NMR analysis of PAMAM dendrimer, generation 5.0, 0.01 M, with CO_2 in CD_3OD, 400 MHz NMR. 86
Figure 4-26. Titration of the gel of PAMAM dendrimer, generation 5.0 by N_2,400 MHz NMR. 87
Figure 4-27. Titration of the gel of PAMAM dendrimer, generation 5.0 by N_2 in the presence of NaOD, room temperature 400 MHz NMR. 88
Figure 5-1. Examples of cyclic host molecules based on cholic acid 92
Figure 5-2. Examples of acyclic host molecules based on cholic acid 93
Figure 5-3. Structure of Tetra-cholic acid cavitand (**3**). 94
Figure 5-4. Guest molecules used. 98
Figure 5-5. ^{1}H NMR of tetra-cholic acid cavitand (DMSO-d_6, 400 MHz). 99
Figure 5-6. Experimental High Resolution ESI-MS Spectrum of Tetracholic Acid Cavitand. ($C_{144}H_{196}N_{12}O_{28}$+2H)/2: 1272.2162. 100
Figure 5-7. Theoretical High Resolution ESI-MS Spectrum of Tetracholic Acid. 100

List of Schemes

Scheme 2-1. Contrast between CB7 binding of MV^{2+} and HEV^{2+} and its effect on the interaction with the cholate assemblies. 46

Scheme 3-1. Steps in the five-electron reduction process of the P5Q macrocycle. 58

Scheme 4-1. Reversible covalent chemistry between CO_2 and amine 68

Scheme 4-2. Converting carbamate to amine by bubbling with N_2 87

Scheme 5-1. Synthesis of Tetra-cholic acid cavitand. 94

Scheme 5-2. Synthesis of **1f** 95

Scheme 5-3. Synthesis of **2c**. 96

List of Tables

Table 1-1. Structural and physical parameters of CB[n][a5] Taken from Isaacs, L. *Chem.Comm.* **2009,** 6, 619. 6

Table 1-2. Values of K_a (M^{-1}) for host-guest complexes of CB[6], CB[6] and CB[8] with various guests[a5] 9

Table 2-1. Equilibrium Association Constants (*K*) for MV^{2+} Complexation by CB7 Measured in Aqueous Media of Variable Composition at 25 ºC. 41

Table 3-1. Electrochemical data for the voltammetric reduction of P5Q in CH_2Cl_2 also containing 0.1 M $TBAPF_6$ 56

Table 4-1. Molecular parameters of PAMAM dendrimers of generation 0.0, 1.0, 2.0 3.0, 4.0 and 5.0..... 67

List of Equations

Equation 2-1 22

Equation 2-2 22

Equation 3-1 51

Equation 3-2 51

Equation 3-3 54

Equation 3-4 54

Equation 3-5 54

Equation 3-6 54

Equation 3-7 55

Equation 3-8 63

Equation 4-1 74

Chapter 1 : Introduction

1.1 Introduction to supramolecular chemistry

The scientific definition of “Suparmolecular chemistry” is: the chemistry of the intermolecular bond, covering the structures and functions of the entities formed by the association of two or more chemical species----- By Jean-Marie Lehn (Figure 1-1 B), *Nobel Laureate* in 1987

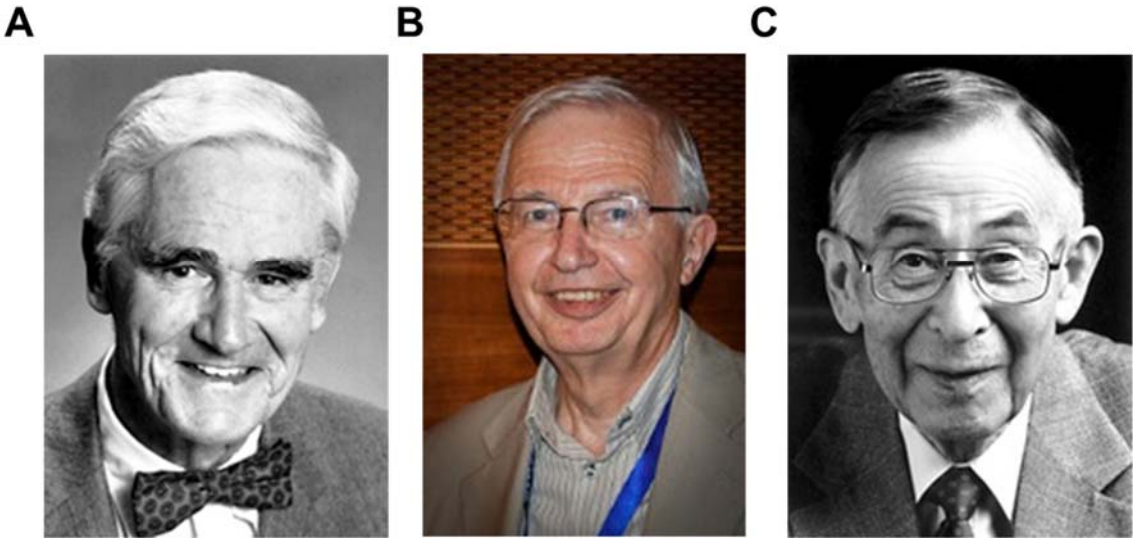

Figure 1-1. (A) Donald J. Cram; (B) Jean-Marie Lehn; (C) Charles Pedersen--Nobel Prize Laureates in Chemistry at 1987

There are many natural supramolecular phenomena: such as DNA cooperative binding self-assembly (Figure 1-2A), enzyme assembly (Figure 1-2B) and so on. In DNA cooperative binding, two separate strands of DNA nucleotides are connected by hydrogen bonding; DNA replications are made possible through the breakdown of the hydrogen bonding between the two strands. In

enzyme assembly, the tertiary structure of proteins is governed by supramolecular interactions, such hydrogen bonds, etc.

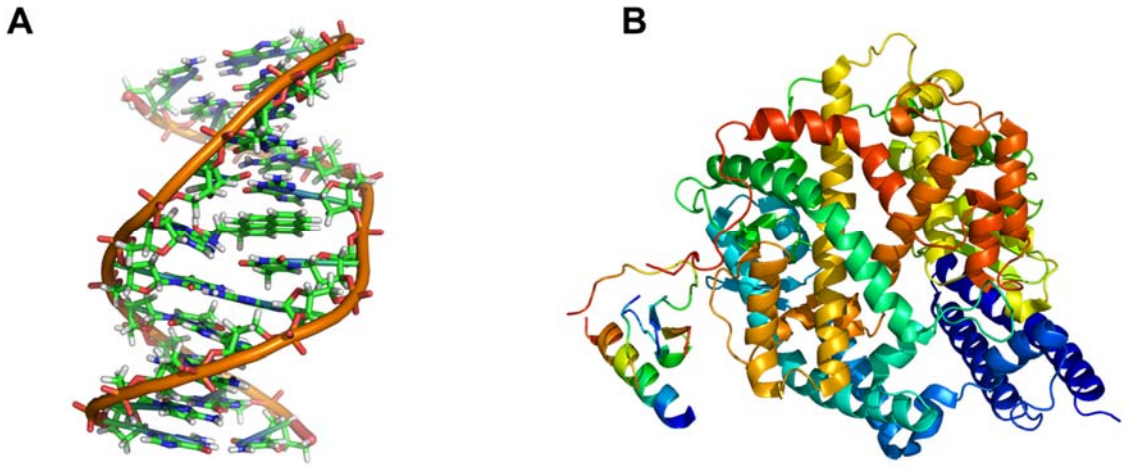

Figure 1-2. (A) DNA assembly; (B) Protein assembly.

The first supramolecular chemistry investigation can be dated back to 1873 when Johannes Diderik postulated the existence of intermolecular interactions. Afterwards Hermann Emil Fischer proposed that the enzyme-substrate interaction is in the form of a “lock” and “key” system. Later, hydrogen bond was described by Latimer and Rodebush in 1920. The synthetic involvement was initiated by Charles J. Pedersen in 1960s with the synthesis of crown ethers. Later on, more and more researchers have been dedicated to this emerging area. The 1987 Nobel Prize in chemistry was awarded to Donald J. Cram, Jean-Marie Lehn, and Charles J. Pedersen to distinguish their pioneering contributions to supramolecular chemistry.

Some of the most important supramolecular interactions are: (1) Ion-dipole interactions; (2) Dipole-dipole interactions; (3) Hydrogen bonding; (4) Interactions

involving π-systems; (5) Van der Waals forces; (6) Close packing; (7) Hydrophobic effect, etc. These kinds of interactions are weak, such as van der Waals forces are as low as 5 kJ/mole, dipole-dipole interactions are 5-50 kJ/mole, and hydrogen bonding is 4-120 kJ/mole. We need to keep in mind that the energy to form a carbon-hydrogen covalent bond is around 100 kJ/mole. The lattice energy of sodium chloride is around 756 kJ/mole. Since the supramolecular interactions are not strong, supramolecular complexes are easier to decompose compared to covalent molecules and ionic compounds.

A supramolecular system consists of at least two independent parts, which could be organic molecules, ions or large assemblies. The first few synthetic examples of supramolecules were systems between macrocyclic compounds and cations (Figure 1-3).[1] Probably, they were isolated and characterized by chance during the synthesis of another target compound with the corresponding salt as one of the reagents.

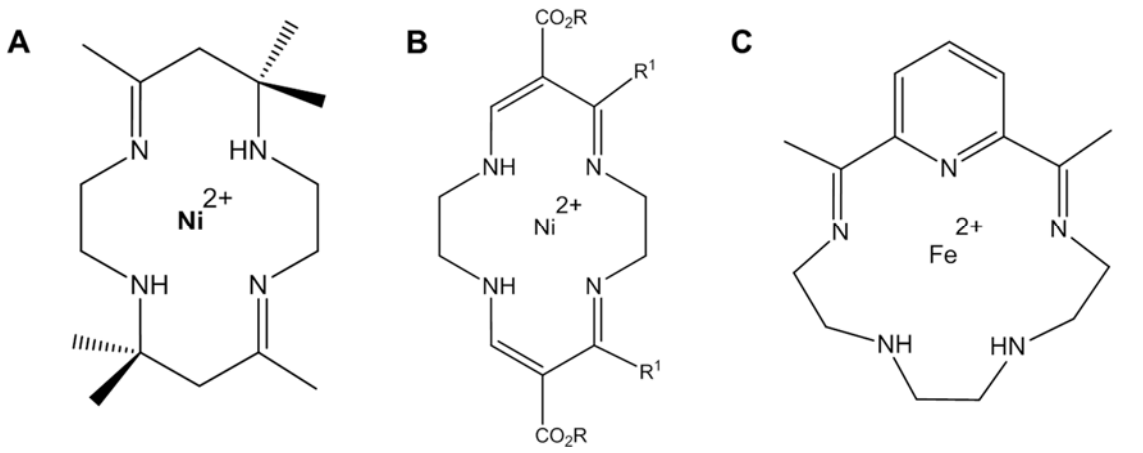

Figure 1-3. (A) First Schiff's base macrocycle from acetone and ethylene diamine by Curtis;[1a] (B) Schiff's base macrocycle by Jager;[1b] (C) Schiff's base macrocycle by Busch.[1c]

Charles J. Pedersen opened the chapter of supramolecular chemistry with the seminal synthesis of crown ethers which can bind metal ions (Figure 1-4A).[2] Jean-Marie Lehn's cryptands were the other example of seminal synthetic supramolecules (Figure 1-4B).[3] Donald J. Cram developed three dimensional molecules, cavitands, which can not only encapsulate metal ions but also bind with organic compounds (Figure 1-4C).[4]

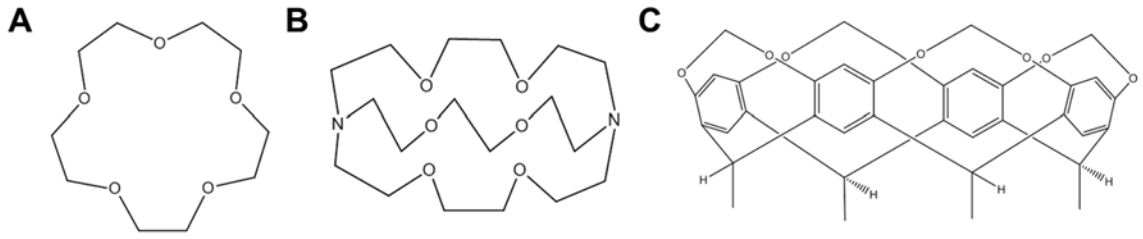

Figure 1-4. (A) Pederson's Crown Ether;[2] (B) Lehn's Cryptand;[3] (C) Cram's Cavitand.[4]

Host-guest chemistry is an important subfield of supramolecular chemistry. Most of supramolecular chemistry can be defined as host-guest chemistry, to

some extent. The host molecule is preferred to have a specific conformation in order to encapsulate the guest molecule. The synthetic involvement into the host-guest chemistry is crucial to advancements in this area. Macrocyclic compounds are ideal as hosts. Macrocyclic molecules have spaces where it can hold ions or molecules. Below are some popular guest molecules: (a) Cyclodextrin (Figure 1-5A); (b) Calixarene (Figure 1-5B); (c) Cucurbituril (Figure 1-5C); (d) Pillararene (Figure 1-5D).

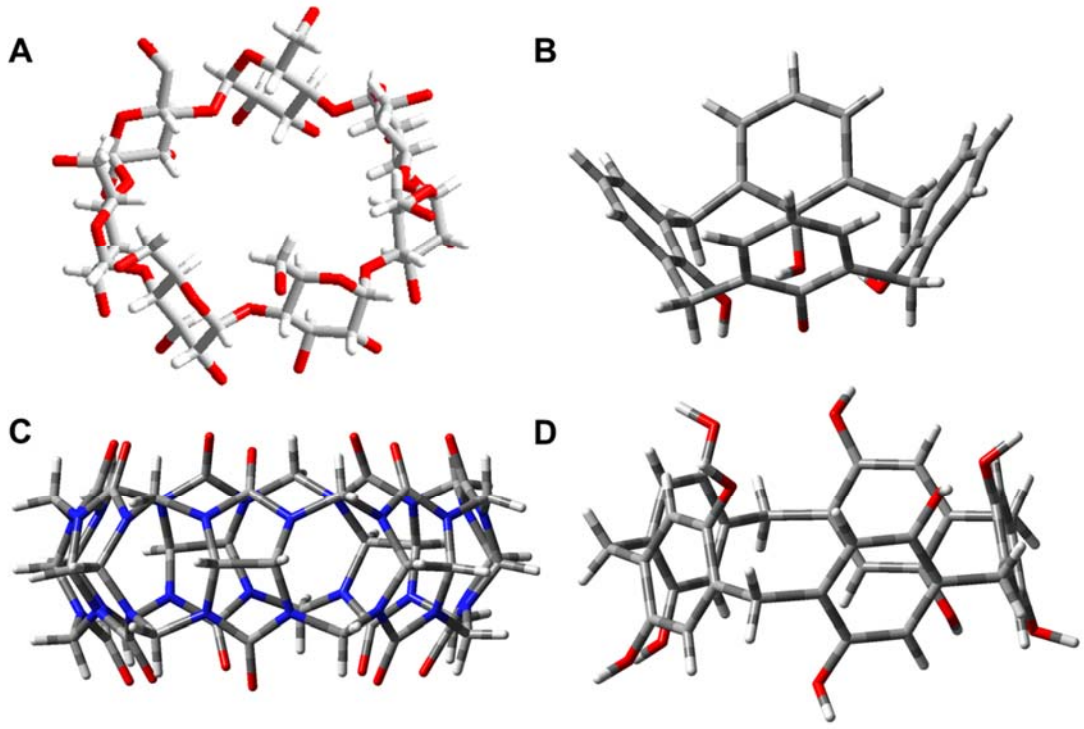

Figure 1-5. (A) β-Cyclodextrin; (B) Calix[4]arene; (C) Cucurbit[7]uril, (D) Pillar[5]arene. (Red: Oxygen; Blue: Nitrogen; White: Hydrogen)

We will discuss cucurbiturils and pillararenes in more details because of their relevance to the work described here.

1.1.1 Introduction to cucurbit[n]urils

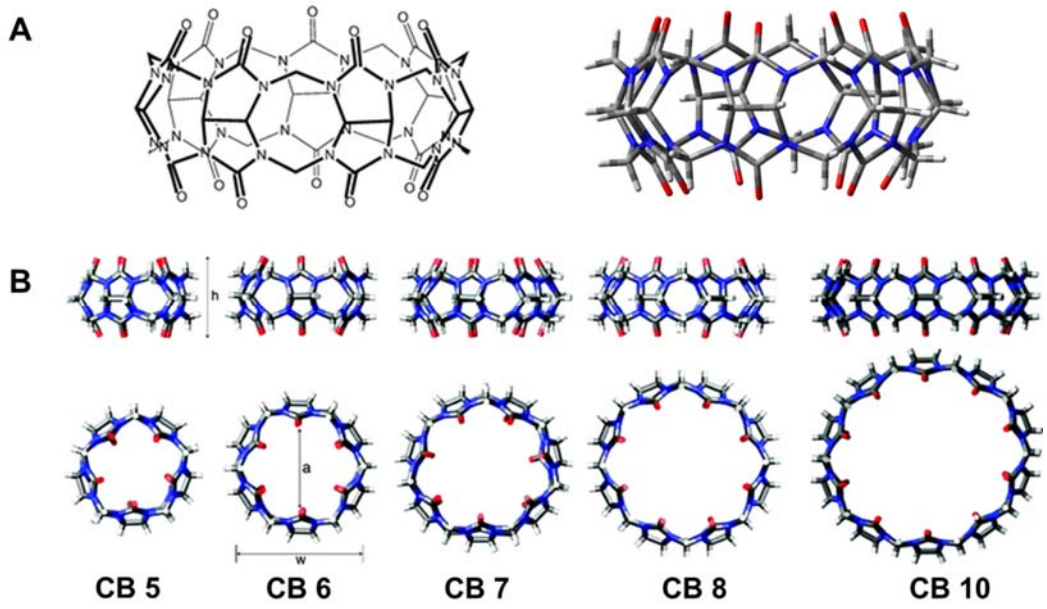

Figure 1-6. (A) Structure of Cucurbit[7]uril; (B) Comparison of the relative sizes of CB5, CB6, CB7, CB8 and CB10.[5] Taken from Isaacs, L. *Chem.Comm.* **2009,** 619.

Table 1-1. Structural and physical parameters of CB[n][a5] Taken from Isaacs, L. *Chem.Comm.* **2009,** 6, 619.

	h / Å	*w* / Å	*a* / Å	*V* / Å^3
CB[5]	9.1	4.4	2.4	82
CB[6]	9.1	5.8	3.9	164
CB[7]	9.1	7.3	5.4	279
CB[8]	9.1	8.8	6.9	479
CB[10]	9.1	11.3-12.4	9.5-10.6	870

[a] Values of *h*, *w*, and *V* account for the van der Waals radii of the various atoms

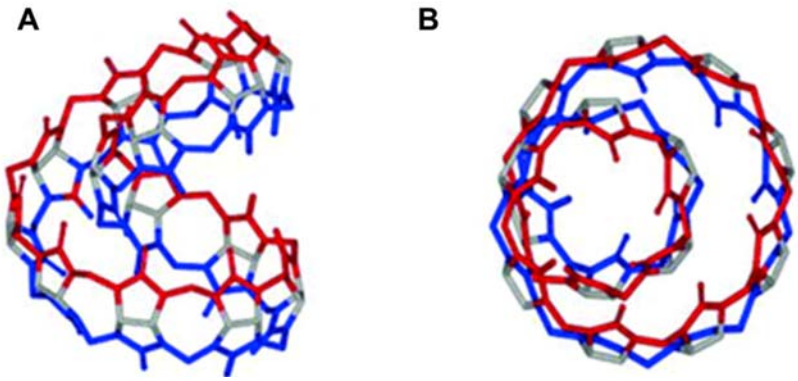

Figure 1-7. (A) Side view of cucurbit[14]uril; (B) Top view of cucurbit[14]uril.[6] Taken from Cheng, X.-J.; Liang, L.-L.; Chen, K.; Ji, N.-N.; Xiao, X.; Zhang, J.-X.; Zhang, Y.-Q.; Xue, S.-F.; Zhu, Q.-J.; Ni, X.-L.; Tao, Z. *Angew. Chem. Int. Ed.* **2013,** *52*, 7252.

The cucurbiturils were first synthesized in 1905. However, their structures were not elucidated until the 1980s. The detailed investigation of cucurbit[n]urils was initiated by W. A. Freeman, W. L. Mock and their coworkers.[7] But only cucurbit[6]uril was investigated until 2000, when Kimoon Kim synthesized cucurbit[5]uril, cucurbit[7]uril and cucurbit[8]uril.[8] Cucurbit[10]uril was first discovered by Anthony Day and his coworkers, but it complexed with cucurbit[5]uril.[9] Pure cucurbit[10]uril was isolated by Lyle Isaacs and his coworkers.[10] In 2013, Zhu Tao and his coworkers successfully detected the existence of cucurbit[14]uril, but it exists in a twisted form (Figure 1-7).[6] Table 1-1 lists the physical parameters of CB[5], CB[6], CB[7], CB[8] and CB[10]. The physical parameters of CB[14] are not provided in this table, since it is formed in a twisted state. CB[5] has the smallest cavity volume of 82 Å. CB[10] has a cavity volume of 870 Å, ten times that of CB[5]. The first CB[10] discovered was a

complex with CB[5]. CB[10] can even accommodate guests as large as cationic calix[4]arenes and tetra(*N*-methylpyridyl)porphyrins.

The solubility of cucurbit[n]uril is a concern. CB[5] and CB[7] have better solubility in neutral water compared to CB[6], CB[8] and CB[10]. All of them are more soluble in acidic conditions or with the assistance of some metal ions.[5]

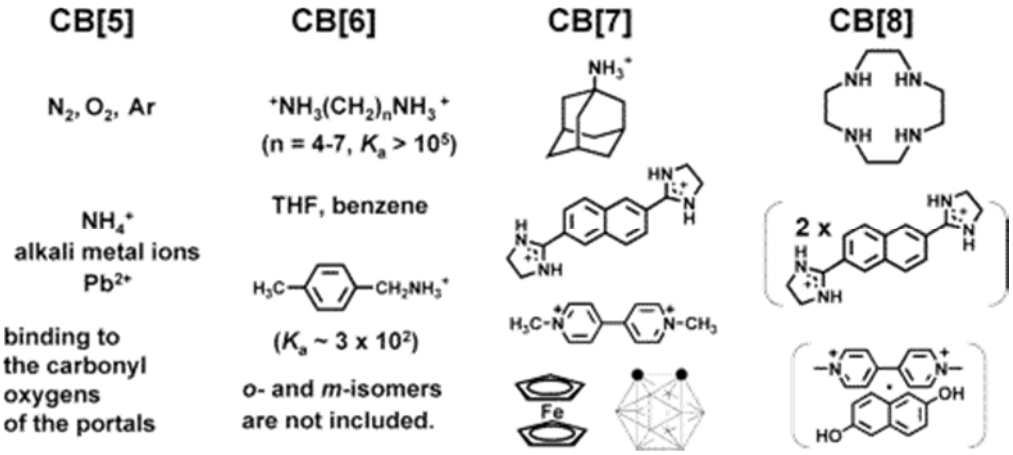

Figure 1-8. Selected guest molecules which can bind with CB[5], CB[6], CB[7] and CB[8] respectively.[11] Taken from Lee, J. W.; Samal, S.; Selvapalam, N.; Kim, H.-J.; Kim, K. *Acc. Chem. Res.* **2003,** *36*, 621.

Cucurbit[n]urils have a hydrophobic cavity and polar carbonyl portals. Since CB homologues vary in cavity and portal size, they have different molecular recognition properties (see Figure 1-8).[11] The difference in size makes them have selective binding properties. CB[5] can only encapsulate small molecules or cations. Two NH_4^+ ions can seal the openings of CB[5]. CB[6] can bind with protonated diaminoalkanes, THF, benzene, etc. CB[7] is able to accommodate protonated adamantylamine, methyl viologen dications, ferrocene and so on. The bigger CB[8] can encapsulate larger molecules, such

as accommodating two 2,6-bis(4,5-dihydro-1*H*-imidazol-2-yl)naphthalene at the same time.

Since CB homologues have different cavity sizes, their binding abilities with the same guest are not the same. Table 1-2 lists the K_a values (K_a: binding constant, M^{-1}) of the binding interactions CB[6], CB[7] and CB[8] with several guests.[5]

Table 1-2. Values of K_a (M^{-1}) for host-guest complexes of CB[6], CB[6] and CB[8] with various guests[a5]

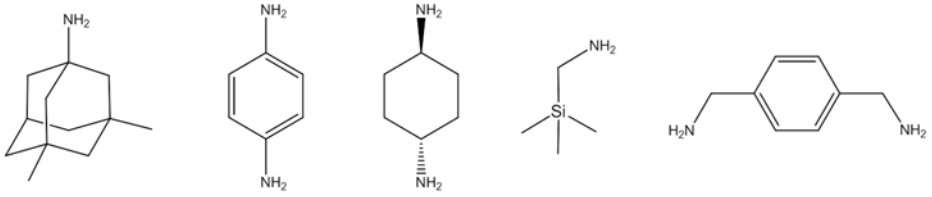

1 **2** **3** **4** **5**

	CB[6]	CB[7]	CB[8]
1	−	2.5×10^4	4.3
2	1860	2.1×10^6	−
3	1.4×10^6	2.3×10^7	−
4	NB	8.9×10^8	NB
5	550	1.8×10^9	−

[a] NB: no inclusion binding detected by ^{1}H NMR spectroscopy. −: not determined.

By analyzing Table 1-2, we can see that the range of values of K_a observed is broad, from 550 to 1.8×10^9. Depending on the sizes of the guest molecules, most of them can only bind with two types of CB[n], and some can only bind with one type of CB[n]. For the same CB[7], the K_a values differ with different guests (CB[7]: from 2.5×10^4 to 1.8×10^9). For the same guest, the K_a values can either be similar or have a large difference with different types of CB[n]

(**5**: 550 for CB[6] and 1.8 × 10^9 for CB[7]; **3**: 1.4 × 10^6 for CB[6] and 1.8 × 10^9 for CB[7]).

1.1.2 Pillar[n]arene in supramolecular chemistry

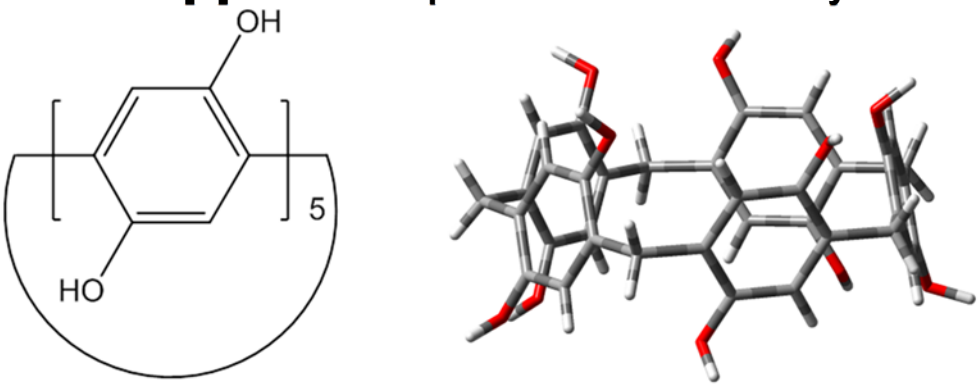

Figure 1-9. Structure of Pillar[5]arene.

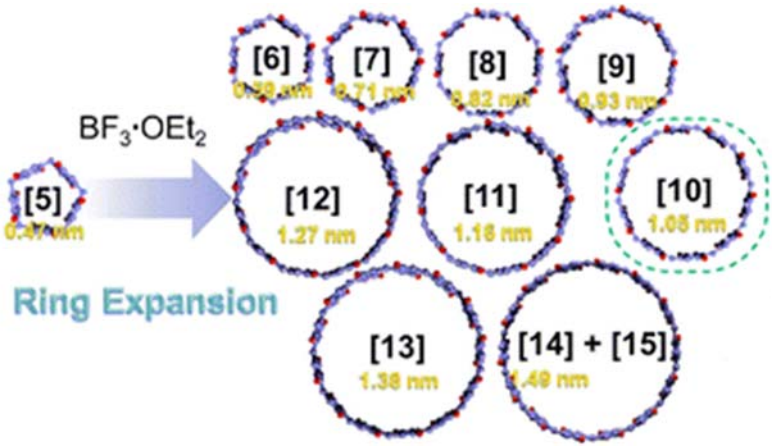

Figure 1-10. Ring expansions from pillar[5]arene reported by Tomoki Ogoshi.[12] Taken from Ogoshi, T.; Ueshima, N.; Sakakibara, F.; Yamagishi, T.-A.; Haino, T. *Org. Lett.* **2014,** *16*, 2896.

The first pillar[n]arene, 1,4-dimethoxypillar[5]arene, was reported by Tomoki Ogoshi.[13] Pillar[5]arene is the most investigated among the pillar[n]arene family, due to its high synthetic yield and conformational stability. Recently, Ogoshi reported a method to increase the yield of pillar[6]arene to 87% using a

templating agent.[14] An interesting thing about this family is that pillar[n]arene is able to go through ring expansion. Ogishi successfully expanded pillar[5]arene to pillar[n]arene (n = 6,7,8,9,10,11,12,13,14 and 15) under kinetic control, though the mechanism of the expansion is not fully understood.[12]

The applications of pillar[n]arenes are broad. However, since pillar[n]arenes do not have very good binding ability, most of pillar[n]arene related research is about functionalized pillar[n]arenes.

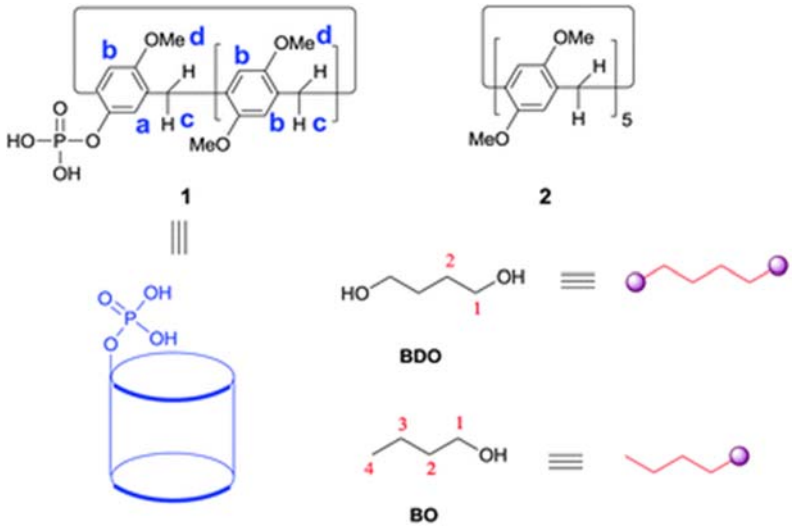

Figure 1-11. (1) Monophosphoryl copillar[5]arene; (2) 1,4-dimethoxyl pillar[5]arene; **BBO.** 1,4-butanediol; **BO.** 1-butanol.[15] Taken from Chen, Y.; He, M.; Li, B.; Wang, L.; Meier, H.; Cao, D. *RSC Adv.* **2013,** *3*, 21405.

Derong Cao and his coworkers prepared a monophosphoryl copillar[5]arene (Figure 1-11, **1**).[15] The phosphoryl group increases the binding ability of **1** (~1.48×10^3 for **BDO** and ~3.45×10^2 for **BO**), compared to **2** (~2.91×10^2 for **BDO**, K_a is too small to be calculated accurately for **BO**). The increased values of K_a are probably from the polar groups on phosphoryl groups,

which have better interaction with the hydroxyl groups on **BBO** and **BO** than the methyl groups on **2**.

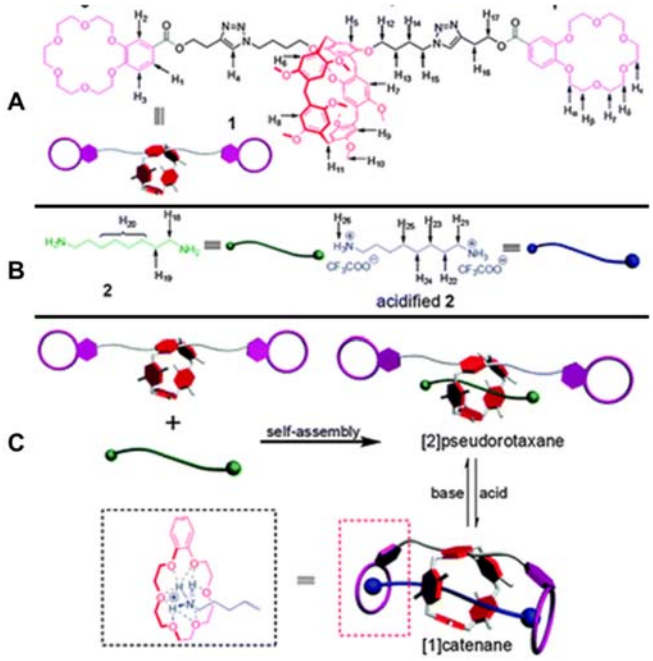

Figure 1-12. (A) Benzo-18-crown-6 functionalized copillar[5]arene; (B) Guest molecules; (C) pH-responsive dynamic[1]catenane.[16] Taken from Yan, X.; Wei, P.; Li, Z.; Zheng, B.; Dong, S.; Huang, F.; Zhou, Q. *Chem. Comm.* **2013,** *49*, 2512.

Feihe Huang and his coworkers reported a difunctionalized pillar[5]arene. They attached one crown ether at each rim of 1,4-dimethoxypillar[5]arene (Figure 1-12A).[16] This difunctionalized pillar[5]arene has two types of binding sites: pillar[5]arene and crown ether. The neutral guest molecule (Figure 1-12B) is able to form a [2]pseudorotaxane with this difunctionalized pillar[5]arene and does not interact with the crown ether (Figure 1-12C). Once the guest molecule is acidified, the two sides of the guest molecule have positive charge to interact with the crown ether to form a [1]catenane (Figure 1-12C).

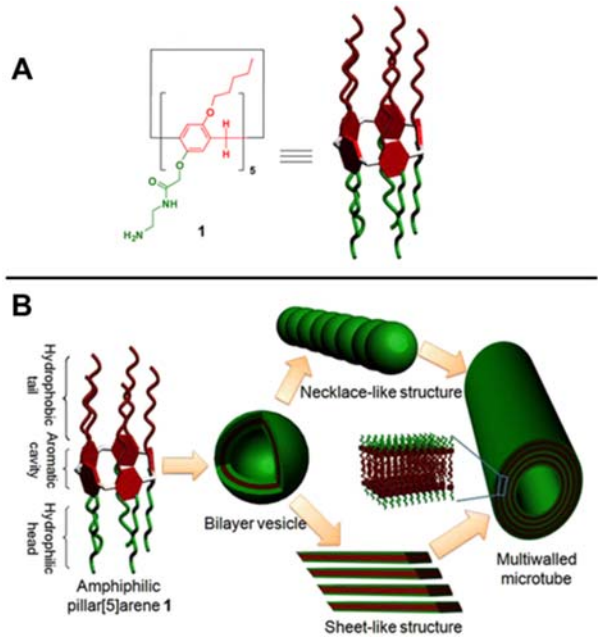

Figure 1-13. (A) Structure of the amphiphilic pillar[5]arene by Feihe Huang; (B) Schematic illustration of the self-assembly process of amphiphilic pillar[5]arene 1 into microtubes.[17] Taken from Yao, Y.; Xue, M.; Chen, J.; Zhang, M.; Huang, F. *J. Am. Chem. Soc.* **2012,** *134*, 15712.

Some people also functionalized all the hydroxyl groups (2n for pillar[n]arene). In 2012, Feihe Huang and his coworkers reported an amphiphilic pillar[5]arene. [17] On each rim of this amphipillic pillar[5]arenes, there are five hydrophilic amino groups; on the other rim, five hydrophobic alkyl chains are attached to it. Huang's amphiphilic pillar[5]arene can come together to form well-defined vesicles under neutral conditions. At low pH, these vesicles transformed into small globular micelles. After four months, the vesicles further self-assembled into microtubes. And the microtubes formed could adsorb 2,4,6-trinitrotoluene by donor-acceptor interactions.

1.2 Introduction to electrochemistry in supramolecular chemistry

The investigation of electrochemistry dates back to the 16th century. The first electric generator was created by Otto von Guericke in 1663. In 1782s, Luigi Galvani made a connection between chemical reactions and electricity, which was the birth of electrochemistry. In 1800, water was electrolyzed into H_2 and O_2 by William Nicholson and Johann Ritter.

The changes of electrical parameters, such as potential, current and charges, are connected with chemical phenomena. The electrical parameters could be used either to monitor chemical changes or to influence chemical reactions.

Most of chemistry characterization methods, such as NMR, UV-Vis, fluorescence, etc, must deal with homogenous bulk solution to get accurate results. Electrochemical processes, most cases, only take place at the interface between electrode and solution has electrochemical processes.

Electrochemistry has many applications in supramolecular chemistry. It can either be used to investigate supramolecular complex properties or to influence supramolecular complex formation.

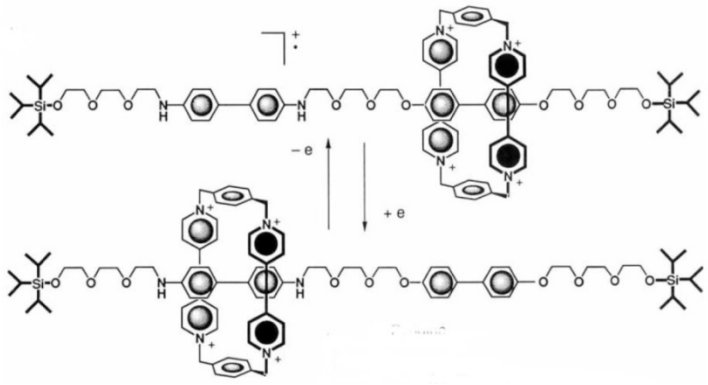

Figure 1-14. Electrochemically switchable molecular shuttle.[18] Taken from Bissell, R. A.; Cordova, E.; Kaifer, A. E.; Stoddart, J. F. *Nature* **1994,** *369*, 133.

Figure 1-14 represents an electrochemically switchable rotaxane by Angel Kaifer and his coworkers.[18] In this bead-thread rotaxane, the thread is composed of two different π-electron donating groups, *i.e.* biphenol and benzidine connected by a polyether chain with tri-isopropylsily groups as stoppers. The bead is the so-called blue box-cycloplane. At room temperature, the bead moves between the biphenol and benzidine group. One electron oxidation of the benzidine can make the bead docking on the biphenol. This rotaxane is also chemically switchable.

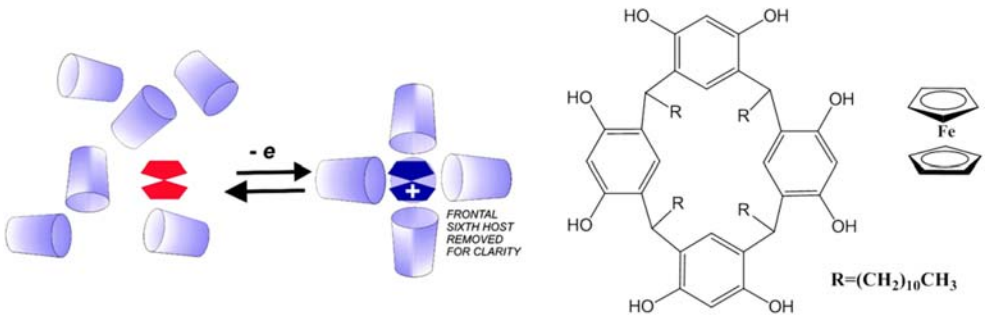

Figure 1-15. Electrochemically driven formation of a molecular capsule around ferrocenium by six resorcinarene.[19] Taken from Philip, I. E.; Kaifer, A. E. *J. Am. Chem. Soc.* **2002,** *124*, 12678.

In 2002, Kaifer and his coworkers reported a molecular capsule around the ferrocenium ion driven by electrochemistry (Figure 1-15).[19] In neutral state of ferrocene, there are no interactions between resorcinarene and ferrocene. When ferrocene is oxidized into ferrocenium, the positive charged forrocenium can attract six resorcinarenes to form a large capsule, since resorcinarene has inner π surface. The hydroxyl groups of resorcinarene attach to the hydroxyl groups from other resorcinarenes by hydrogen bonding, which makes the six resorcinarenes stay together around the ferrocenium.

Electrochemical signal changes can reflect structural or property changes of its associated systems. Chemists use electrochemical signal changes to postulate the related chemical changes in supramolecular chemistry, like UV-Vis, NMR, mass spectroscopy, etc.

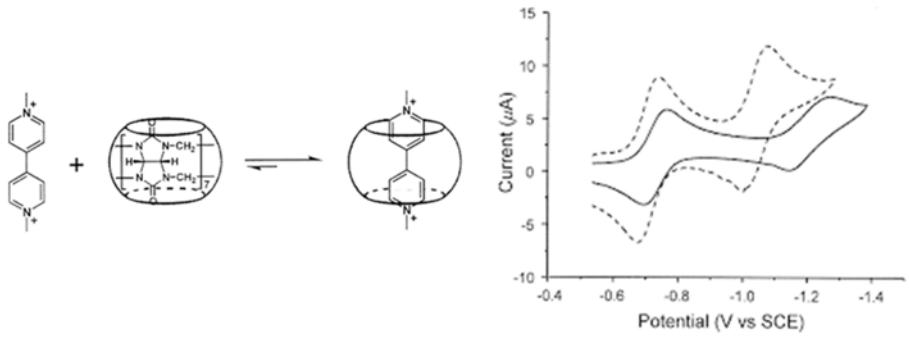

Figure 1-16. Electrochemical investigation of the binding interaction between cucurbit[7]uril and methyl viologen by Angel Kaifer and Kimoon Kim, respectively.[20] Taken from Kim, H.-J.; Jeon, W. S.; Ko, Y. H.; Kim, K. *Proc. Natl. Acad. Sci.* **2002,** *99*, 5007.

Viologen undergoes two one-electron reversible reductions. In 2002, Angel Kaifer and Kimoon Kim simultaneously reported the encapsulation of

methyl viologen into cucurbit[7]uril.[20] Electrochemistry was adopted by both of them to investigate the binding interaction between cucurbit[7]uril and methyl viologen. With the addition of one equivalent of CB7 to methyl viologen, the first half wave potential shifts to a slightly more negative value, while the second half wave potential moves to a much more negative value. The negative shift of the first half wave potential indicates that CB7 prefers to bind with the dication state of viologen rather than the cation radical form. Additionally, the decreased current of MV@CB7 complex means a reduced diffusion coefficient compared to the free viologen, which is determined by the increased size of the MV@CB7 complex.

Chapter 2 : Electrochemistry of Viologen Dications in Cholate Media and Competition between the Cholate Assemblies and the Cucurbit[7]uril Host

2.1 Overview

2.1.1 Cholic acid and cholate

Cholic acid is one of the two major bile acids produced by the liver; the other is chenodeoxycholic acid. Cholic acid plays an important role in the human body. Cholic acid is a white crystalline substance, which is not soluble in water but soluble in alcohol and acetic acid. The salts of bile acids are called bile salts. The salt of cholic acid is called cholate, such as sodium cholate (NaCh).

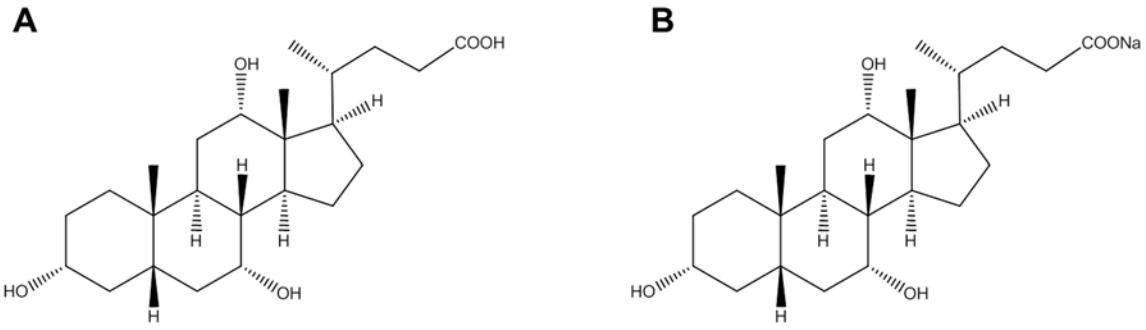

Figure 2-1. (A) Cholic acid; (B) Sodium Cholate

Cholic acid and sodium cholate are very attractive in terms of chemistry. First, it has high levels of functionality, distributed evenly around its framework; second, the functional groups could be differentiated and transformed in various

ways; finally, it is readily available and cheap with a commercial price around one dollar per gram.

2.1.2 Bile salt aggregates

Sodium cholate, bile salt, is an amphiphilic molecule. Its convex face is hydrophobic, because of the methyl groups; while the concave face is hydrophilic, because of the hydroxyl groups.

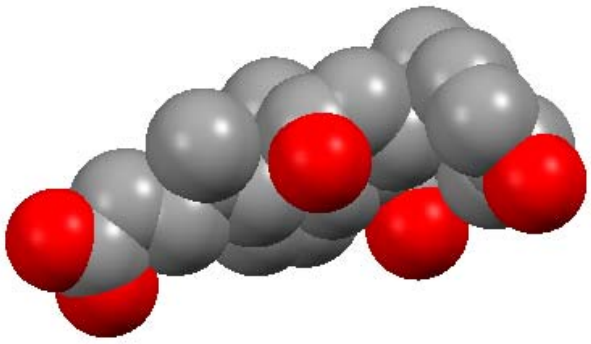

Figure 2-2. 3-D structure of cholic acid.

Bile salt aggregates, in contrast to micelle systems formed by conventional surfactants, increase in size as the concentration is raised.[21] Bile salts solubilize hydrophobic molecules very well.[22] Bile salt aggregates can be regarded as a host system to incorporate guest molecules.

Several models have been proposed for the formation of bile salt aggregates. (1) Small and his coworkers suggested a primary/secondary model:

at low concentrations of bile salt, primary aggregates are formed through the interaction of the hydrophobic convex surfaces of bile salts; as the concentration of monomers increases, the primary aggregates agglomerate into secondary aggregates.[21] (2) Another model suggests that the primary aggregates are formed through the interaction of the hydroxyl groups located on the concave face of the monomers.[23] (3) Some others proposed that the bile salt aggregates are formed as a stepwise aggregation process in which the primary interaction modes are not defined.[24] (4) Recent NMR and theoretical studies reveal that both hydrophobic interactions and hydrogen binding play roles in the formation of bile salt aggregates, and their relative importance depends on the structure of bile salt monomers.[25]

While the effect of sodium cholate on the photophysical behavior of several fluorophores has been investigated in detail,[26] we are not aware of any systematic investigation of the electrochemical properties of redox-active probes in the presence of sodium cholate aggregates. As ideal probes for this work, we selected a series of simple 4,4'-bipyridinium (viologen) dications. The reasons behind this selection are listed below:

(1) The electrochemistry of viologens (V^{2+}) involves two fast one-electron reduction steps, leading successively to a radical cation ($V^{+\bullet}$) and a neutral species (V).

(2) Reduction is associated with the removal of positive charge from the initial viologen dication. Therefore, as reduction proceeds, the resulting viologen species is less water-soluble and more hydrophobic, leading to stronger

interactions with any hydrophobic cavities or docking sites present in the media.

(3) Finally, the overall hydrophobicity of any viologen oxidation state (V^{2+}, $V^{+\bullet}$ or V) can be controlled synthetically by the attachment of different aliphatic groups to the nitrogen atoms in the 4 and 4' positions of the bipyridinium nucleus.

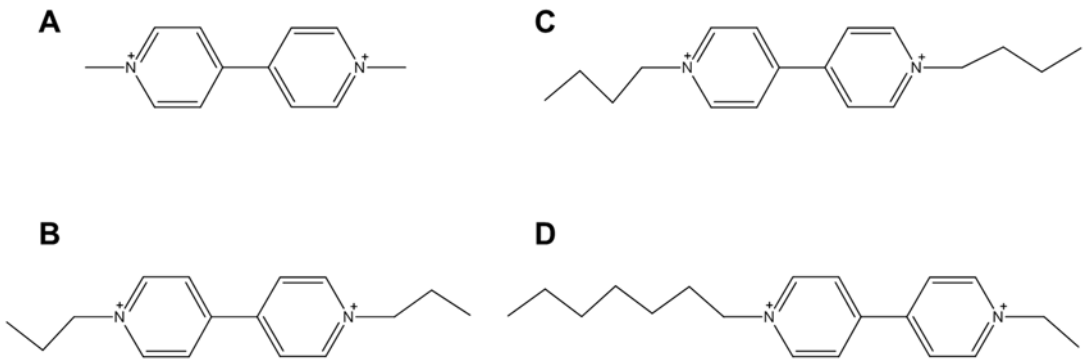

Figure 2-3. (A) Methyl viologen dication; (B) Propyl viologen dication; (C) Butyl viologen dication; (D) Heptyl ethyl viologen dication.

Another interesting aspect of viologens is that they are excellent guests for the formation of inclusion complexes with the host cucurbit[7]uril (CB7).[11, 27] In fact, methylviologen was one of the first guests investigated for complexation by this versatile aqueous host.[20] It is interesting to look at the competition for viologen guests between the hydrophobic cavities formed by cholate assemblies and the CB7 host.

2.2 Results

We selected 0.2 M NaCl as the supporting electrolyte in our electrochemical experiments because the literature contains substantial information on the behavior of sodium cholate in this medium. The cyclic voltammetry (CV) of a viologen (V^{2+}) in aqueous media is characterized by the observation of two redox couples corresponding to the following consecutive, one-electron reduction processes:

$$V^{2+} + e^{-} \leftrightarrow V^{+\cdot} \qquad \text{Equation 2-1}$$

$$V^{+\cdot} + e^{-} \leftrightarrow V \qquad \text{Equation 2-2}$$

At the relatively slow scan rates used in our experiments, the second reduction leads to some precipitation of the fully reduced species (V), which manifest itself in departures from the reversible wave shape, which is especially visible in the second reduction process. More specifically, the accumulation of precipitated V on the electrode surface results in the “stripping” shape of the very sharp anodic peak for the second wave, which reflects the oxidation of V to the more water-soluble radical cation form ($V^{+\bullet}$). The precipitation of reduced species on the working electrode takes place with most viologens, but the distortions from diffusion-controlled voltammetric curves increase with the hydrophobic character of the viologen. In principle, one can try to “push” the cyclic voltammogram into a more reversible shape by either increasing the scan rate or by decreasing the overall viologen concentration in the experiment. However, we decided to use

this voltammetric feature as a way to probe the effect of cholate on the electrochemical processes, with the expectation that hydrophobic cavities created by the cholate assemblies may help solubilize cavities created by the cholate assemblies may help solubilize hydrophobic species and thus contribute to the elimination of the very visible anodic spike on the second redox process.

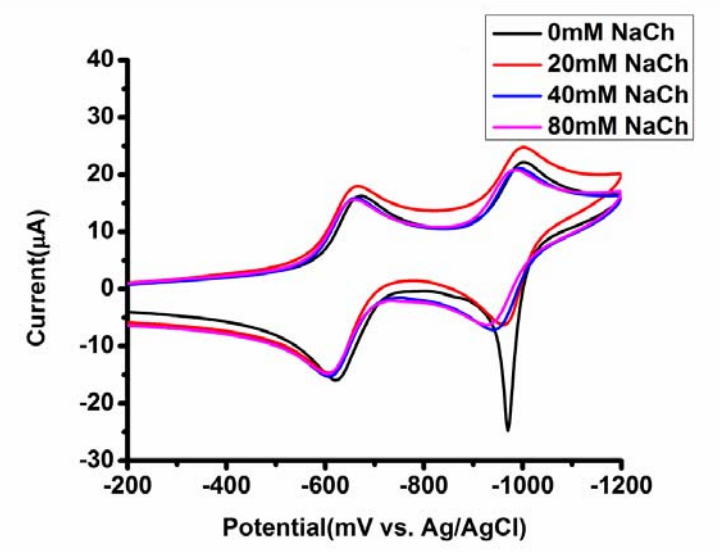

Figure 2-4. Cyclic voltammetric behavior on glass carbon (0.071 cm^2) of 1.0 mM MV^{2+} in 0.2 M NaCl containing variable concentrations of sodium cholate. Scan rate: 0.1 V s^{-1}.

Figure 2-4 show the cyclic voltammetric behavior of the methylviologen (MV^{2+}) in aqueous 0.2 M NaCl containing variable concentrations of sodium cholate. Clearly, cholate additions have a relatively minor effect on the current-potential curves. Perhaps the most notable effect is that the stripping peak corresponding to the oxidation of MV to $MV^{+\bullet}$ is no longer observed in the presence of sodium cholate, even at concentrations as low as 20 mM. This

finding suggests that the cholate aggregates solubilize the hydrophobic, neutral species and prevent its precipitation on the electrode surface, even at relatively low concentrations. On the other hand, the peak potential and currents in the voltammogram are not strongly affected by the presence of cholate.

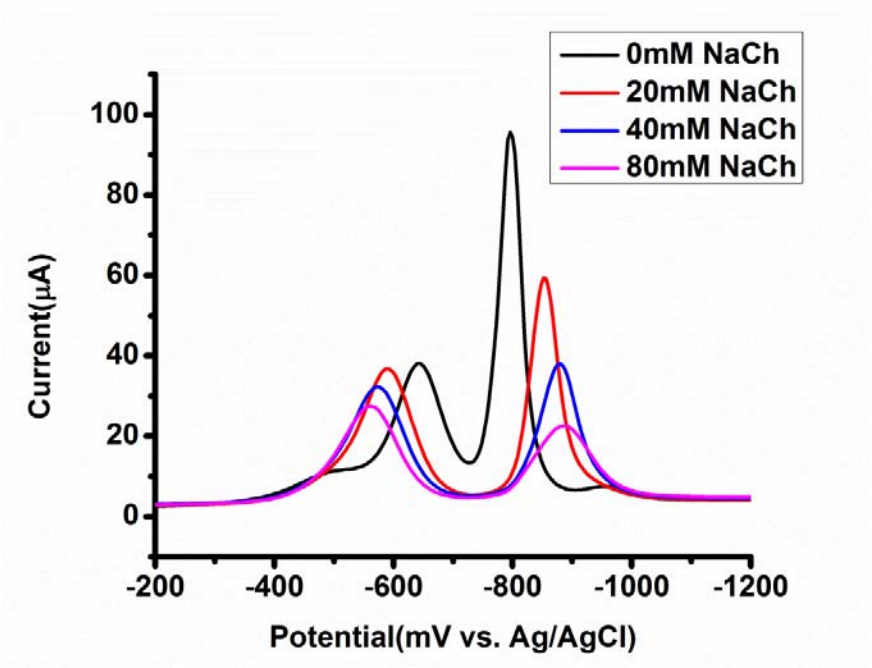

Figure 2-5. Square wave voltammetric behavior of 1.0 mM HEV^{2+} in 0.2 M NaCl and variable concentration of sodium cholate.

Square wave voltammetry (SWV) is another electrochemical technique that can be used to measure the characteristic potentials for the reduction of viologen probes in the presence of cholate. In general terms, the electrochemical data obtained from CV and SWV are very similar, as expected. We carried out voltammetric experiments with all four viologens (Figure 2-6 to Figure 2-11). As a second illustrative example, Figure 2-5 shows the SWV data obtained with asymmetric viologen HEV^{2+}. In this case, the addition of cholate results in clear changes in the peak potentials measured for the two reduction processes of

HEV^{2+}. In SWV, the observed peak potentials are equal to the half-wave potentials ($E_{1/2}$) for the corresponding electrochemical process. And the data in the figure clearly shows that the first one-electron reduction of HEV^{2+} experiences a shift to more positive $E_{1/2}$ as the cholate concentration increases. Conversely, the $E_{1/2}$ value for the second one-electron reduction process moves to more negative values with increasing cholate concentration. However, the second reduction process is more strongly affected by the precipitation of the reduced species, as evidenced by the sharper appearance of the voltammetric peaks, which diminishes their value to monitor any thermodynamic trends. In any instance, the voltammetric data for HEV^{2+} show that the potential difference between the two consecutive $E_{1/2}$ values increases with the cholate concentration, indicating that the presence of cholate assemblies differentially stabilizes the cation radical form, $HEV^{+\bullet}$, in preference to the dicationic and neutral forms (HEV^{2+} and HEV) of the viologen probe. In other words, assuming that the distortions caused by viologen precipitation on the second wave are modest, we can conclude that the comproportionation equilibrium, $HEV^{2+} + HEV \leftrightarrow 2HEV^{+\bullet}$, shifts to the right as the concentration of cholate increases.

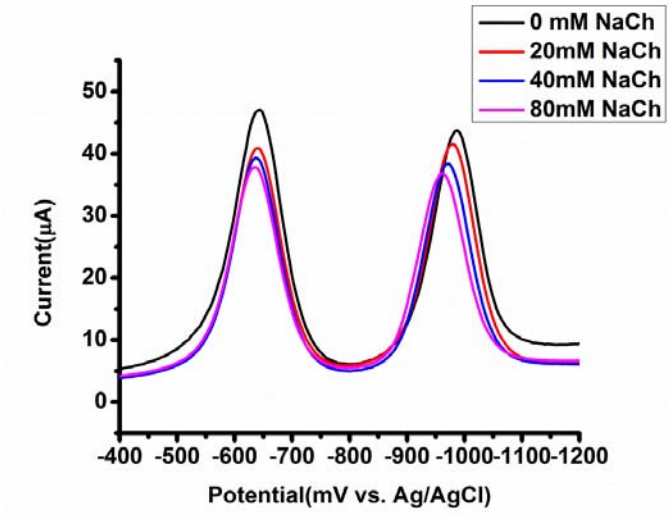

Figure 2-6. Square wave voltammetric behavior of 1.0 mM MV^{2+} NaCl and variable concentrations of sodium cholate.

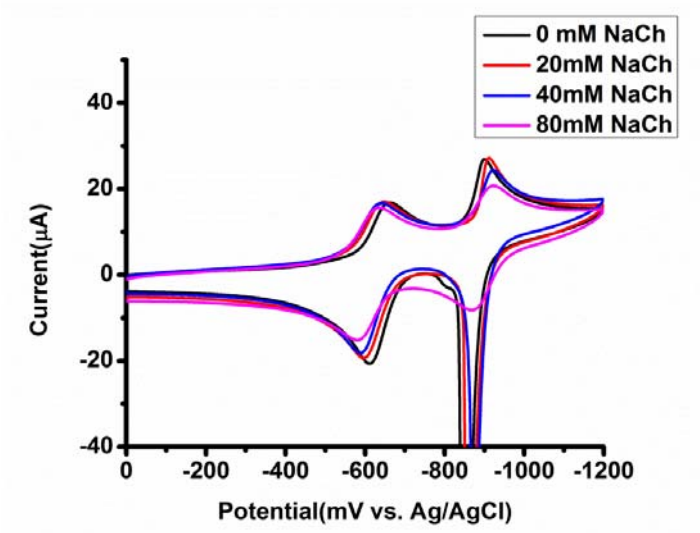

Figure 2-7. Cyclic voltammetric behavior on glassy carbon (0.071 cm^2) of 1.0 mM PV^{2+} in 0.2 M NaCl containing variable concentrations of sodium cholate. Scan rate: 0.1 V s^{-1}.

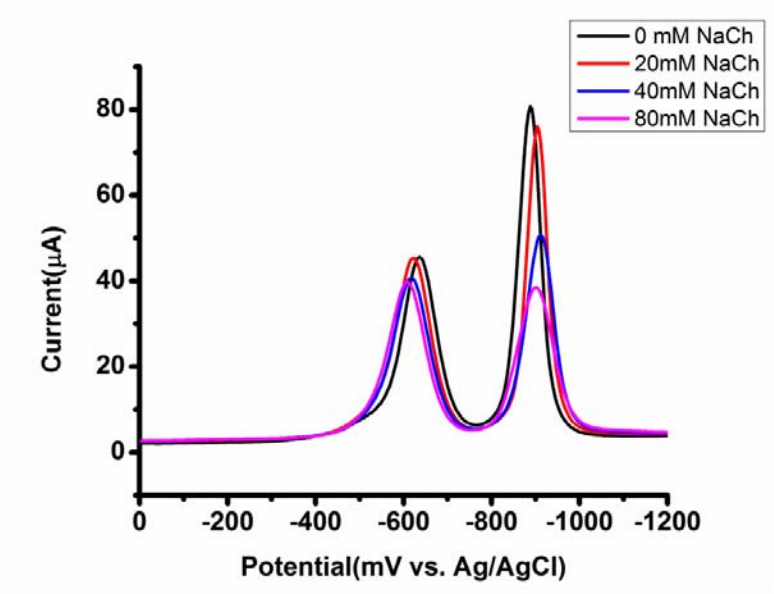

Figure 2-8. Square wave voltammetric behavior of 1.0 mM PV^{2+} in 0.2 M NaCl and variable concentrations of sodium cholate.

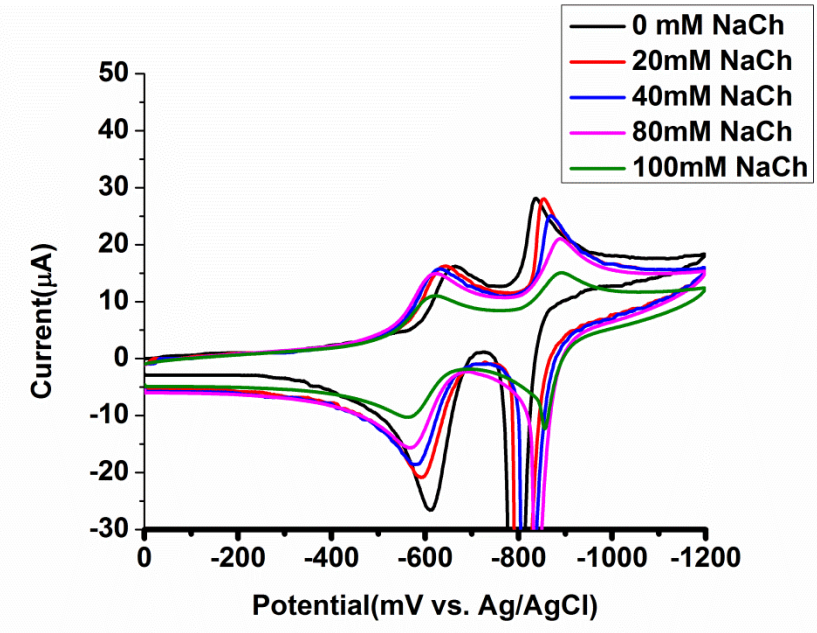

Figure 2-9. Cyclic voltammetric behavior on glassy carbon (0.071 cm^2) of 1.0 mM BV^{2+} in 0.2 M NaCl containing variable concentrations of sodium cholate. Scan rate: 0.1 V s^{-1}.

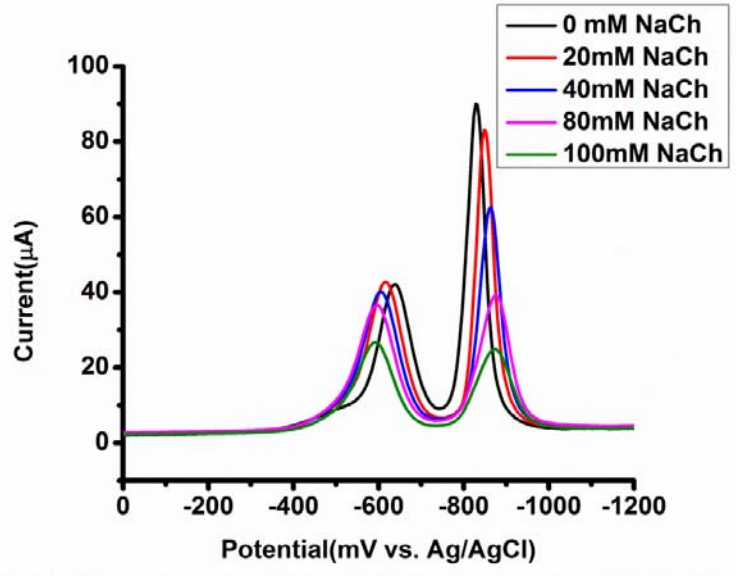

Figure 2-10. Square wave voltammetric behavior of 1.0 mM BV^{2+} in 0.2 M NaCl and variable concentrations of sodium cholate.

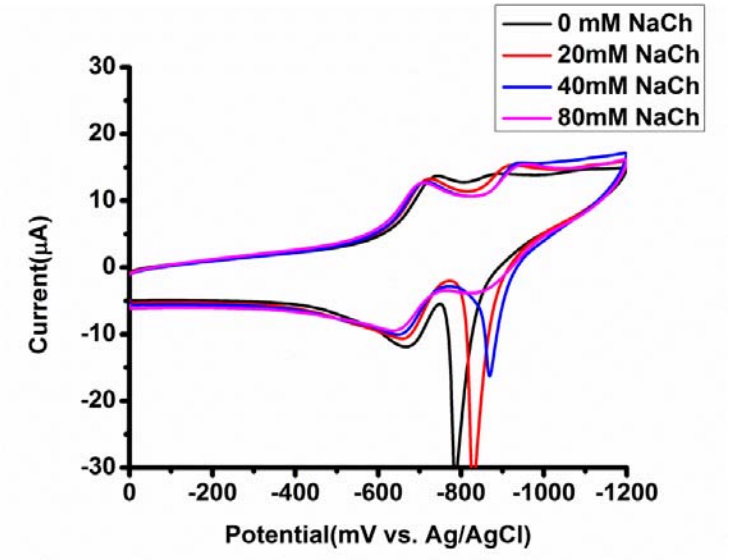

Figure 2-11. Cyclic voltammetric behavior on glassy carbon (0.071 cm^2) of 1.0 mM HEV^{2+} in 0.2 M NaCl containing variable concentrations of sodium cholate. Scan rate: 0.1 V s^{-1}.

We collected all potentials for the first viologen reduction process ($V^{2+} + e^- \leftrightarrow V^{-\bullet}$) and plotted them against the sodium cholate concentration in the medium.

The potential data obtained from SWV are given in Figure 2-12. Very similar data were recorded using CV (Figure 2-13).

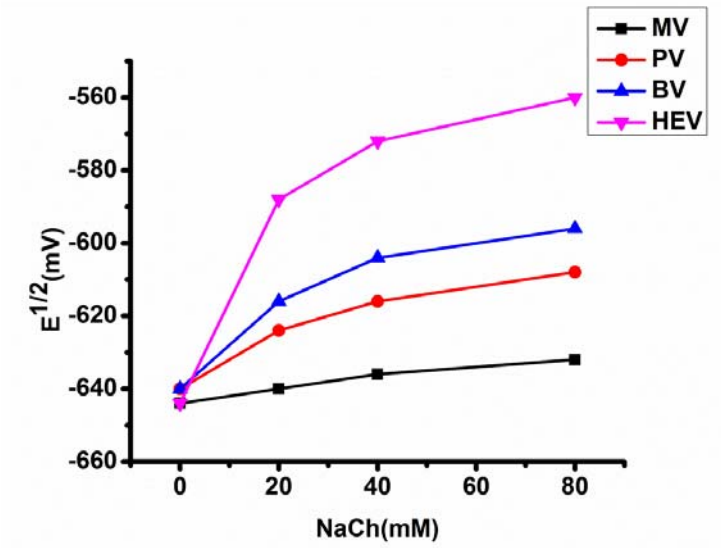

Figure 2-12. Half-wave potentials measured in SWV experiments for the first one-electron reduction of the viologen probes in 0.2 M NaCl and variable concentrations of sodium cholate.

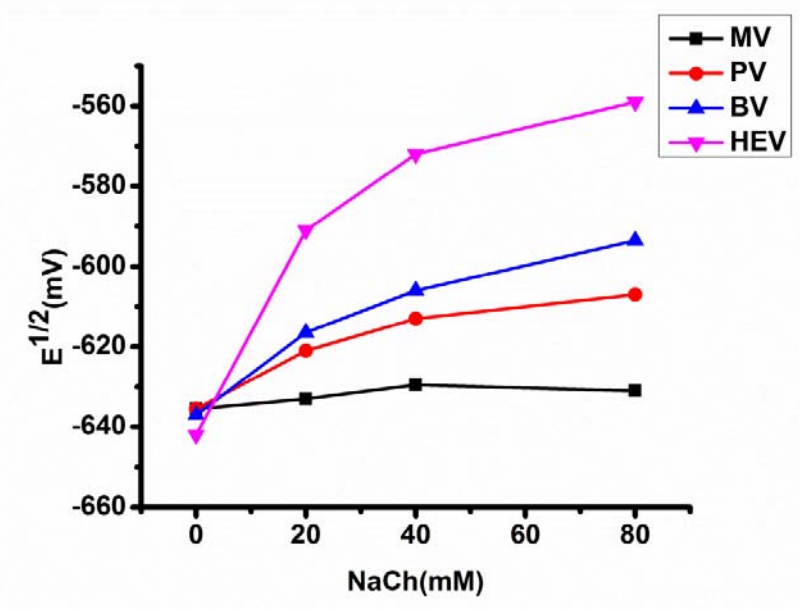

Figure 2-13. Half-wave potentials measured in CV experiments for the first one-electron reduction of the viologen probes in 0.2 M NaCl and variable concentrations of sodium cholate.

Clearly, the presence of the cholate tends to shift the half-wave potential in the anodic direction, indicating that the $V^{+\bullet}$ form is more stabilized by the cholate aggregates than the V^{2+} form for all of the viologens surveyed here. In other words, the first reduction process is thermodynamically favored by the presence of cholate. Similar potential shifts were recorded previously for the first reduction of methylviologen in the presence of sodium dodecyl sulfate,[28] a widely used anionic surfactant that forms conventional micelles. The magnitude of the potential shifts at any cholate concentration increases in going from methylviologen to propylviologen to butylviologen and reaches its maximum with heptyl-ethylviologen. If we accept that the hydrophobic character of the viologen probe increases with the total number of carbon atoms on the two N substituents, then it is clear that the observed potential shifts increase with the hydrophobic character of the viologen probe. While BV^{2+} and HEV^{2+} are the two guests with the most pronounced hydrophobic character, the potential shifts are substantially larger with the latter, suggesting that the longer aliphatic chain (heptyl in HEV^{2+}) has a predominant effect on the interaction with the cholate aggregates. In other words, one heptyl chain is more effective than two butyl chains at promoting interactions with the cholate micelles.

Another interesting trend that is visible in the data relates to the effect of cholate on the observed current levels of the voltammetric waves. While increasing the cholate concentration has little effect on the currents observed with MV^{2+}, diminishing currents across the entire potential range are visible with HEV^{2+} in the presence of sodium cholate. These two viologen probes represent

the extremes in the spectrum of behavior observed, with the intermediate effects on the current levels measured with the remaining viologens.

Overall, our voltammetric data reveal that the more hydrophobic viologen probes interact more strongly with the cholate micelles. Furthermore, the viologen cation radical form ($V^{+\bullet}$) is more strongly stabilized by the cholate micelles than the dicationic form (V^{2+}). In clear contrast to this, the data with the more hydrophobic viologens show the opposite trend for the second reduction process, where $V^{+\bullet}$ is differentially stabilized relative to the neutral form (V). Therefore, we must conclude that the cholate aggregates engage the cation radical species in the preference to the more highly charged, dicationic form and in preference to the neutral and most hydrophobic form. The $V^{+\bullet}$ form offers the best balance between charge and hydrophobic character for interaction with the cavities formed by the anionic cholate micelles.

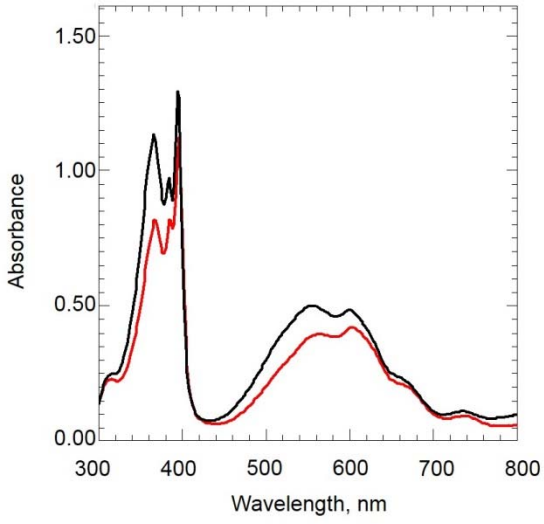

Figure 2-14. Electronic absorption spectra after exhaustive one–electron reduction of a solution containing 1.0 mM MV^{2+} and 200 mM NaCl in the absence (black) and in the presence (red) of 80 mM NaCh.

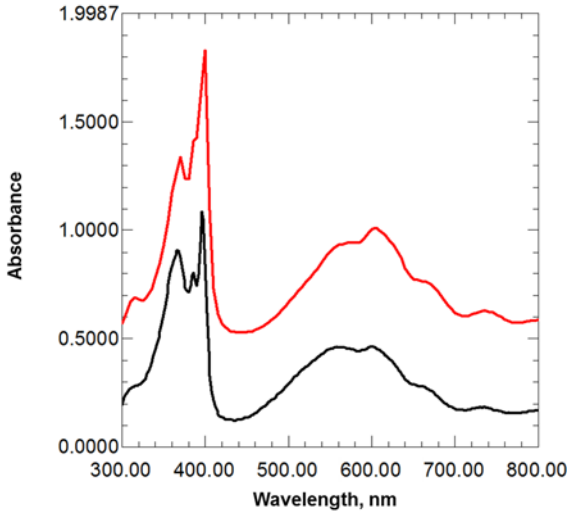

Figure 2-15. Electronic absorption spectra after exhaustive one–electron reduction of a solution containing 1.0 mM PV^{2+} and 200 mM NaCl in the absence (black) and in the presence (red) of 80 mM NaCh.

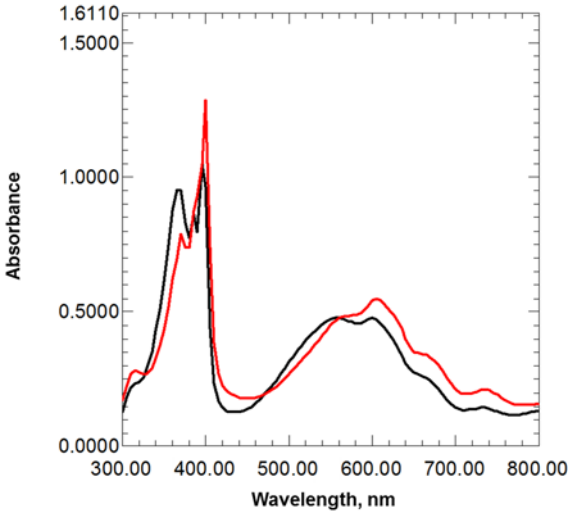

Figure 2-16. Electronic absorption spectra after exhaustive one–electron reduction of a solution containing 1.0 mM BV^{2+} and 200 mM NaCl in the absence (black) and in the presence (red) of 80 mM NaCh.

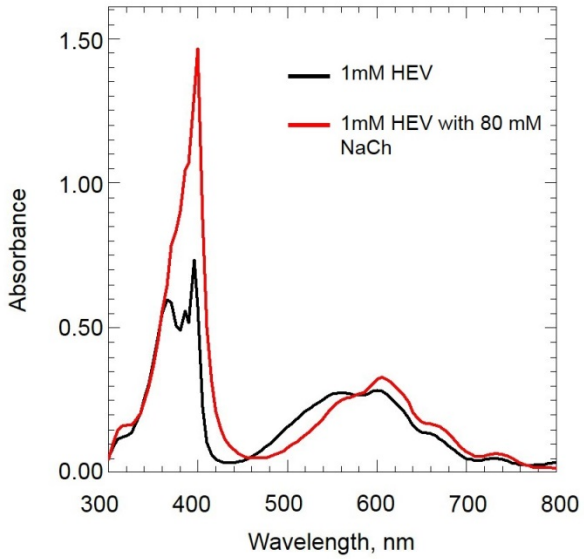

Figure 2-17. Electronic absorption spectra after exhaustive one–electron reduction of a solution containing 1.0 mM HEV^{2+} and 200 mM NaCl in the absence (black) and in the presence (red) of 80 mM NaCh.

It is important to point out that the preferential stabilization of the viologen cation radical form by the cholate micelles is not due to enhanced dimerization. In fact, the cholate aggregates tend to depress the formation of cation radical dimers. This was examined in some detail through spectroelectrochemical experiments. We found that the extent of cation radical dimerization in the presence of cholate assemblies decreases with the strength of the cholate-$V^{+\bullet}$ interaction. The spectra shown in Figure 2-17 and Figure 2-20 clearly show the spectroscopic data for $MV^{+\bullet}$ and $HEV^{+\bullet}$, revealing that the dimerization of the latter is almost completely suppressed by the cholate micelles.

The addition of water-soluble CB7 host to a sodium cholate aqueous solution containing one of the viologen probes opens a number of interesting

questions. For instance, would the viologen be included by CB7, as is the case in the absence of cholate aggregates? If so, would the cholate aggregates compete effectively with CB7 and depress the effective binding affinity for the viologen-CB7 complexes? To address these questions, we first verified by NMR spectroscopy the absence of interactions between the cholate anions and the CB7 host. As expected the ^{1}H NMR spectrum of a 1.0 mM cholate solution in D_2O undergoes only minor changes after the addition of 1.0 mM CB7 (Figure 2-18). The lack of substantial binding interactions is easily rationalized by the considerable cross section of cholate, which prevents its partial or full inclusion in the cavity of CB7.

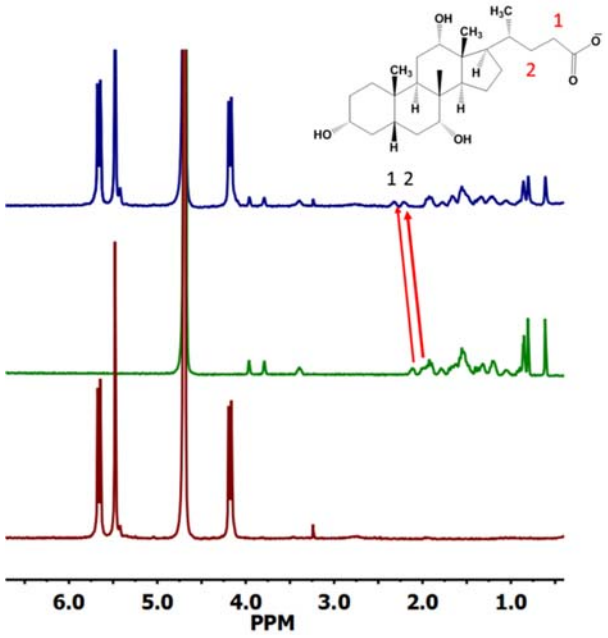

Figure 2-18. ^{1}H NMR spectra (500 MHz, 0.2 M NaCl/D_2O) of (bottom) 1.0 mM CB7, (middle) 1.0 mM NaCh and (top) 1.0 mM NaCh + 1.0 mM CB7.

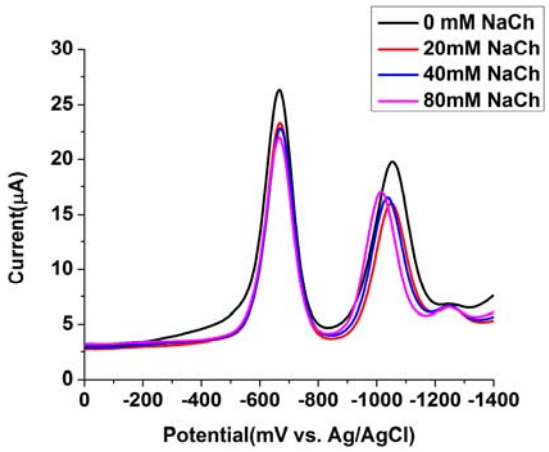

Figure 2-19. Square wave voltammetric behavior of 1.0 mM MV^{2+} in the presence of 1.0 equivalent CB7 in 0.2 M NaCl and variable concentrations of sodium cholate.

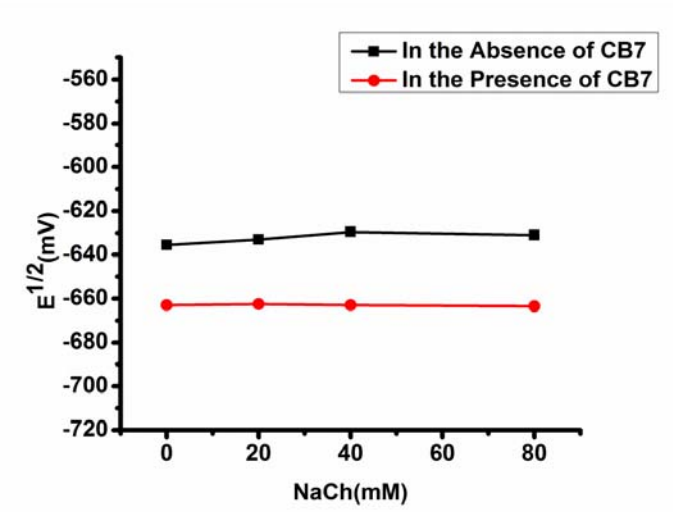

Figure 2-20. Half-wave potentials for the first reduction of methyl viologen (1.0 mM) in the absence and in the presence of 1.0 equiv of CB7 as a function of sodium cholate concentration. The experiments were run in 0.2 M NaCl supporting electrolyte.

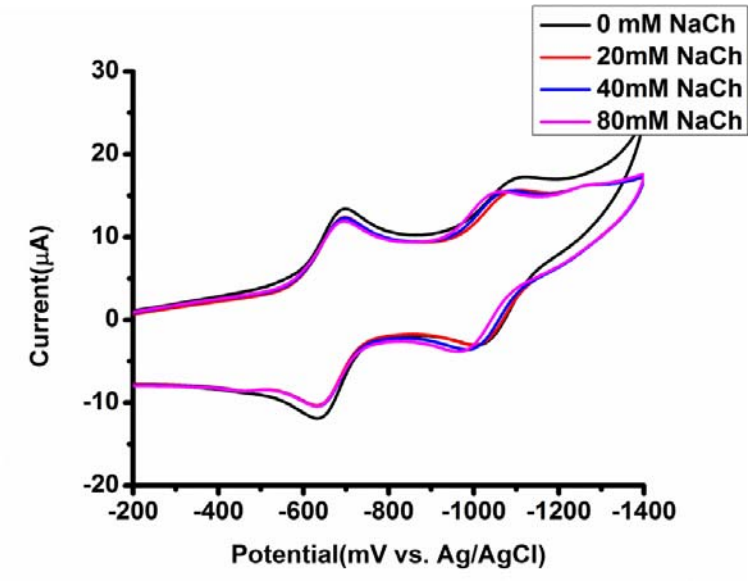

Figure 2-21. Cyclic voltammetric behavior on glassy carbon (0.071 cm^2) of 1.0 mM MV^{2+} in the presence of 1.0 equivalent CB7 in 0.2 M NaCl containing variable concentrations of sodium cholate. Scan rate: 0.1 V s^{-1}.

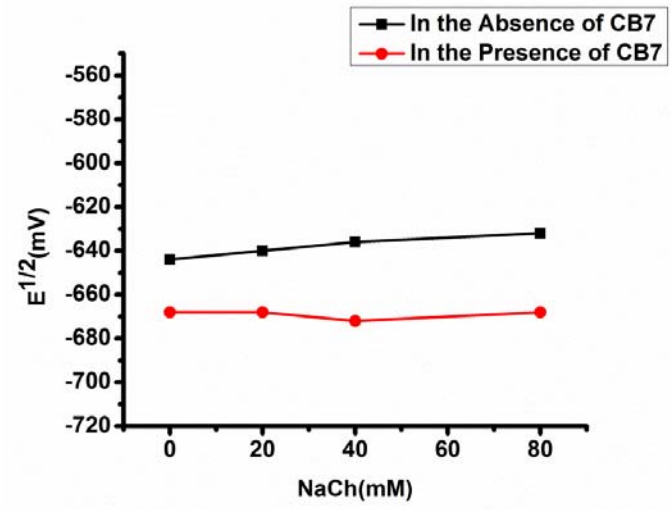

Figure 2-22. Half-wave potentials measured in CV for the first reduction of methylviologen (1.0 mM) in the absence and in the presence of 1.0 equiv CB7 as a function of sodium cholate concentration. The experiments were run in 0.2 M NaCl supporting electrolyte.

Upon addition of 1.0 equiv of CB7 to a solution containing 1.0 mM MV^{2+} in 0.2 M NaCl, the corresponding inclusion complex, CB7•MV^{2+}, is formed and the $E_{1/2}$ value for the first reduction of the viologen guest shifts ca. -25 mV compared to the value measured in the absence of CB7. This is in excellent agreement with previous reports from our group and means that one-electron reduction slightly weakens the binding affinity of the inclusion complex. More accurately, the stability of the CB7•$MV^{+\bullet}$complex is just 2.4 kJ mol^{-1} lower that of the CB7•MV^{2+} complex. Our previous work has shown that both the MV^{2+} and $MV^{+\bullet}$ species remain bound inside the CB7 cavity. Figure 2-20 shows that the half-wave potential for the first reduction of MV^{2+} in the presence of 1. 0 equiv of CB7 remains unchanged as the sodium cholate concentration increases from 0 to 80 mM, while in the host's absence the potential values exhibit modest shifts as observed before (Figure 2-4). Very similar data were recorded by using CV (Figure 2-21 and Figure 2-22). This finding suggests strongly that the formation of the CB7•MV^{2+} complex is not affected by the cholate micelles. In other words, the formation of the complex with CB7 prevents interactions with the micelles.

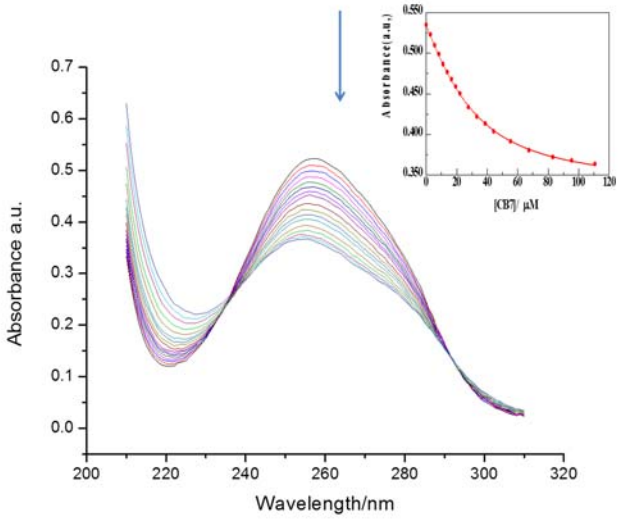

Figure 2-23. Electronic absorption spectrum of 25.6 uM MV•Cl_2 in 280.0 mM NaCl/H_2O in the presence of increasing concentrations (0.0-102.3 uM, in the direction of the arrow) of CB7. Insert shows the best fit of the experimental data to the 1:1 binding model. (CB7•MV^{2+}: λ_{max} = 253 nm, ε = 1.1 x 10^4 $M^{-1}cm^{-1}$ at 25 °C)

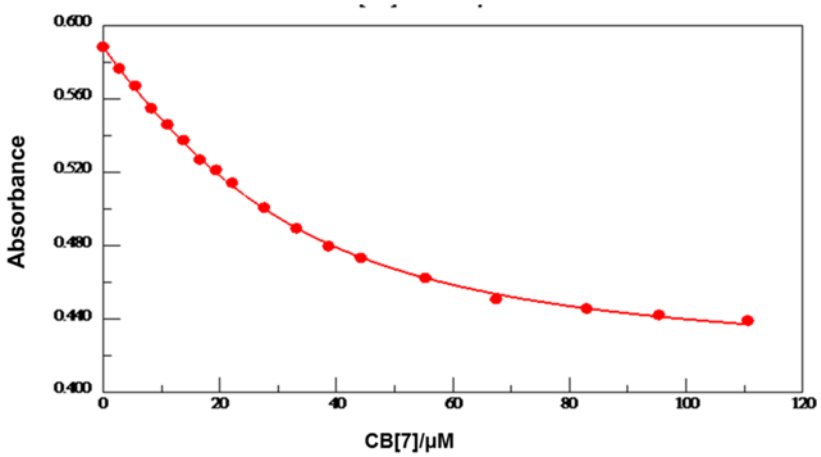

Figure 2-24. Absorbance versus CB7 concentration of aqueous solutions containing 25.6 μM methylviologen at 200.0 mM NaCl and 80.0 mM NaCh. The continuous lines show the best fit of the experimental data to 1:1 binding isotherms.

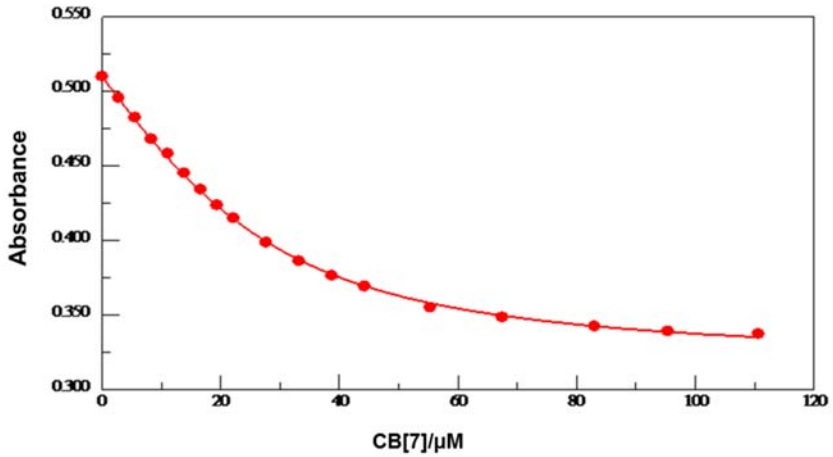

Figure 2-25. Absorbance versus CB7 concentration of aqueous solutions containing 25.6 μM methylviologen at 240.0 mM NaCl. The continuous lines show the best fit of the experimental data to 1:1 binding isotherms.

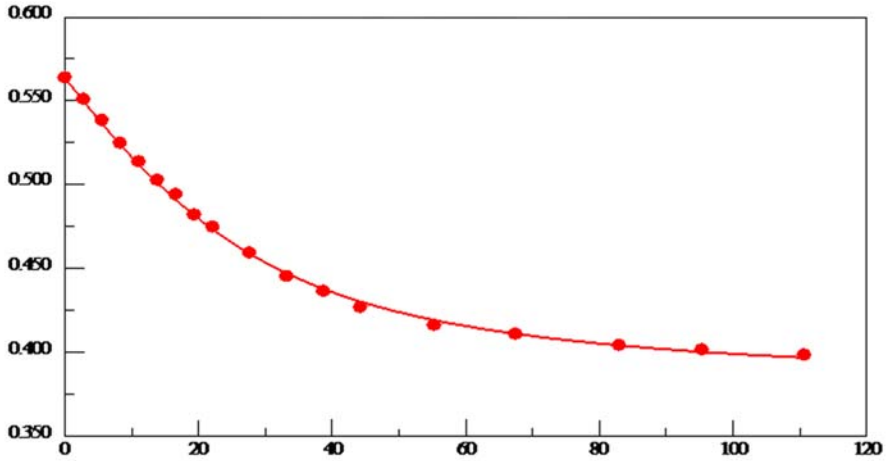

Figure 2-26. Absorbance versus CB7 concentration of aqueous solutions containing 25.6 μM methylviologen at 200.0 mM NaCl and 40.0 mM NaCh. The continuous lines show the best fit of the experimental data to 1:1 binding isotherms.

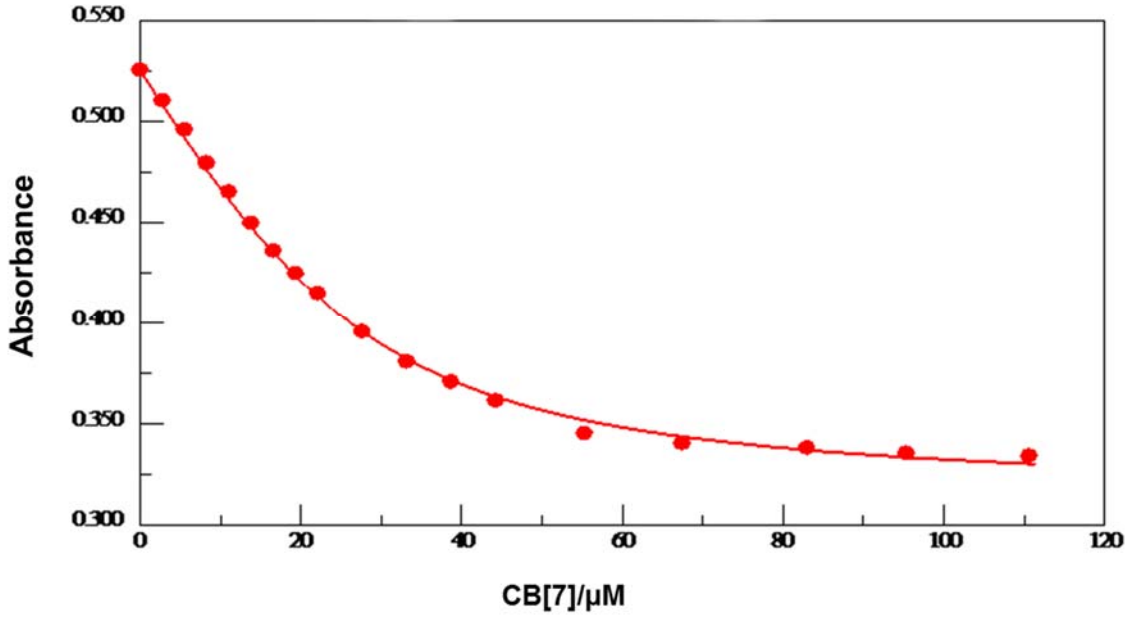

Figure 2-27. Absorbance versus CB7 concentration of aqueous solutions containing 25.6 μM methylviologen at 200.0 mM NaCl. The continuous lines show the best fit of the experimental data to 1:1 binding isotherms.

To confirm this result, we measured the apparent equilibrium association constant (K) for the CB7•MV^{2+} complex in 0.2 M NaCl solution containing variable concentrations (0, 40, and 80 mM) of sodium cholate. The K values were determined as described before, using the diminishing effect of CB7 on the absorbance of the UV absorption band of the viologen at 253 nm. By fitting the absorbance versus CB7 concentration data to a 1:1 binding isotherm (Figure 2-24, Figure 2-25, Figure 2-26 and Figure 2-27), we obtained the values given in Table 2-1.

Table 2-1. Equilibrium Association Constants (*K*) for MV^{2+} Complexation by CB7 Measured in Aqueous Media of Variable Composition at 25 ºC.

entry	[NaCl]/mM	[NaCh]/mM	K/M^{-1a}
1	200	0	1.3×10^5
2	200	40	9.7×10^4
3	240	0	1.0×10^5
4	200	80	6.7×10^4
5	280	0	6.4×10^4

[a] The K values were determined with an error margin of ± 5%

Clearly, the addition of sodium cholate to the solution depresses the measured K values, While this could be taken initially as a sign that the cholate micelles are effectively competing with CB7 for methylviologen, a more careful analysis of the data is necessary because it is well know that variable concentrations of alkali metal ions do affect the K values between MV^{2+} and CB7 in aqueous solution. In fact, our group has shown that increasing concentrations of NaCl decrease the observed *K* values.[29] Therefore, we performed experiments in which the added concentrations of sodium cholate were replaced by identical concentrations of added NaCl. By comparing the measured K value in a medium containing 200 mM NaCl and 40 mM sodium cholate with that observed in 240 mM NaCl (Figure 2-25), we can truly assess the effect of the cholate aggregates and separate it from the effect caused by the sodium ions. The measured K values are basically within experimental error in these two media (entries 2 and 3 in Table 2-1) thus suggesting that the cholate micelles do not compete effectively with the CB7 receptors at hosting the MV^{2+} ions. Similar K values were also

measured in media containing either 200 mM NaCl and 80 mM sodium cholate or 280 mM NaCl (Figure 2-23) (entries 4 and 5 in Table 2-1), leading to the same conclusion; that is, the observed reductions in the K values from that measured in 200 mM NaCl solution (entry 1) are due to the increased concentrations of sodium ions, which compete for CB7 with the MV^{2+} guest by binding to the rims of carbonyl oxygens that line the cavity portals of the host.

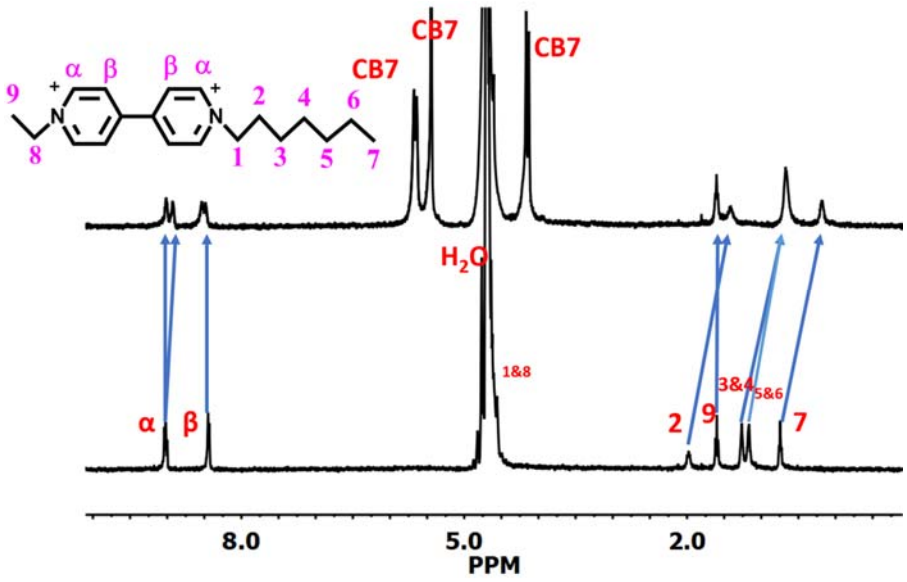

Figure 2-28. ^{1}H NMR spectra (500 MHz, 0.2 M NaCl/D_2O) of 1.0 mM HEV^{2+} (bottom) in the absence and (top) in the presence of 1.0 equiv of CB7.

NMR spectroscopic experiments can be used to pinpoint the main molecular region of a guest that is engulfed by the CB7 cavity when the corresponding inclusion complex is formed. In the case of MV^{2+}, we have shown that CB7 is centered on the 4,4'-bipyridinium nucleus,[20a] as anticipated in order to optimize the ion-dipole interactions between each of the positively charged nitrogens and the carbonyl rims on the portals. However, the main CB7 binding

site of more hydrophobic viologen derivatives could be different. For instance, we have shown that CB7 binds BV^{2+} by including one of the butyl chains.[30] This is the case with aliphatic chains of four carbon atoms or longer. Therefore, we carried out NMR spectroscopic experiments to determine the main CB7 binding site on the inclusion complex with the HEV^{2+} guest. The ^{1}HNMR spectra in Figure 2-28 clearly show that the addition of 1.0 equiv of CB7 to a D_2O solution containing 1.0 mM HEV^{2+} results in measurable upfield shifts for all of the signals corresponding to the protons on the heptyl chain while the methyl protons on the other end of the molecule are unchanged. The modest changes in the chemical shifts of the pyridinium proton resonances are consistent with our previous reports for guests in which the central viologen nucleus remains unbound by CB7. All of these data clearly demonstrate that the main CB7 binding site in HEV^{2+} is the heptyl chain.

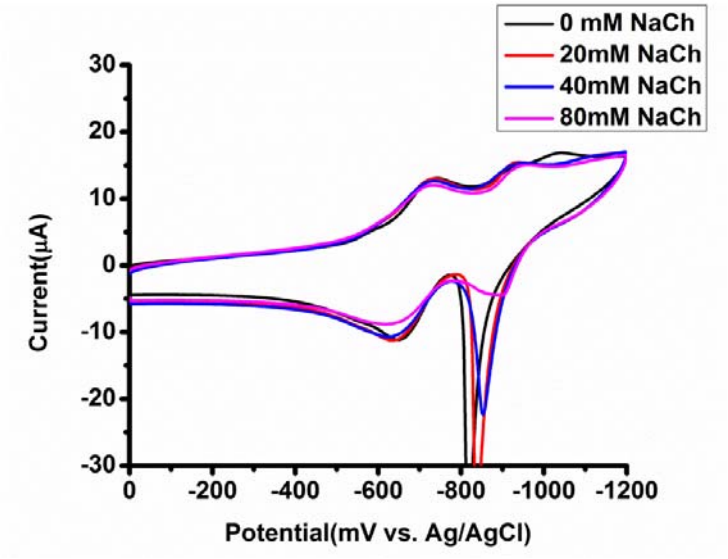

Figure 2-29. Cyclic voltammetric behavior on glassy carbon (0.071 cm^2) of 1.0 mM BV^{2+} in the presence of 1.0 equivalent CB7 in 0.2 M NaCl containing variable concentrations of sodium cholate. Scan rate: 0.1 V s^{-1}.

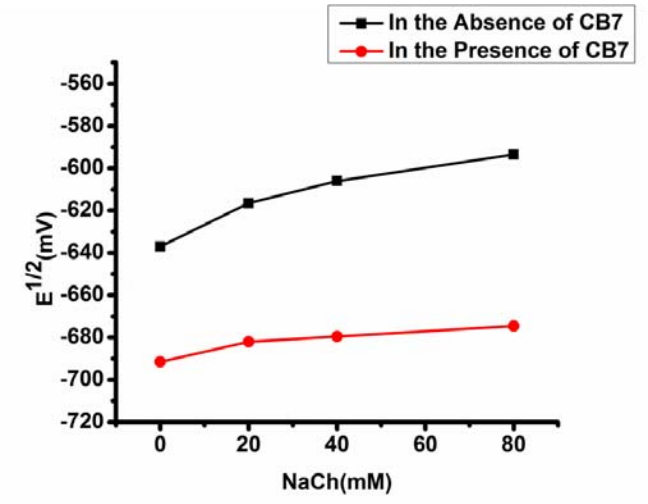

Figure 2-30. Half-wave potentials measured in CV for the first reduction of BV^{2+} (1.0 mM) in the absence and in the presence of 1.0 equiv CB7 as a function of sodium cholate concentration. The experiments were run in 0.2 M NaCl supporting electrolyte.

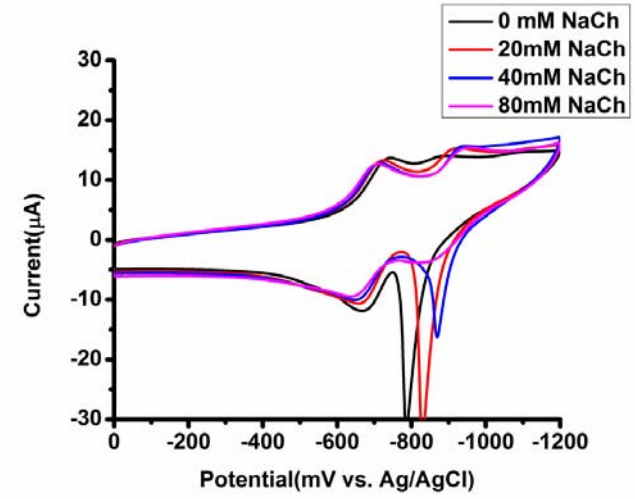

Figure 2-31. Cyclic voltammetric behavior on glassy carbon (0.071 cm^2) of 1.0 mM HEV^{2+} in the presence of 1.0 equivalent CB7 in 0.2 M NaCl containing variable concentrations of sodium cholate. Scan rate: 0.1 V s^{-1}.

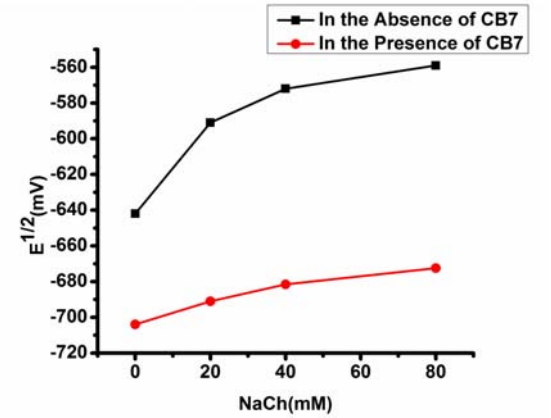

Figure 2-32. Half-wave potentials for the first reduction of HEV^{2+} (1.0 mM) in the absence and in the presence of 1.0 equiv of CB7 as a function of the sodium cholate concentration. The experiments were run in 0.2 mM NaCl supporting electrolyte.

What is the effect of CB7 complexation of HEV^{2+} on the interaction of this viologen guest with the cholate aggregates? Figure 2-32 shows that the half-wave potential shifts caused by the addition of sodium cholate on the first reduction process are substantially diminished by the presence of 1.0 equiv of CB7. In fact, the cholate-induce potential shifts measured with the CB7•HEV^{2+} complex are intermediate between those measured with the CB7•MV^{2+} and CB7•PV^{2+} complexes (Figure 2-12). This result is consistent with the viologen guest interacting with the cholate aggregates through its ethyl end, while the heptyl end remains included by the CB7 host.

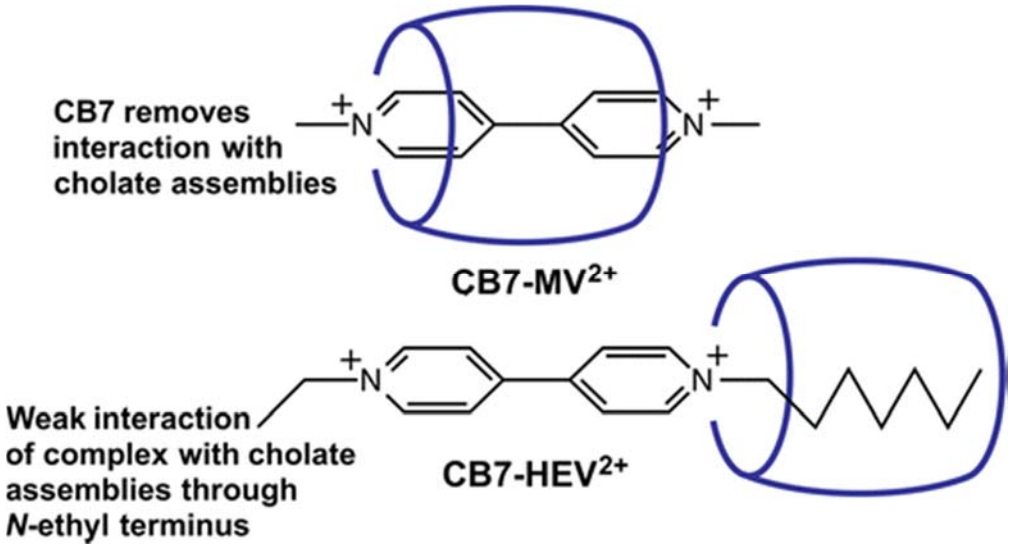

Scheme 2-1. Contrast between CB7 binding of MV^{2+} and HEV^{2+} and its effect on the interaction with the cholate assemblies.

2.3 Discussion

The voltammetric data presented here are consistent with a variable degree of interaction between the surveyed viologen probes and cholate aggregates formed in aqueous solution. The strength of the viologen-cholate aggregate interactions increases with the hydrophobic character of the viologen, following the order MV^{2+}<PV^{2+}<BV^{2+}<HEV^{2+}. For each viologen probe, the cation radical ($V^{+\bullet}$) is the oxidation state that undergoes preferential stabilization by the cholate aggregates, leading to a cholate-induced increase in the comproportionation equilibrium constant ($V^{2+} + V \leftrightarrow 2V^{+\bullet}$). The preference of the anionic cholate micelles for the cation radical probably stems from an ideal balance between charge and hydrophobic character in the intermediate oxidation state. The fully oxidized viologen dications (V^{2+}) are less hydrophobic, and the

fully reduced, neutral species (V) lack positive charge to provide electrostatic assistance in the interaction with the anionic cholate assemblies. Increasing the concentration of cholate lead to more pronounced voltammetric effects, including the observed anodic shift in the $V^{2+}/V^{+\bullet}$ half-wave potential, and the decreased current levels. Although no clear break points are visible in our experiments when these parameters plotted against cholate concentration, the observed results are in general agreement with the postulated growth of cholate assemblies and the development of better-defined hydrophobic cavities within them as the sodium cholate concentration increases.[26] In general terms, sodium cholate has similar effects on the electrochemical properties of MV^{2+} as traditional, micelle-forming anionic surfactants, such as sodium dodecyl sulfate[28] and sodium decyl sulfate.[31]

A central motivation to carry out this work was to assess how effectively the cholate assemblies can compete with the CB7 receptors at hosting the viologen probes. Our results clearly indicate that the CB7 inclusion complexes are very stable and the cholate assemblies simply cannot compete effectively against CB7. In this regard, it must be noted that CB7 is a rigid molecular receptor, with a well-defined cavity, which can effectively interact with the viologen probes. In contrast, the cholate micelles are dynamic assemblies in which cavities are formed and disrupted along with the continuous assembly and disassembly of the cholate aggregates. The static hydrophobic cavity supplied by each CB7 receptor is thus much more stable in time than any of the dynamic cavities afforded by the cholate assemblies.

The binding interactions between viologen probes and the CB7 host depend on the structure of the viologen probe (Scheme 2-1). In our experiments, we detected two clear extremes of behavior. MV^{2+} forms a highly symmetric inclusion complex with CB7 in which the host encircles the bipyridinium group, with the two terminal methyl groups protruding out of the host. This leads to the complete sequestration of MV^{2+} and the disruption of its rather weak interaction with the cholate aggregates. Alternatively, HEV^{2+} forms an asymmetric inclusion complex in which the heptyl chain is included by CB7. The other end of the viologen (N-ethyl) is still free to interact with the cholate micelles. However, the presence of CB7 has an overall weakening effect on the interactions between the cholate assemblies and the HEV^{2+} probe.

In conclusion, the experimental results reported here indicate that all of the surveyed viologen probes interact with cholate assemblies and the oxidation state that is preferentially stabilized is the partially reduced, cation radical. However, the CB7 host forms very stable inclusion complexes with all of the viologen probes, leading to a substantial decrease in the interactions between the viologens and the cholate aggregates. Because many CB7 complexes are as stable or more stable than the CB7-viologen complexes, our findings suggest that cholate-containing aqueous solutions afford a relatively structured medium in which to investigate the binding interactions between various guests and CB7.

Chapter 3 :The Cathodic Voltammetric Behaviour of Pillar[5]quinone in Nonaqueous Media. Symmetry Effects on the Electron Uptake Sequence

3.1 Overview

The pillar[n]arenes constitute an interesting family of synthetic supramolecular receptors, which have attracted considerable attention in the last decade.[32] Their ease of functionalization[33] makes them particularly attractive compared to other supramolecular host families. We are specifically interested in the preparation and electrochemical properties of pillar[n]quinones.[34] Currently, pillar[5]quinone[35] (P5Q, see structure Figure 3-1) is the only known member of this series of multi-quinone macrocyclic hosts, although various pillar[5]arenes have also been reported in which just one or two aromatic rings are oxidized to quinones.[36] A number or structurally related calix[n]quinones are known and their electrochemical properties have been investigated in nonaqueous solution.[37] However, calix[n]arenes are conformationally more complicated than pillar[n]arenes, and, as a result, the electrochemical behavior of calix[n]quinones is typically rather complex, reflecting the equilibration among multiple conformers. Our expectation was that P5Q might exhibit simpler voltammetric behavior that could be understood in terms of straightforward pentagonal symmetry considerations.

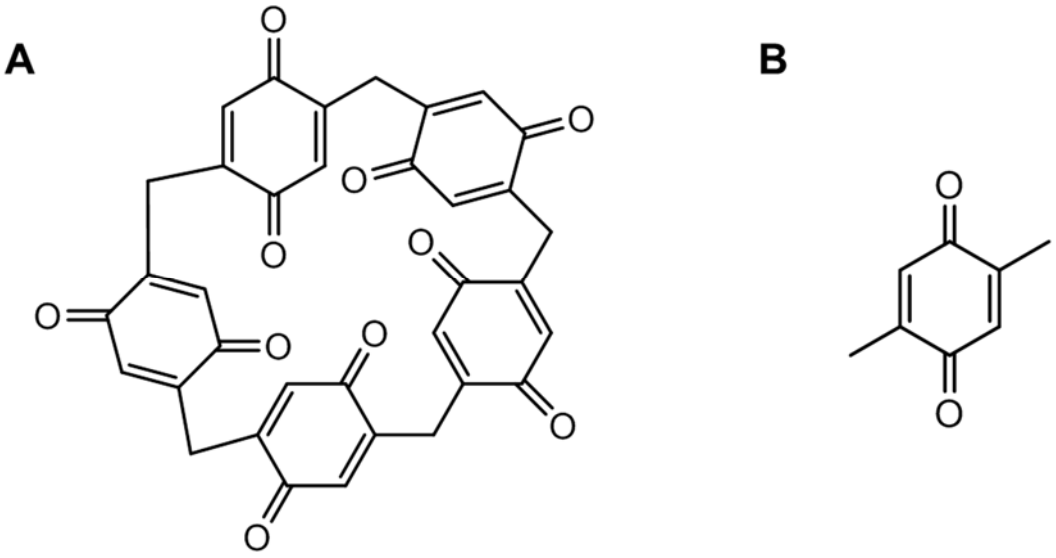

Figure 3-1. (A) Structure of pillar[5]quinone (P5Q); (B) structure of the model quinone compound, *p*-xyloquinone(XQ).

P5Q was recently reported as an active constituent of the cathode in all-solid-state lithium organic batteries with composite polymer electrolytes.[38] In this work, we focus on the nonaqueous electrochemical behavior of P5Q, which reflects in a unique way the symmetry of this macrocyclic compound.

3.2 Results

3.2.1 Studies of the electron uptake sequence

The voltammetric behavior of simple quinones in nonaqueous solvents is very well established. Under aprotic conditions, quinones undergo two consecutive, reversible one-electron reductions. The first reduction (Equation 3-1)

leads to the formation of the corresponding radical anion, which, in turn, can be further reduced to a dianion (Equation 3-2) at more negative potentials.

$$Q + e^- \leftrightarrow Q^{-\cdot} \qquad \text{Equation 3-1}$$

$$Q^{-\cdot} + e^- \leftrightarrow Q^{2-} \qquad \text{Equation 3-2}$$

Since P5Q contains five identical quinones in its macrocyclic structure, we selected *p*-xyloquinone (XQ, see Figure 3-1) as the most suitable model compound. Using square wave voltammetry (SWV), its cathodic electrochemical behavior in dichloromethane solution shows the two anticipated cathodic waves (Figure 3-2) at half-wave potentials of -0.67 and -1.19 V vs Ag/AgCl. It must be noted that the second cathodic wave is broader than the first. This is not particularly surprising, as Evans has reported on the differences between the two consecutive reduction waves observed with simple quinones.[39] The second reduction wave is typically less developed or broader than the first wave, partially due to the larger sensitivity of the dianion to residual protic species or to the slower rates of heterogeneous electron transfer for the second one-electron reduction process. However, in normal pulse voltammetry (NPV) conditions, the two consecutive waves exhibit similar heights (Figure 3-2), as expected for consecutive one-electron reductions.

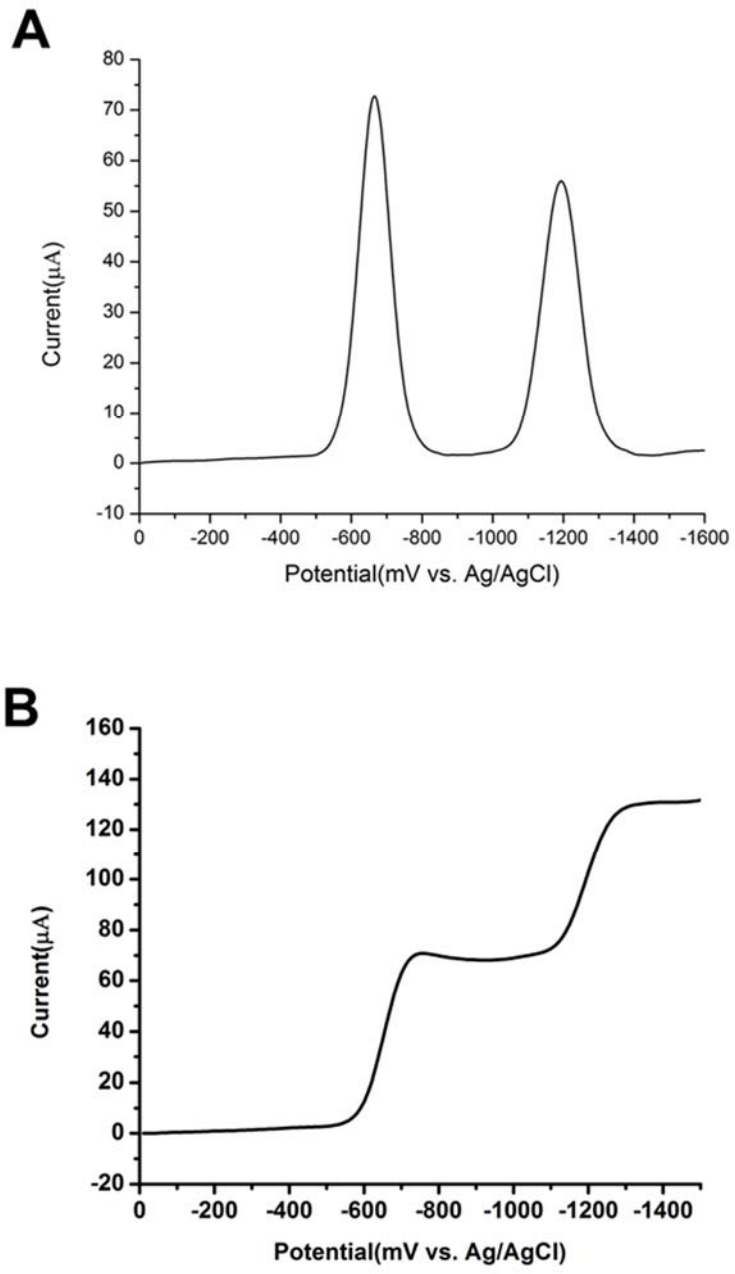

Figure 3-2. Cathodic voltammetric behavior on glassy carbon (0.07 cm^2) of 1.0 mM XQ in CH_2Cl_2 solution also containing 0.1 M $TBAPF_6$ as the supporting electrolyte. (A) Square wave voltammetry. (B) Normal Pulse Voltammetry.

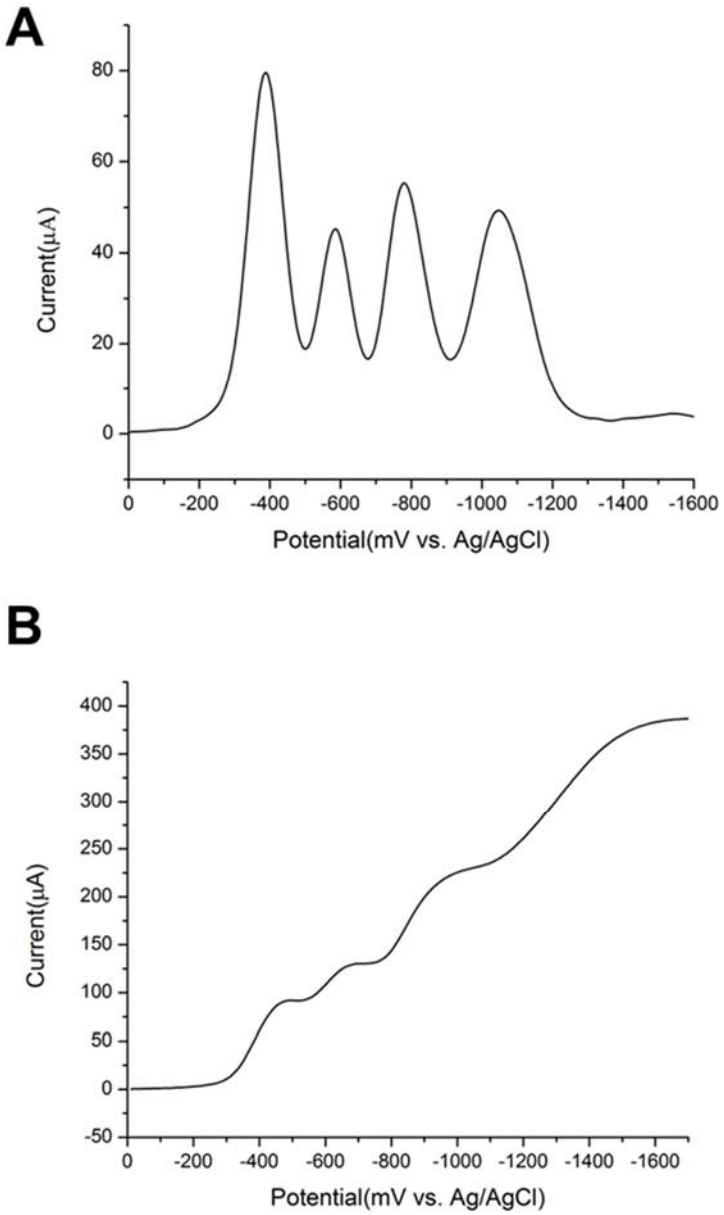

Figure 3-3. Cathodic voltammetric behavior on glassy carbon (0.07 cm^2) of 1.0 mM P5Q in CH_2Cl_2 solution also containing 0.1 M $TBAPF_6$ as the supporting electrolyte. (A) Square wave voltammetry. (B) Normal Pulse Voltammetry.

The voltammetric behavior of P5Q is depicted in Figure 3-3. Assuming a poor level of communication between adjacent quinone groups in the macrocycle, we would like to anticipate the observation of two five-electron waves: the first

one corresponding to the uptake of one electron by each of the quinone units (Equation 3-3), and the second one corresponding to the uptake of a second electron per quinone to yield a macrocyclic compound with 10 negative charges (Equation 3-4). However, the experimental data clearly differ from these expectations, as show in Figure 3-3. Four peaks with variable intensities are observed in the square wave voltammogram; similarly, four different waves are observed in the normal pulse voltammogram. In order to assign each of these voltammetric features to reduction events associated with the uptake of well-defined numbers of electrons, we turned to a methodology that combines voltammetric data with diffusion coefficient measurements obtained with NMR spectroscopic techniques. We have previously reported on the combined use of these techniques to determine the number of electrons involved in the oxidation of dendrimer-like species containing multiple ferrocene centers.[40]

$$P5Q + 5e^- \leftrightarrow P5Q^{5-} \qquad \text{Equation 3-3}$$

$$P5Q^{5-} + 5e^- \leftrightarrow P5Q^{10-} \qquad \text{Equation 3-4}$$

$$i = \frac{nFAD_0^{1/2}C_0^*}{\pi^{1/2}(\tau - \tau')^{1/2}} \qquad \text{Equation 3-5}$$

$$\frac{(i_d)_{P5Q}}{(n_{P5Q})\sqrt{D_{P5Q}}} = \frac{(i_d)_{XQ}}{(n_{XQ})\sqrt{D_{XQ}}} \qquad \text{Equation 3-6}$$

In NPV, the limiting current (i_d) reached after each wave under conditions diffusion control is given by Equation 3-4, where *n* is the number of electrons involved, *F* is Faraday's constant, *A* is the projected area of the electrode, D_0 represents the diffusion coefficient, C_0^* is the bulk concentration of electroactive

species, and τ and τ' are the times associated with current measurements in the NPV experiment. If we use the same electrode, concentration of electroactive species and NPV time parameters for two different reducible compounds, such as XQ and P5Q, it is clear that Equation 3-6 exists. Therefore, if we independently measure the diffusion coefficients of P5Q and XQ (D_{P5Q} and D_{XQ}) using NMR spectroscopic techniques, the NPV limiting current for the first reduction of XQ, which is known to involve the uptake of a single electron (n_{XQ}=1), and the NPV limiting current for any reduction wave of P5Q, we can determine the number of electrons (n_{P5Q}) involved in the latter reduction process using Equation 3-6.

The diffusion coefficient values were measured using the Pulse Gradient Stimulated Echo (PGSE) NMR spectroscopic method, which we have used often in previous work. We obtained values of 4.01×10^{-5} and 7.98×10^{-5} cm^2/s for P5Q and XQ, respectively in CD_2Cl_2 solution at 25 ºC. Since the medium composition in the NMR spectroscopic and voltammetric experiments is different (CD_2Cl_2 for NMR and 0.1 M $TBAPF_6$-CH_2Cl_2 for electrochemistry), it is necessary to correct for the viscosities of both solutions in order to obtain the diffusion coefficient values of P5Q and XQ under voltammetric conditions. We used an Ostwald viscometer to measure the viscosities of both solvent systems and found that the D_0 values under voltammetric conditions are related to those measured under NMR conditions by the simple equations:

$$D_0 = 0.959(D_0)_{NMR} \qquad \text{Equation 3-7}$$

Therefore, the corrected D_0 values for P5Q and XQ are 3.85×10^{-5} and 7.65×10^{-5} cm^2/s, respectively. Table 3-1 gives the half-wave potential ($E_{1/2}$) values, and limiting currents for each of the four waves observed in the voltammetric reduction of P5Q. The limiting current for the first one-electron reduction wave of XQ under NPV conditions (Figure 3-2) was determined to be 69.3 ± 2.3 μA. Therefore, the limiting currents and the diffusion coefficients can be used to determine the number of electrons involved in the reduction event corresponding to each one of the waves.

Table 3-1. Electrochemical data for the voltammetric reduction of P5Q in CH_2Cl_2 also containing 0.1 M $TBAPF_6$

Wave	$E_{1/2}$, V vs Ag/AgCl	i_d, μA[b]	n_{cum}[c]	n[d]
1	-0.388	92.4 ± 1.6	1.9	1.9
2	-0.596	132.3 ± 4.6	2.7	0.8
3	-0.800	224.9 ± 5.1	4.6	1.9
4	-1.080	374.7 ± 22	7.7	3.1

[a] Obtained directly from the peak potential values measured in SWV experiments. Error margin: ±0.005V. [b] Limiting current values were measured from the initial baseline, giving rise to cumulative numbers of electrons (n_{cum}), which, in turn, were used to obtain the number of electrons (n) associated with each wave. [c] Cumulative number of electrons (± 10%) corresponding to the particular wave.

The experimental and calculated data shown in Table 3-1 indicate that the four successive waves observed in the voltammetric reduction of P5Q correspond to 2, 1, 2, and 3 electrons, respectively. In order to rationalize this finding we must take into account the structure and geometry of the P5Q macrocycle and accept that there is some level of electronic communication between adjacent quinone units in P5Q.

As mentioned before, if the quinone groups were completely independent from each other, the cathodic voltammetric behavior of P5Q would consist of two consecutive five-electron waves. Accepting that adjacent quinone groups maintain a level of electronic communication is necessary to rationalize the observed voltammetric behavior. If we consider the uptake of electrons by the five connected quinone units, it is clear that the pentagonal symmetry plays a significant role. Uptake of the first electron is followed at a very similar potential by the uptake of a second electron, as both negative charges can be primarily located in quinone units that are not directly adjacent (Scheme 3-1). This leaves a neutral quinone group in between two charged quinones and two adjacent, uncharged quinones completing the $P5Q^{2-}$ macrocycle. Therefore, uptake of the third electron must proceed in one of the two adjacent, uncharged quinones, in order to minimize the repulsive interactions among the three charged quinone units at this state. After uptake of the third electron, the macrocycle only contains two uncharged quinones, and both are equivalent, as each is directly connected to two anion radicals. Therefore, the $P5Q^{5-}$ species is formed by the uptake of the last two electrons at very similar potentials (Scheme 3-1). These simple arguments, based on the minimization of repulsive interactions on the reduced macrocycle, explain the sequence of the first three voltammetric waves and their associated numbers of electrons (2-1-2). The last wave, however, clearly corresponds to three electrons, thus leading to the octa-anion, $P5Q^{8-}$. Within the investigated potential range, the fully reduced deca-anion, $P5Q^{10-}$, is not observed in dichloromethane solution. This highly charged anionic species would

correspond to the uptake of two electrons per quinone group, which could be expected on the basis of the electrochemical behavior of XQ and many other quinones. However, the spatial proximity of the quinone groups in the P5Q macrocycle may hinder the accumulation of ten negative charges in such a small molecular volume and prevent the formation of the deca-anion in the low polarity medium in which we conducted our voltammetric experiments.

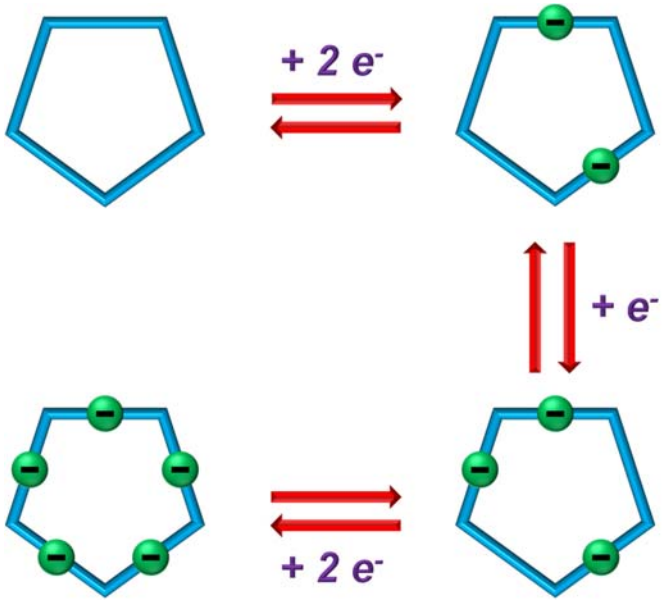

Scheme 3-1. Steps in the five-electron reduction process of the P5Q macrocycle.

3.2.2 Binding interaction studies

We expected pillar[5]quinone would be a good host molecule. Also, since quinone is electroactive, it would be interesting to investigate the binding interaction between pillar[5]quinone and guest molecules, when the charge state of pillar[5]quinone changes.

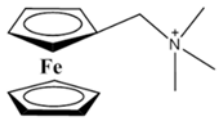

1

Figure 3-4. The guest molecule studies

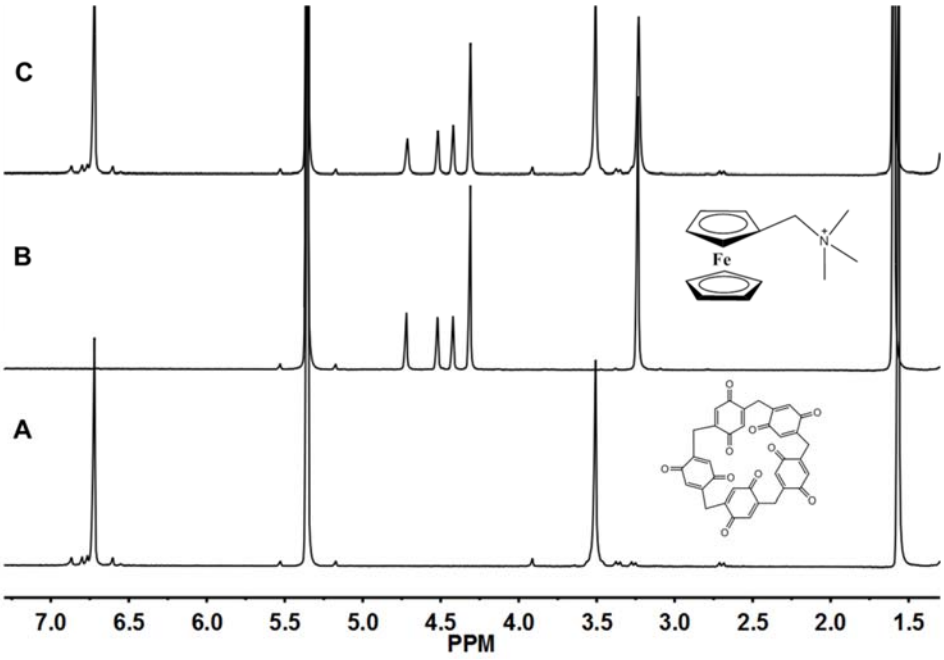

Figure 3-5. (A) ^{1}H NMR spectrum of P5Q 1.0 mM in CD_2Cl_2; (B). ^{1}H NMR spectrum of the guest molecule (Figure 3-4) 1.0 mM in CD_2Cl_2; (C) ^{1}H NMR spectrum of P5Q and the guest molecule with a 1:1 ratio

^{1}H NMR spectroscopic studies indicate that there are no obvious interactions between P5Q and guest molecule **1**. Even when the ferrocene derivative was oxidized to ferrocenium, the two positive charge (one on ferrocenium, the other on nitrogen) did not make the interaction stronger (Figure 3-6). However, when P5Q was reduced, we could see shifts to more positive values of all the four peaks of P5Q in the presence of guest molecule **1**(Figure 3-7).The reason could be that reduced P5Q has negative charges on the rim and

1 has a positive charge. With more electrons taken by P5Q, it has more negative charges, which increases its binding ability towards the guest molecule **1**.

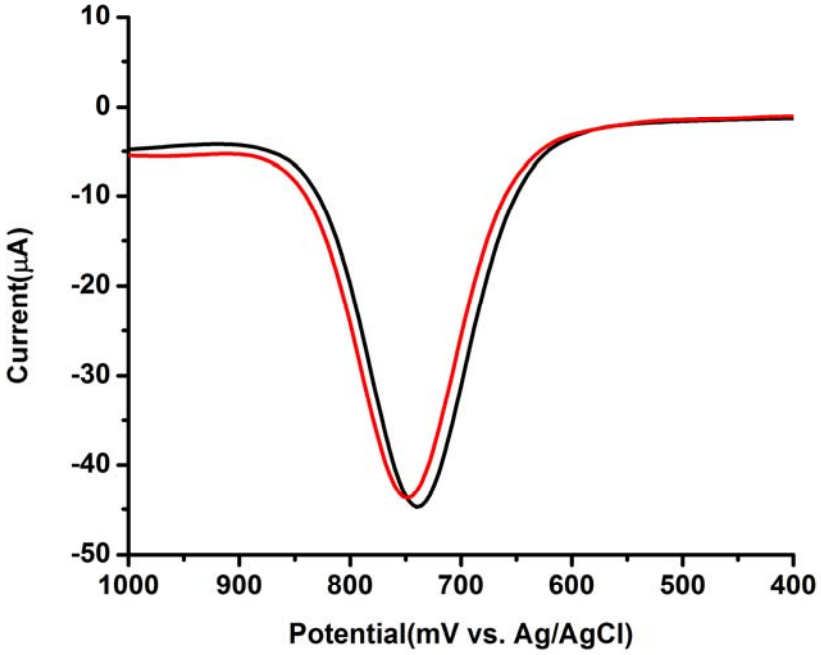

Figure 3-6. **Black:** SWV of guest molecule **1** (1 mM) in the absence of P5Q; **Red:** SWV of guest molecule **1** (1 mM) in the presence of 1 mM P5Q.

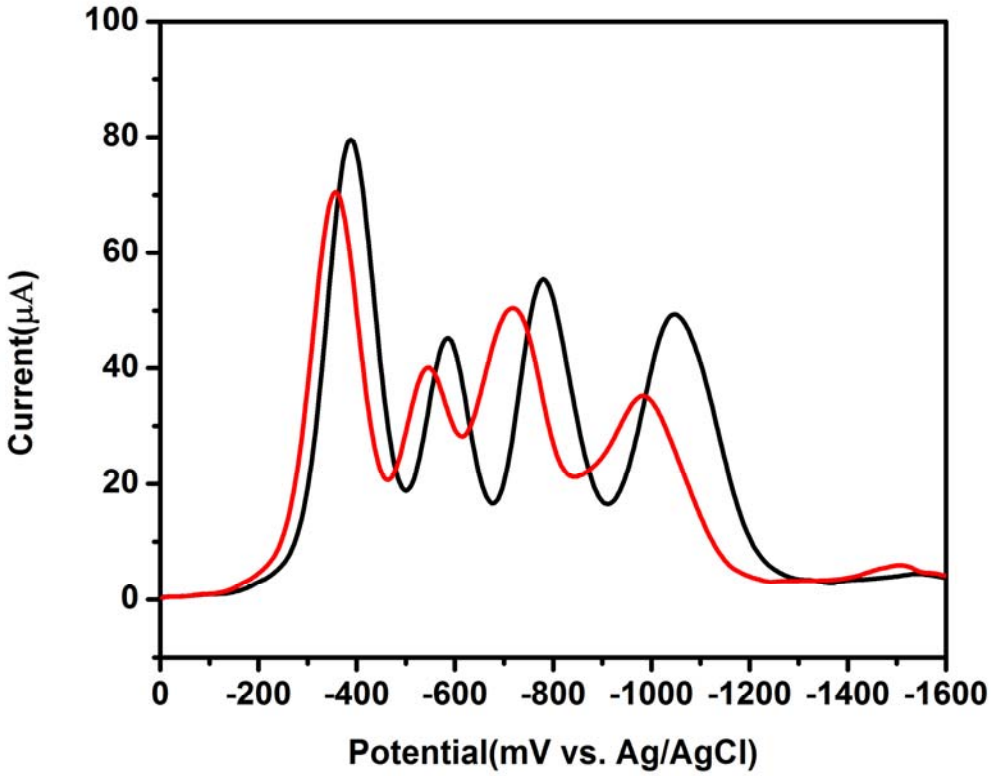

Figure 3-7. **Black:** SWV of P5Q (1 mM) in the absence of guest molecule **1**; **Red:** SWV of P5Q (1 mM) in the presence of 1 mM guest molecule **1**.

3.3 Experimental section

3.3.1 Synthesis

Pillar[5]quinone was prepared by oxidation of the readily available 1,4-dimethoxypillar[5]arene with Oxone/iodobenzene according to the method reported by Shivakumar and Sanjayan, which is easily scalable and does not

require chromatographic purification. The isolated P5Q was characterized by its published ^{1}H and ^{13}C NMR spectroscopic and mass spectrometric data.

All other chemicals were commercially available and used without further purification.

3.3.2 Electrochemical experiments

A single compartment glass cell was used for all voltammetric experiments. Typically the cell was fitted with a glassy carbon working electrode (0.071cm^2), a Pt auxiliary electrode, a Ag/AgCl reference electrode and nitrogen inlet Teflon tubing. Nitrogen gas was purified before use and bubbled through the solution to remove dissolved oxygen before the measurements. During the voltammetric measurements, nitrogen flow was maintained above the solution to minimize re-dissolution of oxygen. The working electrode was polished on a soft, felt surface using aqueous alumina (0.05μm) slurry for lubrication. Before use the working electrode surface was rinsed extensively with water and sonicated to remove any particulate left from polishing.

The square wave voltammetric experiments were run with a step potential of 4 mV, pulse amplitude of 25 mV and 15 Hz of frequency. The normal pulse voltammetric experiments were run at a scan rate of 100 mV/s, a sample width of 17 ms and a pulse width of 50 ms.

3.3.3 NMR diffusion measurements

^{1}H PGSE NMR measurements were performed by using the standard stimulated echo pulse sequence on a Bruker 400 MHz spectrometer at 300 K without spinning. The shape of the gradients was rectangular, their duration (δ) was 4 ms. And their strength (G) was varied during the experiments. The delay between gradient pulses was 54 ms. All spectra were recorded on a spectrometer equipped with a GAB z-gradient unit capable of producing magnetic pulsed field gradients in the z-direction up to 0.5 T/m. The semilogarithmic plots of $\ln(I/I_0)$ vs G^2 were fitted using an Office Excel© software; the R factor was always higher than 0.99. The dependence of the resonance intensity (I) on a constant diffusion time and on a varied gradient strength (G) is described by Equation 3-8:

$$\ln(I/I_0) = -(\gamma\delta)^2 D(\Delta - \delta/3)G^2 \qquad \text{Equation 3-8}$$

Where I is the intensity of the observed spin-echo, I_0 is the intensity of the spin-echo without gradients, D is the diffusion coefficient, Δ is the delay between the midpoints of the gradients, δ is the length of the gradient pulse and γ is the gyromagnetic ration. Illustrative examples are shown in Figure 3-8 and Figure 3-9.

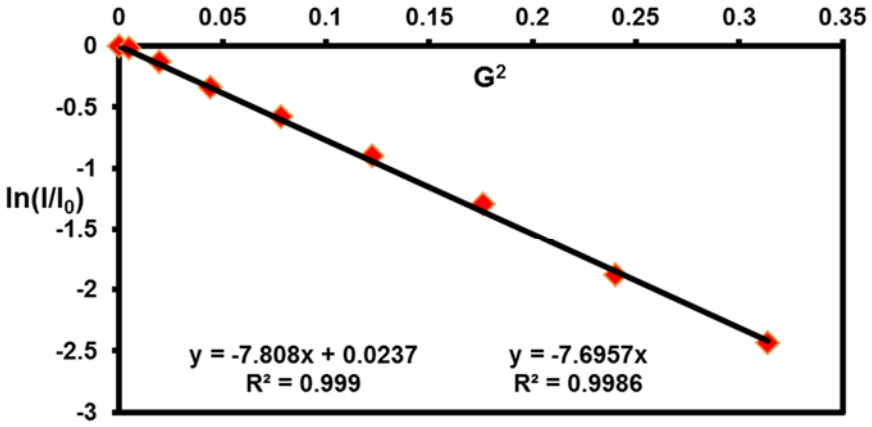

Figure 3-8. Normalized signal decay as a function of gradient strength for P5Q in CD_2Cl_2.

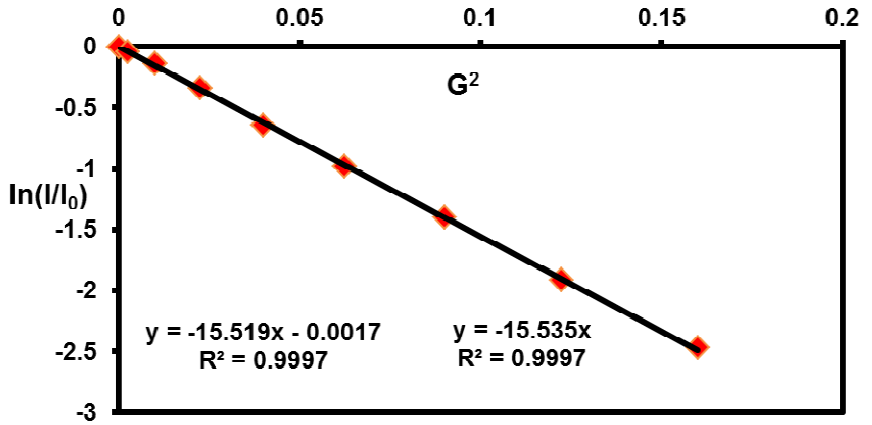

Figure 3-9. Normalized signal decay as a function of gradient strength for XQ in CD_2Cl_2.

Chapter 4 : Investigation of Gel Formation of PAMAM Dendrimers with CO_2

4.1 Overview

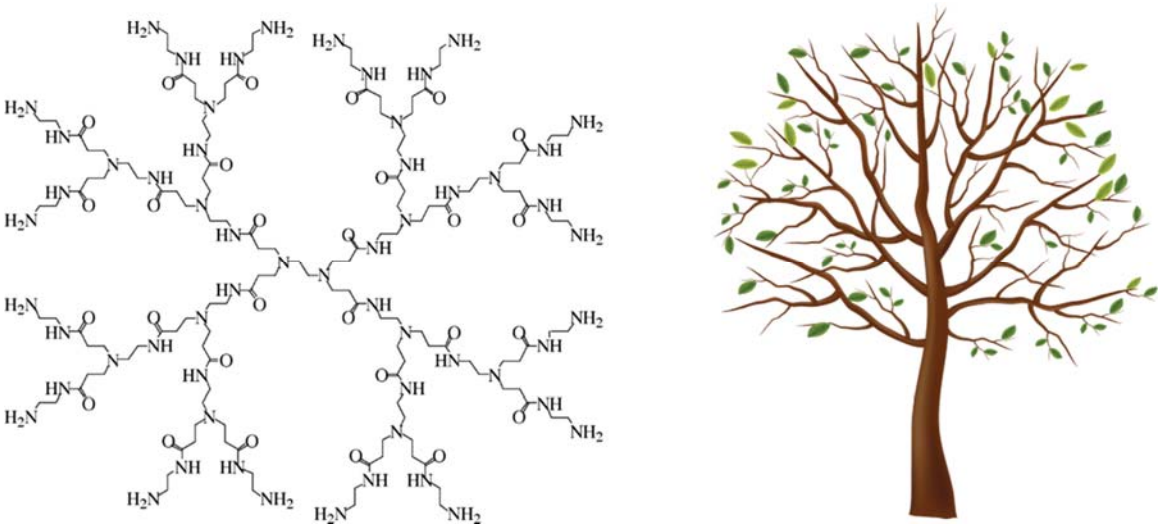

Figure 4-1. Structure of generation 2.0 PAMAM Dendrimer

Dendrimers are tree-like molecules (Figure 4-1). The name, dendrimer, means tree in Greek word. It was first reported in 1978 by Fritz Vogtle.[41] A dendrimer generally has a core with branches growing around it. Dendrimers are generally symmetrical around their cores. Their surface groups, generally, have functionalities. Some dendrimers may have also internal functionalization[42] Dendrimers are classified by generations. With only the core named as generation 0, each addition of branching cycle increases the generation by 1.0.The molecular weight is generally doubled when the generation increases by 1.0. Its molecular weight can be up to several thousand grams per mole.

A gel is a solid, jelly like material. It contains a three-dimensional network spanning a volume of liquid. The three-dimensional structure can be either formed by physical bonds or chemical bonds.

Considering the tree-like structure of PAMAM dendrimers, it would be interesting to investigate their gelation ability. For PAMAM dendrimers, from generation 0.0 to generation 5.0, they are not gel in methanol or water, though generation 5.0 has a diameter of around 5 nm. A gel could be formed if a larger three dimensional structure could be formed. It is a well-known reaction that amine and carbon dioxide can react with each other to form carbamate and ammonium readily, and carbamate and ammonium can attract with each other via salt bridge. The functional group of PAMAM dendrimer is amine. We used carbon dioxide to react with PAMAM dendrimers to investigate if the gelation ability of PAMAM dendrimers could be enhanced.

4.2 Results and discussions

The type of dendrimers used in this chapter is called PAMAM dendrimers, ethyleneamine core, generation n (n=0.0, 1.0, 3.0 and 5.0). Their head groups are amines and the cores are ethyleneamines (Figure 4-2A). Generation 0.0 only has an ethyleneamine core and four terminal groups, but no branch groups. Figure 4-2B shows how to name the generations of PAMAM dendrimers: with each increase of a cycle of branch groups, the generation increases by one (Figure 4-2B).

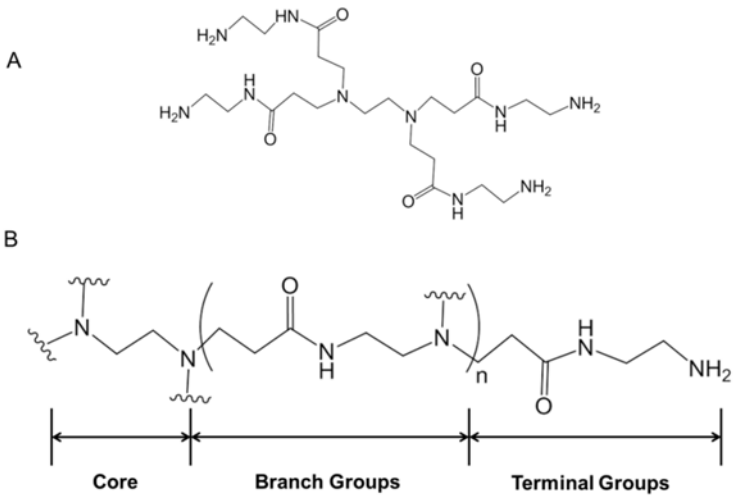

Figure 4-2. (A) Structure of PAMAM dendrimer, ethylenediamine core, generation 0.0 (B) General structure of PAMAM dendrimer, generation *n*.

Table 4-1. Molecular parameters of PAMAM dendrimers of generation 0.0, 1.0, 2.0 3.0, 4.0 and 5.0.

Generation	Molecular Weight	Measured Diameter(Å)	Surface Group
0	517	15	4
1.0	1430	22	8
2.0	3256	29	16
3.0	6909	36	32
4.0	14215	45	64
5.0	28826	54	128

Table 4-1 lists the physical parameters of PAMAM dendrimers of generation 0.0, 1.0, 2.0, 3.0, 4.0 and 5.0. From this table, we see the molecular weight of generation 0.0 is only 517 g/mole; the MW for generation 5.0 is 28826, almost 58 times than that of generation 0.0. The diameter of generation 5.0 (54 Å)

is almost four times than that of generation 0.0 (15Å). Generation 5.0 has 128 surface groups, but generation 0.0 only has 4 surface groups.

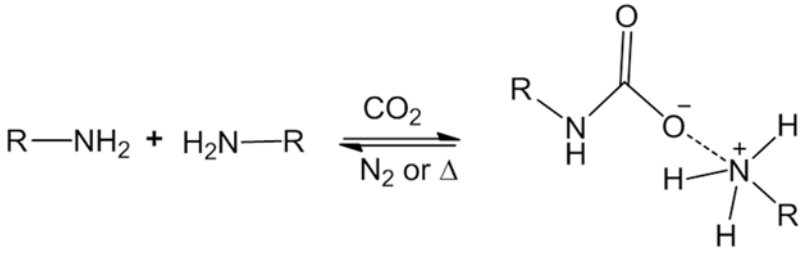

Scheme 4-1. Reversible covalent chemistry between CO_2 and amine

It is a well-known reaction that carbon dioxide reacts rapidly with amines at ordinary temperatures and pressures to produce a carbamate ion and a protonated base (ammonium), which are connected by a salt bridge (Scheme 4-1).[43] The reaction between CO_2 and amines is basically an acid-base equilibrium. Additionally, this process is reversible upon N_2 bubbling or heating.[44] Considering the tree-like structure of PAMAM dendrimers and their head groups (amines), CO_2 would be a good agent to crosslink dendrimers. It would be interesting to investigate the gelation ability of PAMAM dendrimers with CO_2. Also, since the reaction between CO_2 and amines is reversible, if a gel is formed with PAMAM dendrimers, the gel could be converted to its original PAMAM dendrimer structure upon N_2 bubbling.

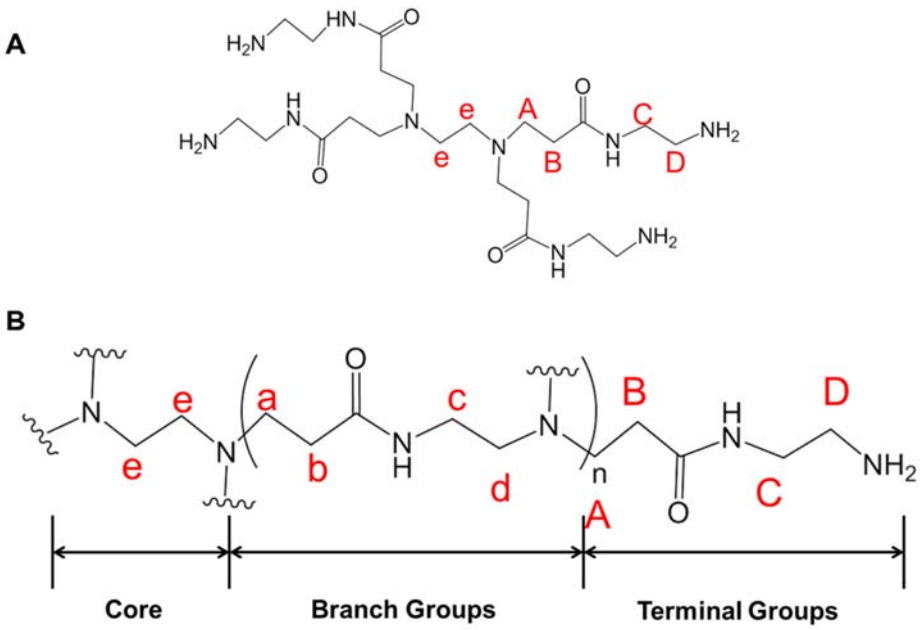

Figure 4-3. Schematic representation of PAMAM dendrimers, generation n, indicating the lettering scheme used to identify the methylene groups. (A) generation 0.0; (B) generation *n*.

Figure 4-3 shows how to use label to identify the methylene and nitrogen groups, adopted from ^{1}H NMR chemical shift labeling by Richard Crooks and his coworkers. All generations have ethylene cores, which are assigned as letter *e*. Since their structures are symmetrical, we could assume all the branch methylenes have similar chemical shifts (which are assigned as letter *a*, *b*, *c* and *d*). The terminal groups are close to the amine groups, it would be reasonable to assume that the methylene groups on the terminal parts have a little different chemical shifts(*A*, *B*, *C* and *D* for the methylene groups in the terminal part). Figure 4-4, Figure 4-5, Figure 4-6 and Figure 4-7 are the ^{1}H NMR chemical shift assignments for PAMAM dendrimer generation 0.0, 1,0, 3.0 and 5.0 in D_2O.

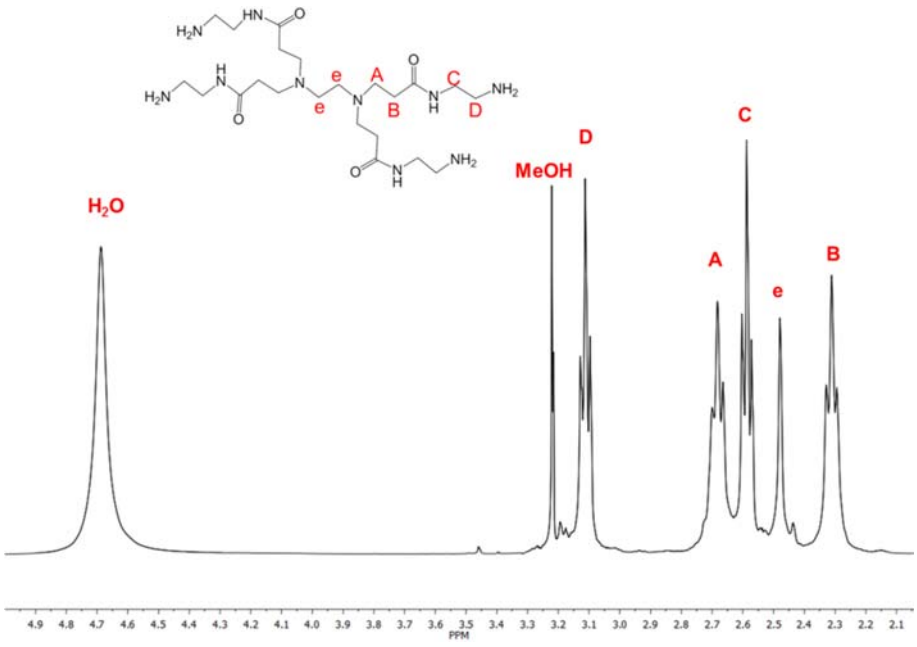

Figure 4-4. ^{1}H NMR chemical assignment for PAMAM dendrimer, generation 0.0 in D_2O, 400 MHz NMR.

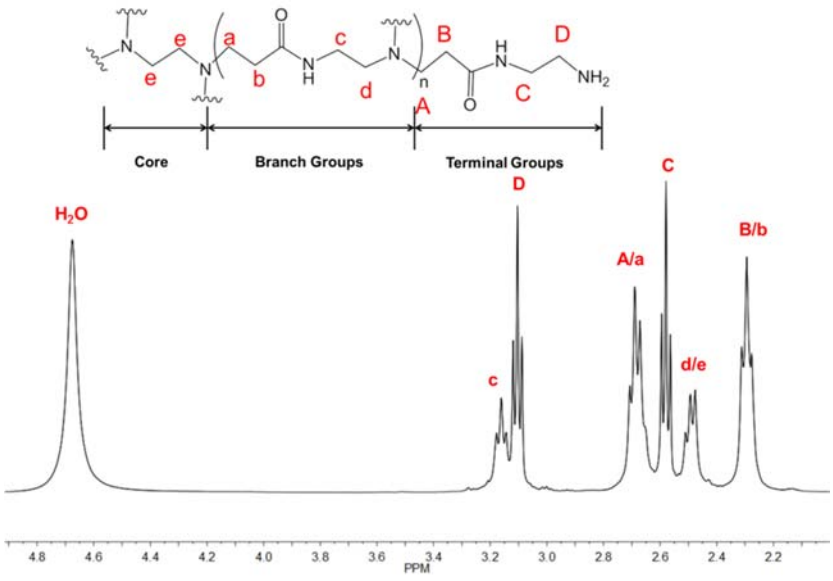

Figure 4-5. ^{1}H NMR chemical assignment for PAMAM dendrimer, generation 1.0 in D_2O, 400 MHz NMR.

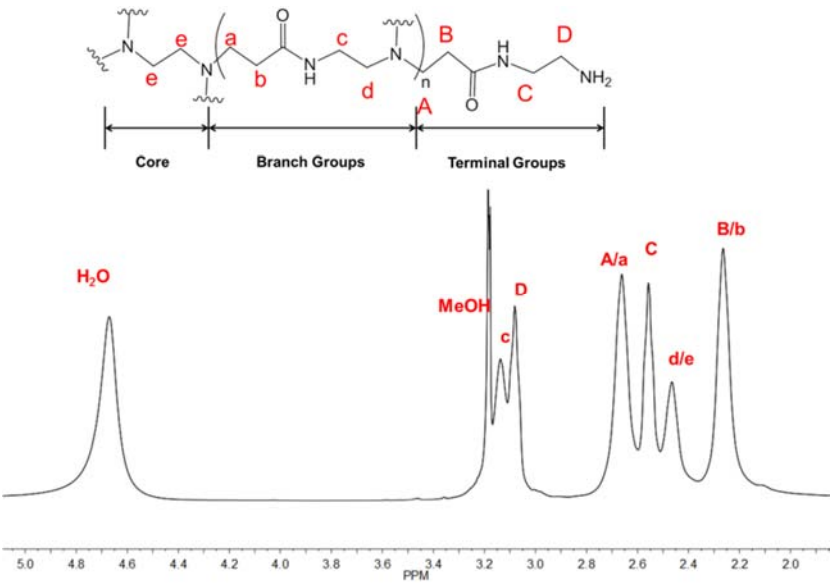

Figure 4-6. ^{1}H NMR chemical assignment for PAMAM dendrimer, generation 3.0 in D_2O, 400 MHz NMR.

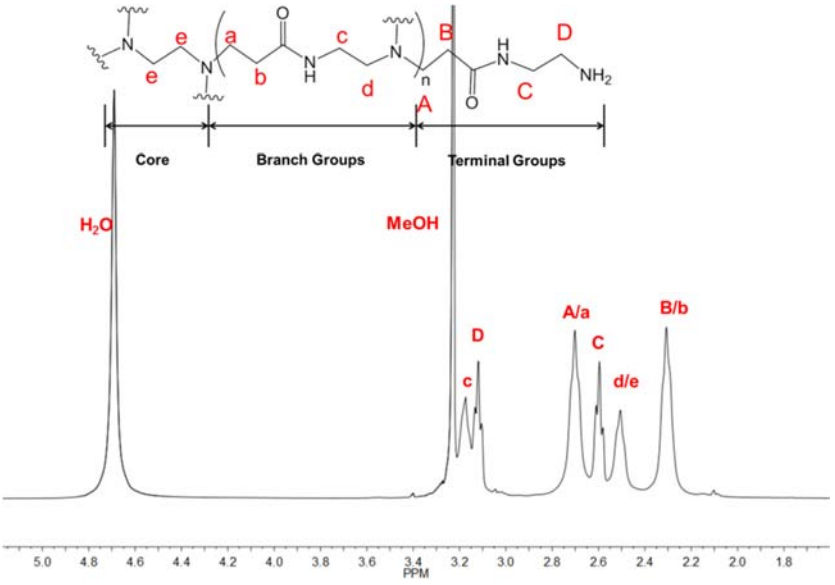

Figure 4-7. ^{1}H NMR chemical assignment for PAMAM dendrimer, generation 5.0 in D_2O, 400 MHz NMR.

4.2.1 Gelation studies of PAMAM dendrimers in D_2O

Since the reaction between CO_2 and amines produces carbamate ion and protonated bases (ammonium), we expected carbamate ions and protonated bases would be produced on the head groups (amines) of PAMAM dendrimers if bubbled with CO_2. We used ^1H NMR spectroscopy to investigate the gelation reaction firstly in D_2O. Dendrimers were dissolved in D_2O in a NMR tube. A small amount of CO_2 was introduced into the NMR tube one time, and then ^1H NMR spectrum was recorded. Many cycles of bubbling and NMR measurements were done to record as detailed as possible the reaction process and enough time was allowed so that all the amine groups were reacted. For each generation, we prepared several solutions of different concentrations. The highest concentration we prepared for generation 0.0 was 0.32 M; 0.5 M for generation 1.0; 0.1 M for generation 3.0; 0.01 M for generation 5.0. Figure 4-8 and Figure 4-9 show the NMR spectrum changes during CO_2 bubbling for generation 0.0 and generation 5.0 respectively. However, there was no gel formed for all of the generations at all of the concentrations used.

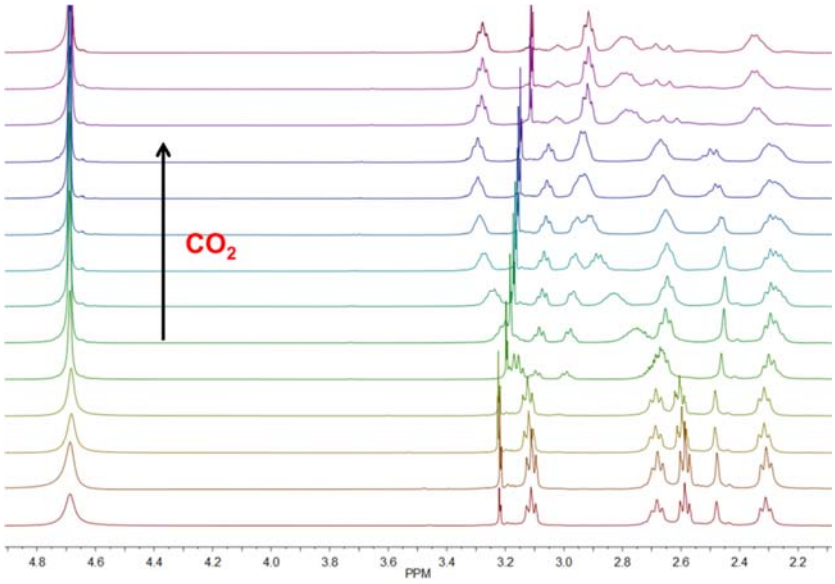

Figure 4-8. ^{1}H NMR spectra of the bubbling of CO_2 into PAMAM dendrimer, generation 0.0. Down: no bubbling of CO_2. From down to up, the amount of CO_2 introduced increases.

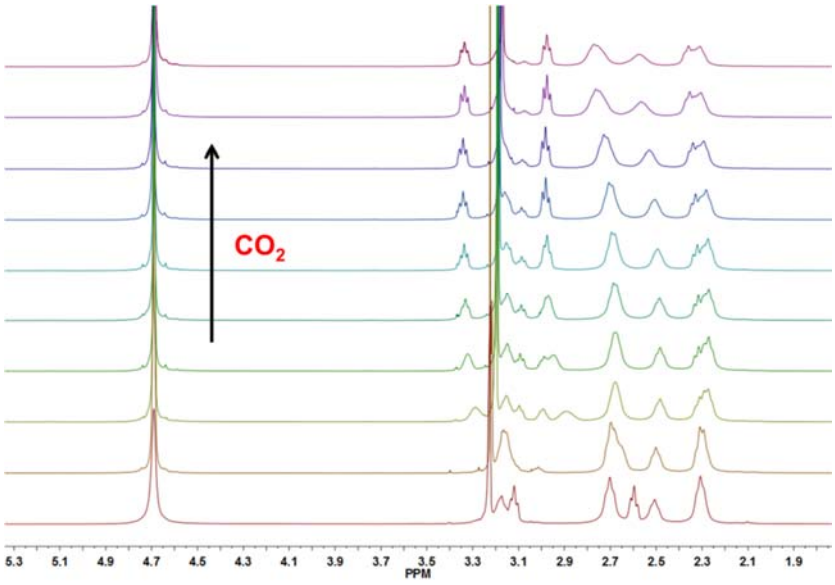

Figure 4-9. ^{1}H NMR spectra of the bubbling of CO_2 into PAMAM dendrimer, generation 5.0. Down: no bubbling of CO_2. From down to up, the amount of CO_2 introduced increases.

In order to know why gel was not formed, we first need to know what these chemical shifts mean. We first titrated generation 5.0 with DCl in D_2O to

see how the formation of ammonium would reflect on the spectra and which peaks correspond to the α-methylene and β-methylene protons from ammonium part. Then we titrated PAMAM dendrimer, generation 1.0 with $NaDCO_3$ to produce carbamate, then titrated the produced carbamate in generation 1.0 with DCl to see how the spectrum would change.

$$RNH_2 + HCO_3^- \leftrightarrow RNHCO_2^- + H_2O \quad \text{Equation 4-1}$$

DCl would react with the amine to produce ammonium. Figure 4-10 is the ^1H NMR spectra during the titration of generation 5.0 with DCl. It clearly shows how the peaks change during the formation of ammonium and which peaks correspond to the α-methylene β-methylene protons from the ammonium part. The HCO_3^- from $NaHCO_3$ can react with amine group to produce carbamate (Equation 4-1). We titrated Generation 1.0 with $NaHCO_3$ to see how the formation of carbamate would reflect on the ^1H NMR spectra.

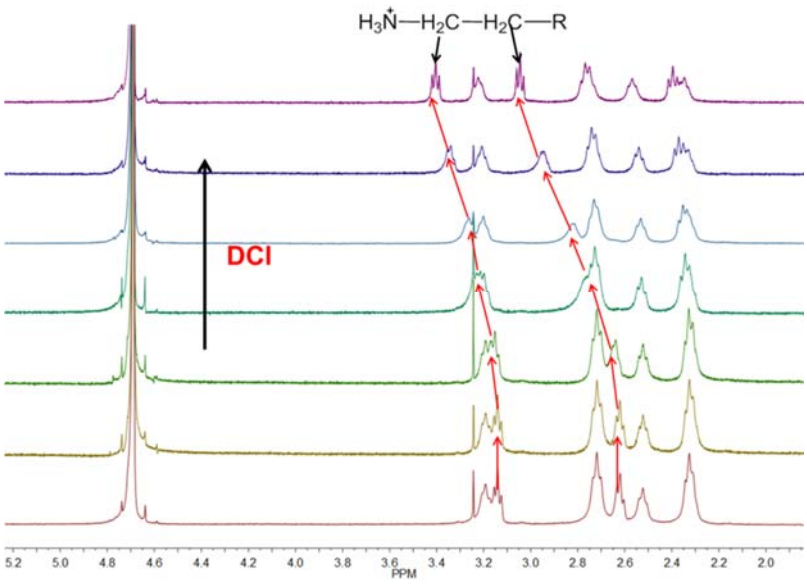

Figure 4-10. Titration of PAMAM dendrimer, generation 5.0 with DCl in D_2O, 400 MHz NMR.

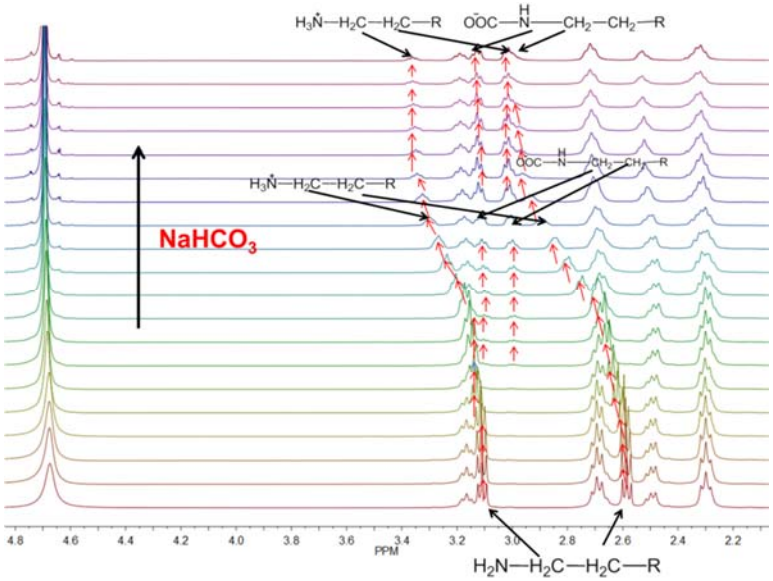

Figure 4-11. Titration of PAMAM dendrimer, generation 1.0 with $NaHCO_3$ in D_2O, 400 MHz NMR.

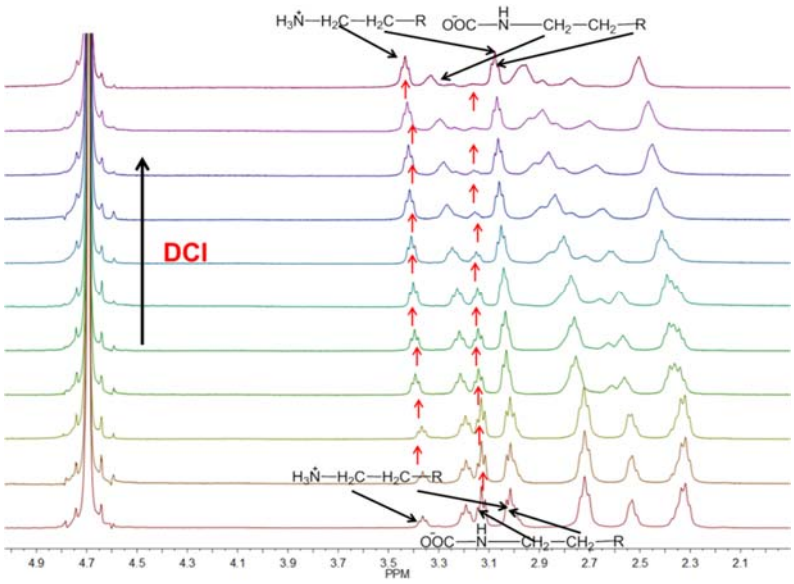

Figure 4-12. Titration of the solution already titrated with $NaHCO_3$ with DCl in D_2O, 400 MHz NMR.

From Figure 4-11, we can see how chemical shifts for the α-methylene protons and β-methylene protons from carbamate were produced during the formation of carbamate, when we were titrating it the $NaDCO_3$. Then we titrated the resulted solution (the last spectrum in Figure 4-11) with DCl to convert the head groups to ammoniums. From Figure 4-12, we can see how the intensity corresponding to the α-methylene and β-methylene protons from carbamate decreased and how the intensity for the α-methylene and β-methylene protons from ammonium increased. The down field shifts of other chemical peaks in Figure 4-12 are probably resulted from the addition of DCl, which made the solution acidic.

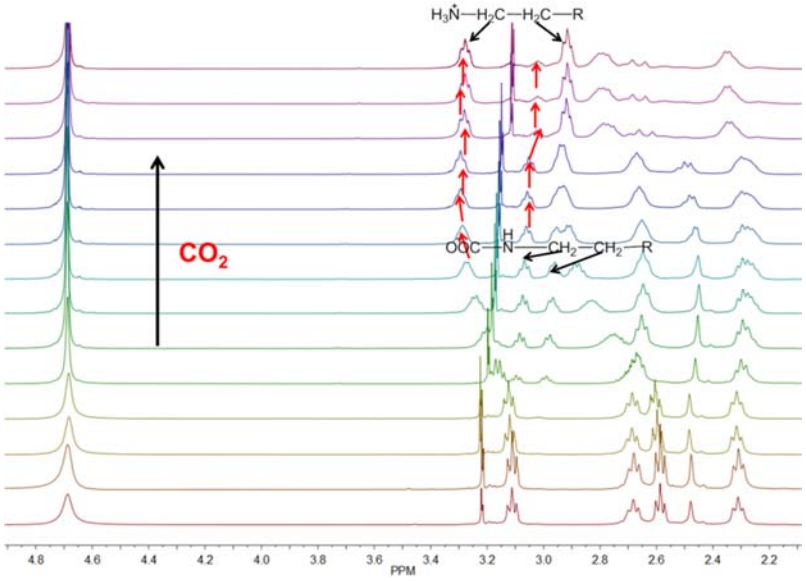

Figure 4-13. Analysis of the reaction between CO_2 and PAMAM dendrimer, generation 0.0.

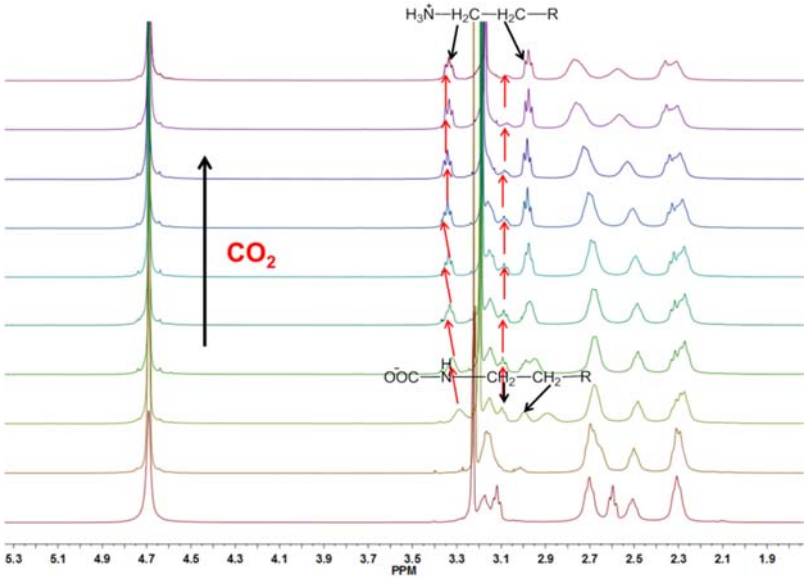

Figure 4-14. Analysis of the reaction between CO_2 and PAMAM dendrimer, generation 5.0.

Now let us go back to the titrations between PAMAM dendrimers and CO_2 in D_2O. From Figure 4-13 and Figure 4-14, which are corresponding generation 0.0 and generation 5.0, we can see at the early stage of the reaction between

CO_2 and dendrimers, during which there was not much CO_2 bubbled into dendrimer solution, there was carmabate formed. However, with more CO_2 introduced into the solution, the intensity for the chemical shifts from α-methylene and β-methylene of carbamate decreased. The intensity for the chemical shifts corresponding the α-methylene and β-methylene from ammonium increased. The reason behind could be that the solubility of CO_2 in H_2O is not low. CO_2 reacts with water to produce H_2CO_3. The acidity of the PAMAM dendrimer solution would increase with bubbling of CO_2. Though, there were some carbamate ions formed, the increased acidity converted them into ammonium, like the fact in the titration with DCl (in Figure 4-12) . Also, since H_2O is a protic solvent and H_2CO_3 is able to dissociate into many types of ions, the existence of large amount of other cations and anions would interfere with the interaction between carbamate anions and ammonium cations on the terminals of dendrimers.

4.2.2 Gelation of PAMAM dendrimer with CO_2 in CD_3OD

We switched to CD_3OD as the solvent for gelation studies. CD_3OD is less protic than D_2O. We studied PAMAM dendrimer, generation 0.0, 1.0 and 5.0. There is almost no difference between the ^1H NMR spectra of dendrimers in D_2O and CD_3OD, only some weak shifts due to solvent change. (Figure 4-15, Figure 4-16 and Figure 4-17)

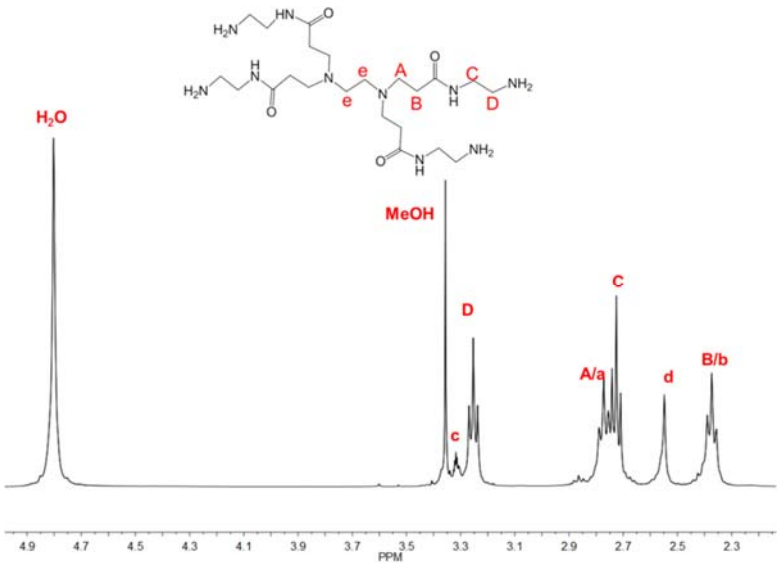

Figure 4-15. ^{1}H NMR chemical assignment for PAMAM dendrimer, generation 0.0 in CD_3OD, 400 MHz NMR.

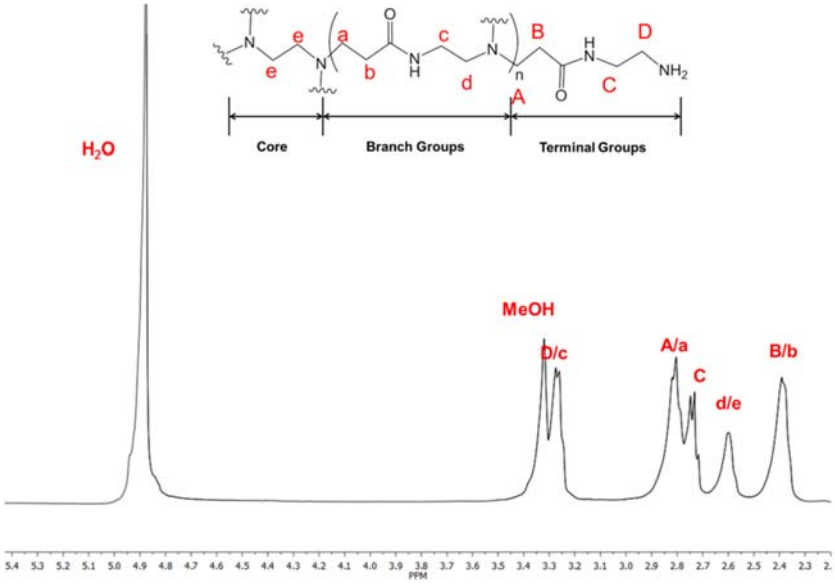

Figure 4-16. ^{1}H NMR chemical assignment for PAMAM dendrimer, generation 1.0 in CD_3OD, 400 MHz NMR.

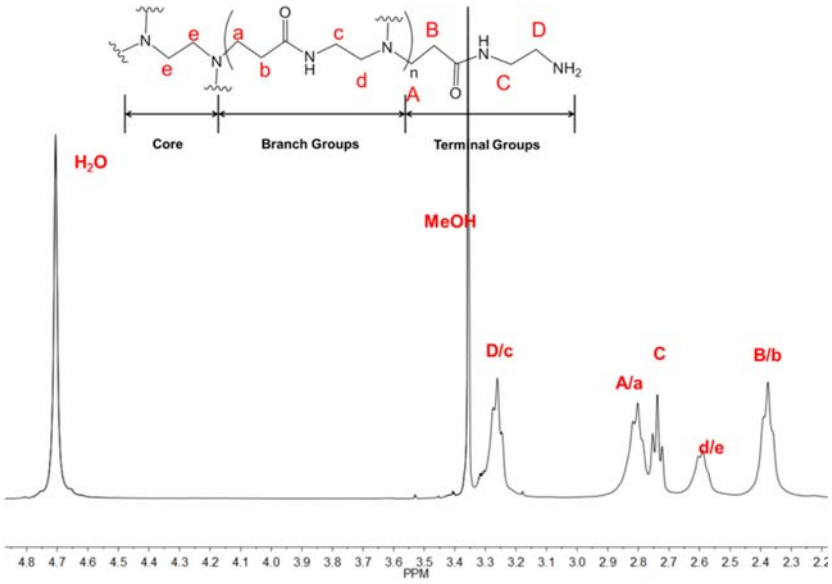

Figure 4-17. ^{1}H NMR chemical assignment for PAMAM dendrimer, generation 5.0 in CD_3OD, 400 MHz NMR.

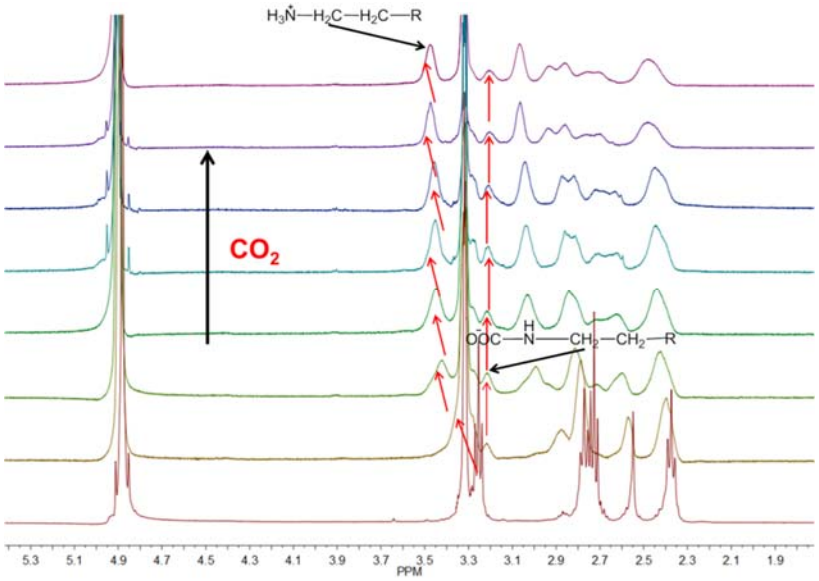

Figure 4-18. ^{1}H NMR analysis of PAMAM dendrimer, generation 0.0, 0.01 M titrated with CO_2 in CD_3OD, 400 MHz NMR.

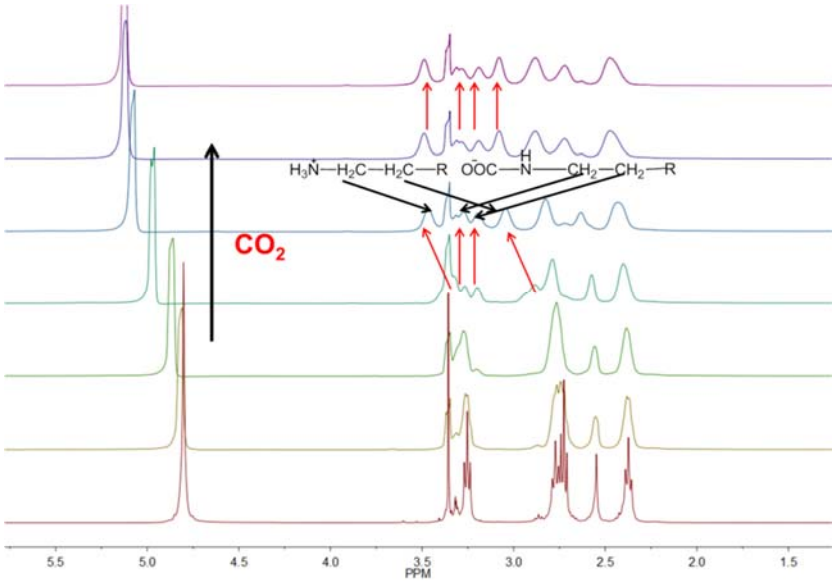

Figure 4-19. ^{1}H NMR analysis of PAMAM dendrimer, generation 0.0, 0.16 M with CO_2 in CD_3OD, 400 MHz NMR.

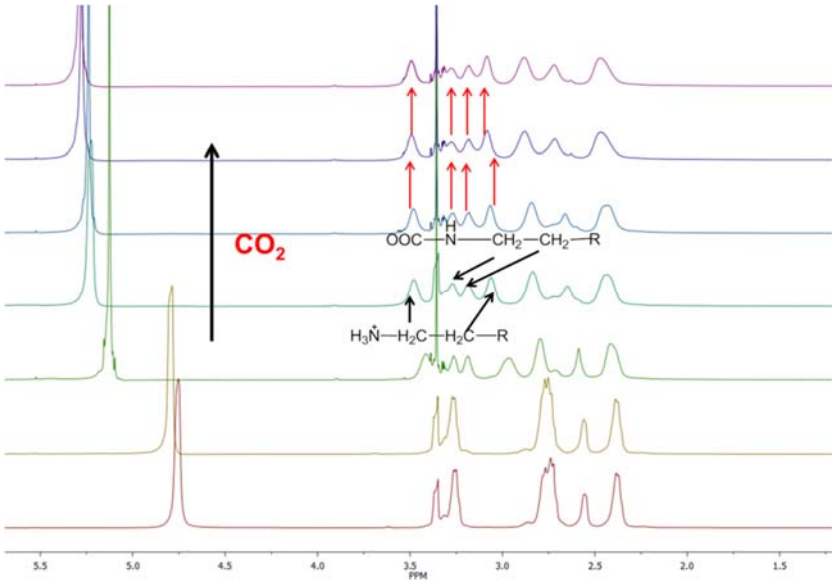

Figure 4-20. ^{1}H NMR analysis of PAMAM dendrimer, generation 0.0, 0.32 M with CO_2 in CD_3OD, 400 MHz NMR.

For generation 0.0, we first prepared a concentration of 0.01 M of PAMAM dendrimer. The bubbling speed of CO_2 was made as slow as possible so that we could observe the details of the reaction. However, no gel or even precipitates

were formed. Based on Figure 4-18, we can see that carbamate ions formed. With the amount of CO_2 introduced increased, we can see the intensity for the α-methylene and β-methylene protons from ammonium got stronger, and these for carbamate decreased. But there were still some carbamate ions existing at the final stage. The reason for the failure of the gel formation could be there was no enough gelation agents (PAMAM dendrimer). So we increased the concentration to 0.16M, and did the same titration with CO_2. In this case (Figure 4-19), the intensity for the chemical shifts for the α-methylene and β-methylene protons from carbamate is stronger compared than these in 0.01 M of dendrimer (Figure 4-18). The same situation applied in the case of a concentration of 0.32 M (Figure 4-20): more carbamate ions were produced compared to the solution of 0.01M. The increased amount of carbamate ions is necessary for the formation of gel, since it is the salt bridge between carbamate and ammonium that connect adjacent dendrimers, which is one of the crucial elements for the construction of a three dimensional structure spanning a volume of liquid. But unfortunately, there was still no gel formed. But the fact that with the increase of the concentration of dendrimers, the amount of carbamate ions formed increased means that the amount of dendrimers in a certain volume of liquid is important for gelation.

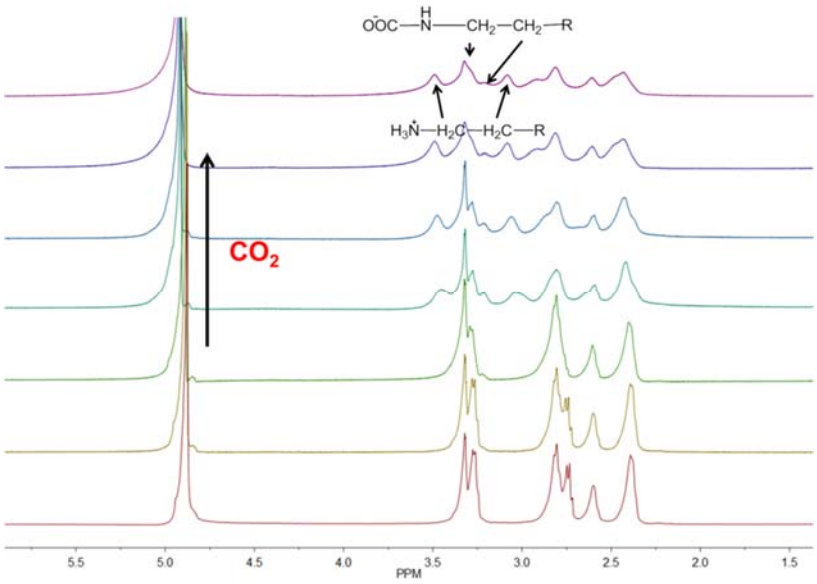

Figure 4-21. ^{1}H NMR analysis of PAMAM dendrimer, generation 1.0, 0.01 M with CO_2 in CD_3OD, 400 MHz NMR.

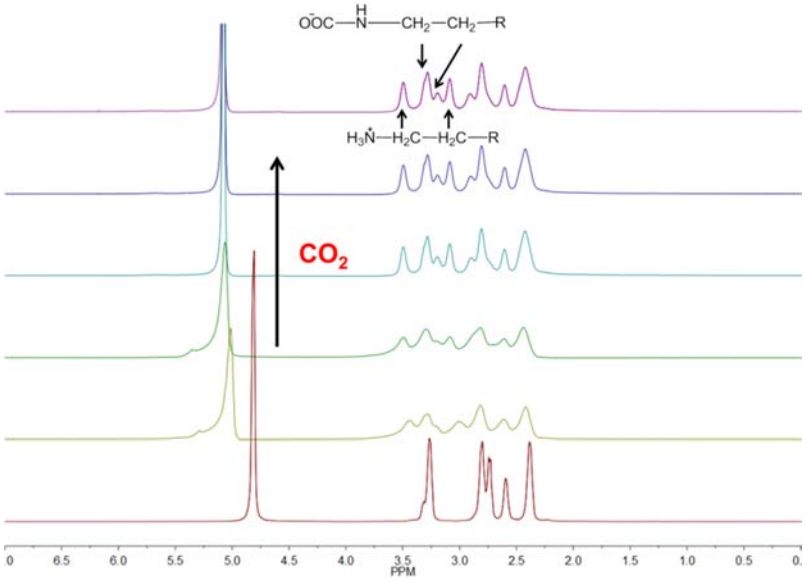

Figure 4-22. ^{1}H NMR analysis of PAMAM dendrimer, generation 1.0, 0.08 M with CO_2 in CD_3OD, 400 MHz NMR.

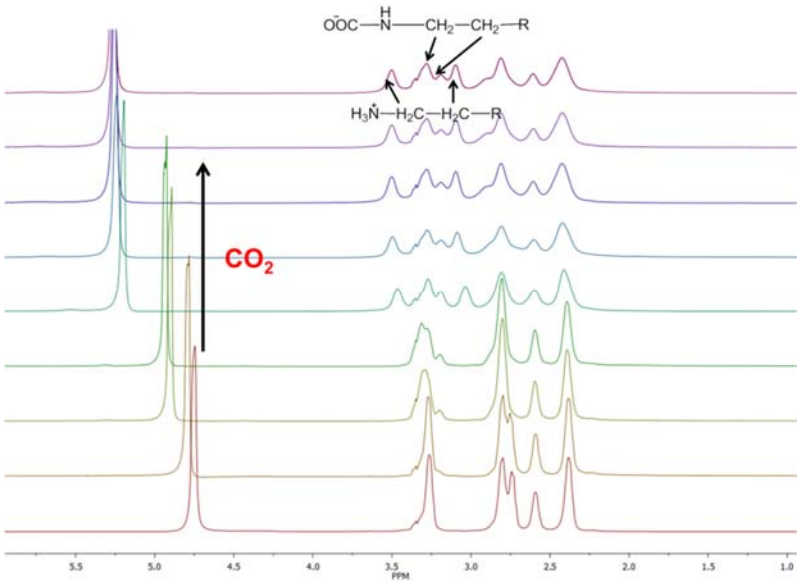

Figure 4-23. ^{1}H NMR analysis of PAMAM dendrimer, generation 1.0, 0.16 M with CO_2 in CD_3OD, 400 MHz NMR.

Then we tested PAMAM dendrimer, generation 1.0. Generation 1.0 has a diameter of 22 Å, larger than that of generation 0.0 (15 Å), and 16 surface groups compared to only 4 for generation 0.0. It would be reasonable to expect a better gelation ability of generation 1.0, considering the larger space it occupies and more surface groups it has. We prepared three different concentrations: 0.01 M, 0.08 M and 0.16 M. The 0.01 M solution was used to compare the gelation ability with generation 0.0 under the same PAMAM concentration. There was also a 0.01 M solution of generation 0.0. The 0.08 M and 0.16 M solution were selected to compare with the 0.16 M and 0.32 M solution of generation 0.0 under the same concentration of surface groups, respectively, since the surface groups of generation 1.0 are two times of those of generation 0.0. Figure 4-21 is the CO_2 titration with a 0.01 M solution of generation 1.0. There was no gel or precipitates formed. However, by analyzing the intensity of the chemical shifts for the α-

methylene and β-methylene protons for carbamate, there was a certain amount of carbamate formed similar to that in 0.01 M solution of generation 0.0 (Figure 4-18). In the 0.08 M solution and the 0.16 M solution (Figure 4-22 and Figure 4-23), the fact we can tell is that in both cases, there was a certain amount of carbamate ions produced. There was almost no difference between the amounts of carbamate ions between generation 0.0 and 1.0, under the same concentrations of surface groups. However, in the 0.08 M solution and 0.16 M solution of generation 1.0, there were some white precipitates formed, though no gel formed. This may indicate that generation 1.0 has better gelation ability, probably due to its larger molecular diameter and more surface groups on a single dendrimer.

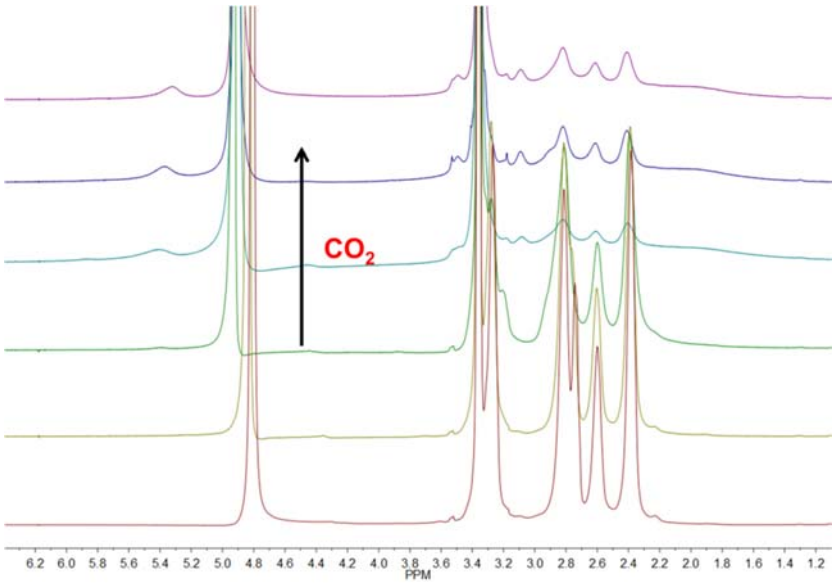

Figure 4-24. ^{1}H NMR analysis of PAMAM dendrimer, generation 5.0, 0.005 M with CO_2 in CD_3OD, 400 MHz NMR.

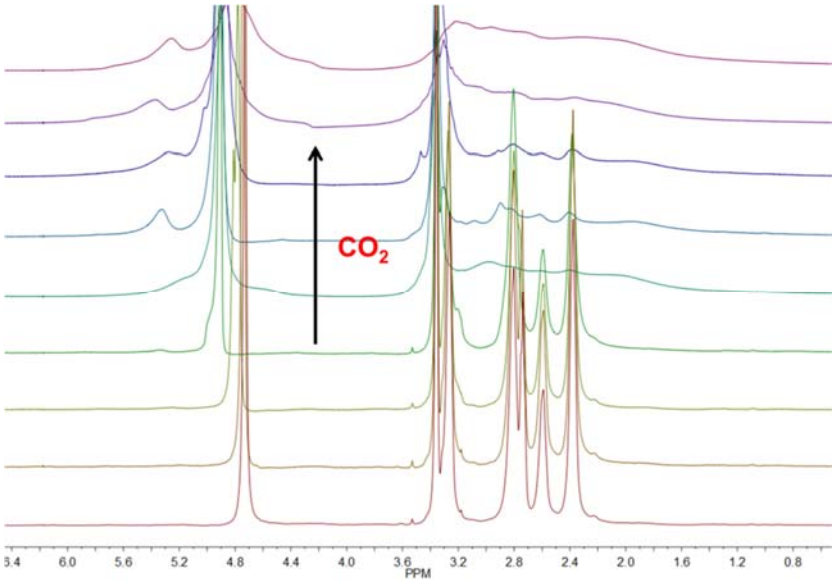

Figure 4-25. ^{1}H NMR analysis of PAMAM dendrimer, generation 5.0, 0.01 M, with CO_2 in CD_3OD, 400 MHz NMR.

Generation 5.0 has a diameter of 54 Å and 128 surface groups. We first prepared a 0.005 M solution of generation 5.0. Then CO_2 was introduced to the solution slowly. We were not able to record very detailed chemical shift changes (Figure 4-24), because there were white precipitates formed after only several CO_2 bubbles were introduced. With more CO_2 bubbled, more and more aggregates (sol) formed until the solution was totally white. We continued to bubble the sol with CO_2, and it gradually turned to clear with a jelly like solid formed, which means the gel formed. Additionally, the chemical shift peaks for generation 5.0 at the gel stage were broad. The broad chemical shift peak is a common phenomenon in solid state NMR. When we increased to higher concentrations of generation 5.0, gel was observed and broad chemical shift peaks were recorded, too (Figure 4-25).

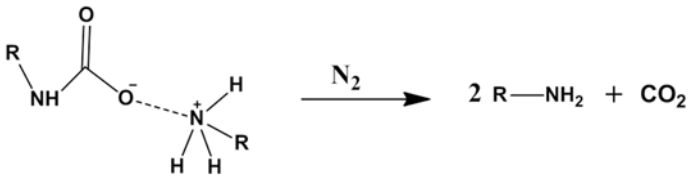

Scheme 4-2. Converting carbamate to amine by bubbling with N_2

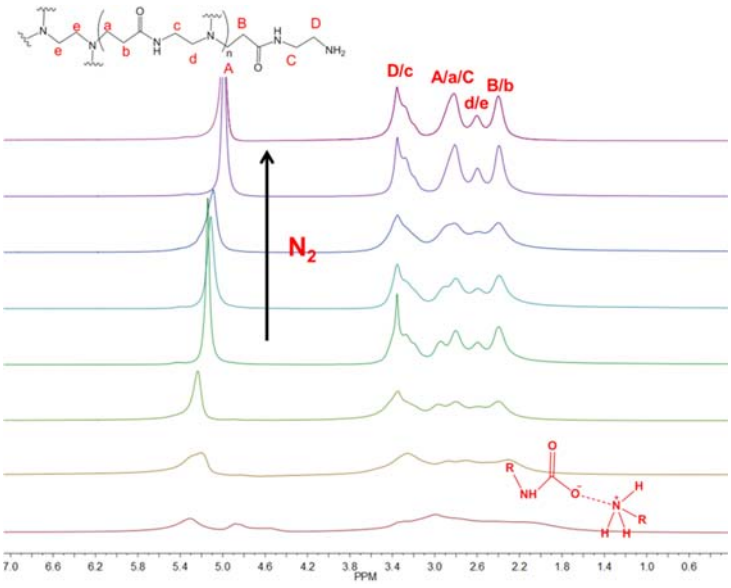

Figure 4-26. Titration of the gel of PAMAM dendrimer, generation 5.0 by N_2,400 MHz NMR.

Carbamate can be converted back to its corresponding amine by heating or nitrogen (Scheme 4-2). In our case, we selected nitrogen as the converting agent, hoping to convert the gel to its original dendrimer. Since, only generation 5.0 has gel formed, the only choice for the reversible studies was the gel of generation 5.0. Similar to CO_2 titration, we titrated the gel with ultra-pure nitrogen slowly and recorded the corresponding ^1H NMR spectra. Figure 4-26 shows how the chemical shift changed during the bubbling of N_2. In the last stage of the bubbling, on the NMR spectra, the chemical shifts for the methylene protons on

the original generation 5.0 dendrimer structure could be identified, though there were some overlaps. Also, the gel disappeared and liquid was formed.

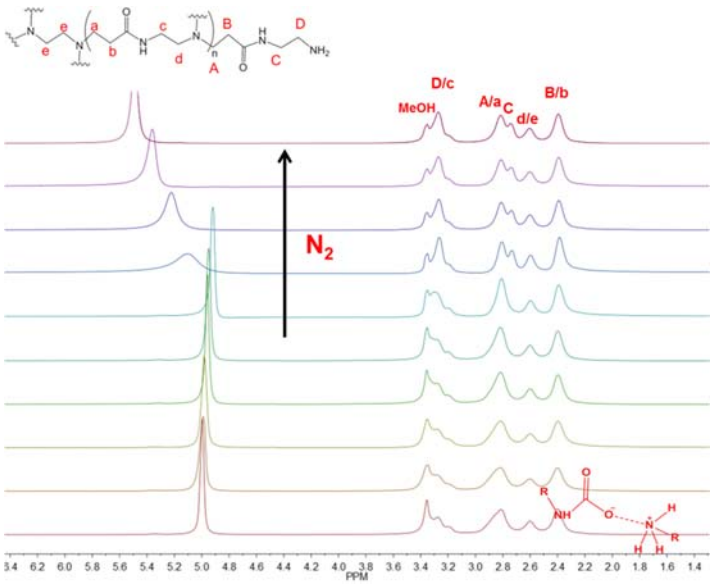

Figure 4-27. Titration of the gel of PAMAM dendrimer, generation 5.0 by N_2 in the presence of NaOD, room temperature 400 MHz NMR.

Since CO_2 is produced during the carbamate conversion, we did the other experiment by adding NaOD to the gel, and then bubbled with N_2, hoping NaOD would neutralize carbonic acid produced and more clear spectra would be obtained. Figure 4-27 shows that in the presence of NaOD, gel was converted to its original dendrimers, and we have clear peaks for dendrimers. There was no overlap between the chemical shifts of the methylene groups from *A/a* and *D* anymore.

4.3 Conclusion

Based on the results in this chapter, we realized that H_2O is not a good solvent for gelation of PAMAM dendrimers. No matter how much the concentration is, how long the diameter of a dendrimer is, and how many surface groups a dendrimer has. CO_2 in an aqueous solution of PAMAM dendrimers would produce carbamate ions, but most of the carbamate ions produced at early stage would be converted to ammonium. The reason could be that CO_2 has a good solubility in H_2O; with more CO_2 introduced, the acidity gets stronger, which may be harmful for the existence of carbamate. Also, aqueous acidic solution would have many cations and anions, which may interfere with the salt bridge between carbamate and ammonium.

In the case of methanol, methanol is not as protic as H_2O. There may not be so many cations and anions related carbonic acid formed during CO_2 titration, which may provide a beneficial environment for the salt bridge between carbamate and ammonium. Also, the fact in generation 0.0, in the three concentrations we used (0.01 M, 0.16M and 0.32 M) there was even no precipitates formed; in the case of generation 1.0, there were no precipitates formed in 0.01M, but some precipitates formed in 0.16M and 0.32M. The 0.08 M solution of generation 1.0 has the same amount of surface groups as the 0.16 M solution of generation 0.0; the 0.16 M solution of generation 1.0 has the same amount of surface groups as the 0.32 M solution of generation 0.0. However, only in the cases of generation 1.0 (0.08 M and 0.16 M), there were precipitates

formed, not in the cases of generation 0.0 (0.16 M and 0.32M). The longer molecular diameter of generation 1.0 (25 Å) may explain this difference.

In the case of generation 5.0, even with a concentration as low as 0.005M, there was gel formed. If we remember the fact that generation 5.0 has a molecular diameter of 54 Å, 128 surface groups and the amount of braches it has, it would not be a surprise that the gelation ability of generation 5.0 is the best. However, when generation was in D_2O, though some carbamate ions and ammonium ions formed during the titration, other ions in D_2O may interfere with the interaction between carbamate and ammonium, which may destroy the gelation.

Also, we successfully converted the gel of generation 5.0 to its original PAMAM dendrimer by bubbling with nitrogen, which means the gelation of PAMAM dendrimer of generation 5.0 is reversible.

Chapter 5 : Synthesis of a Tetra-cholic Acid Cavitand

5.1 Overview

One important field of supramolecular chemistry is the design and synthesis of new host molecules. Efficient synthetic receptors capable of selective substrate binding in aqueous solution play an important role in understanding of molecular recognition and self-assembly in chemical and biological systems.[45] At the beginning, a few studies used bile acids in micellar system. Afterwards, people started to use bile acids to build supramolecular host systems.[46]

Bile acid based molecular and supramolecular assemblies can be divided into two main categories:

(1) Cyclic compounds: a) Cyclocholates (Figure 5-1A[47]) are macrocyclic polyesters with two to six steroid units formed by head-to-tail cyclization of bile acids; b) Cholaphanes (Figure 5-1B[48]) are bile acid based macrocycles that consist of two to four bile acid units joined together by various spacer groups; c) other cyclic compounds (Figure 5-1C and D[49]).

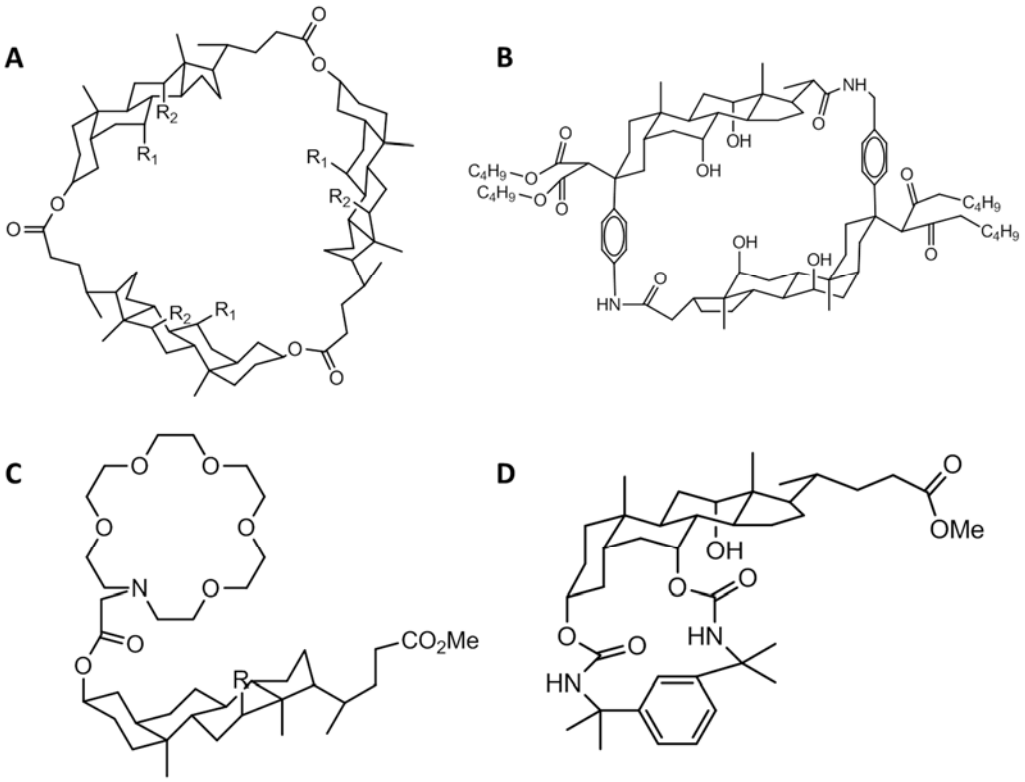

Figure 5-1. Examples of cyclic host molecules based on cholic acid

(2) Acyclic compounds: a) Cleft-type structures which can wrap around a substrate molecule (Figure 5-2A[50]); b) Other acyclic structures

(Figure 5-2B[51] and C[52]).

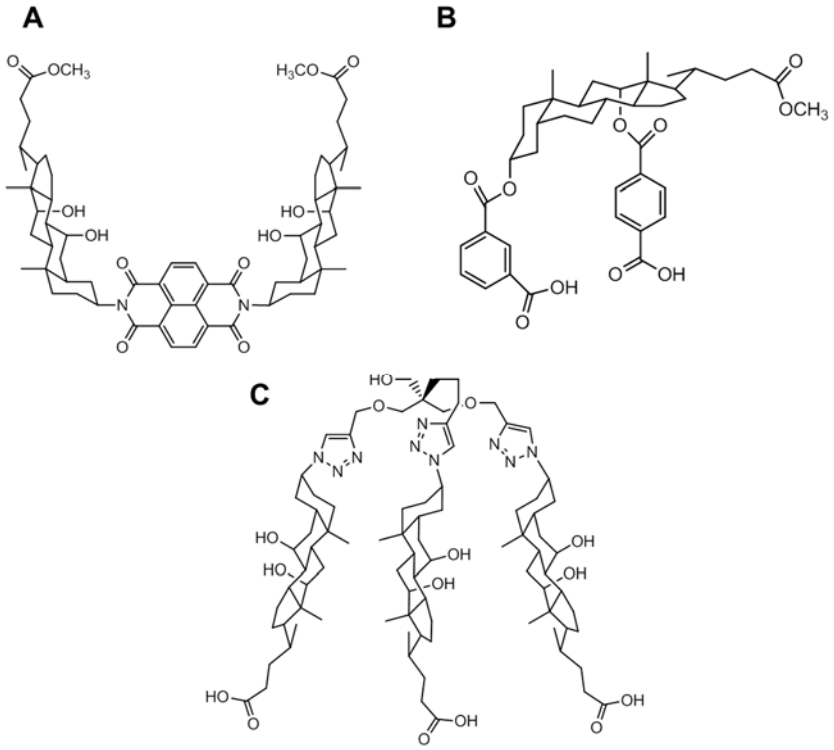

Figure 5-2. Examples of acyclic host molecules based on cholic acid.

The host molecule in this investigation is based on cholic acid and cavitand.

5.2 Results and discussions

5.2.1 Synthesis

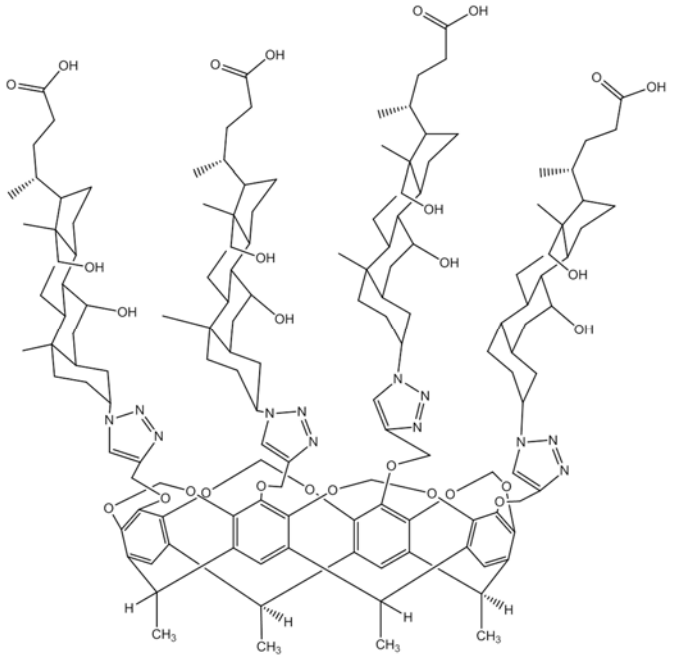

Figure 5-3. Structure of Tetra-cholic acid cavitand (**3**).

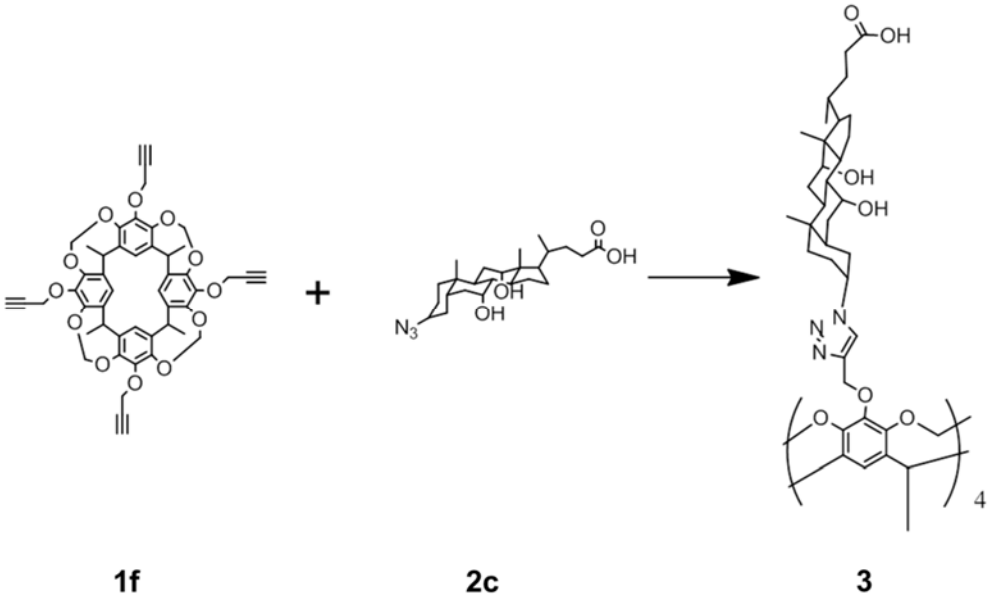

Scheme 5-1. Synthesis of Tetra-cholic acid cavitand.

For the target host molecule (**3**) in this investigation, four cholic acids (**2c**) were connected to the cavitand (**1f**). **1f** has four methyl groups as the feet. Because cholic acid has hydrophobic groups and hydrophilic groups, the host molecule designed (**3**) could form a hydrophobic cavity, when the methyl groups on the cholic acid are inwards, or a hydrophilic cavity, when the hydroxyl group is inwards. Cavitand is one of the first synthetic host molecules in history. It has a rigid cavity. Scheme 5-1 gives the synthesis scheme of the tetra-cholic acid cavitand (**3**). It consists of two synthesis lines: (1) synthesis of the cavitand (**1f**, Scheme 5-2); (2) synthesis of the azido cholic acid (**2c**, Scheme 5-3). Finally, the propargyloxy cavitand was connected with azido cholic acid through click chemistry (Scheme 5-1).

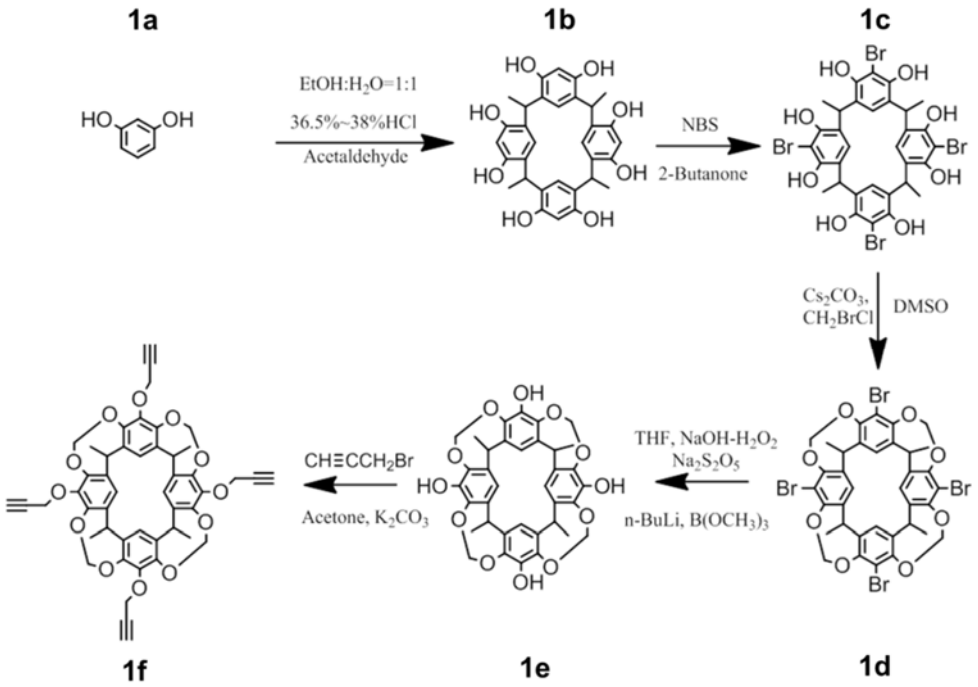

Scheme 5-2. Synthesis of **1f**.

The synthesis of **1f** is as discussed below. **1a** was reacted with acetaldehyde with ethanol as the solvent and the addition of HCl to provide **1b**[53] (yield 8.89%). **1b** is flexible in structure, with several conformations. In order to make a rigid structure, a second covalent bond between two adjacent benzenes was necessary. Methylene group was selected to bridge the hydroxyl groups on two adjacent benzenes. To avoid bridging two –OH groups on the same unit, one –OH group among the three –OH groups needed to be protected. Bromination was applied to protect the –OH group in the center. **1b** was brominated by NBS with 2-butanone as the solvent to give **1c**[53] (yield 37.3%). The bromochloromethane was the bridging agent to react with **1c** to produce **1d** [54](yield 67.1%) In order for the cavitand to be able to click with cholic acid, it needed to have an alkyne group or azide group. An alkyne group was used in this synthesis. Bromide was replaced by –OH group with the assistance of n-BuLi and $B(OCH_3)_3$ to provide **1e**;[55] the isolated product had a 30% yield. Then an alkyne was connected to the –OH group by propargyl bromide and K_2CO_3. The final product **1f**[56] had a yield of 89.38%.

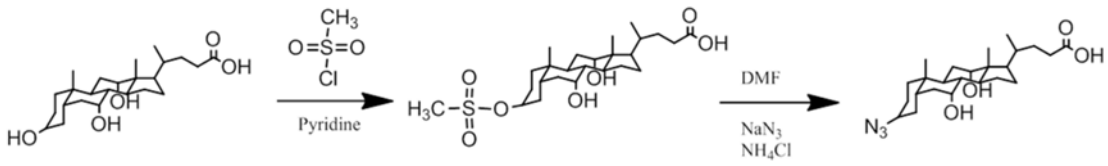

2a **2b** **2c**

Scheme 5-3. Synthesis of **2c**.

Since **1f** was functionalized with alkyne groups, the left choice for functionalization of cholic acid was azide. There are three hydroxyl groups on the

concave face of cholic acid. We just needed to modify one hydroxyl group. It is not easy to replace the hydroxyl group directly with azido group. The –OH group was replaced with mesylate group first. Since the size of mesylate is relative large, the replacement only happened at the location in **2b**.[52, 55] Probably, since the other two hydroxyl groups were surrounded by cyclohexanes, the steric effect disfavored the mesylate replacement on the other two places. The yield for the mesylate step was 77%. Azide group substituted the mesylate group to produce **2c**[52] with a 68.3% yield.

Click chemistry just needs benign reaction conditions, has high yields and only creates easy to remove byproducts. The click reaction between **1f** and **2c** (Scheme 5-1) was catalyzed by freshly produced Cu(I) in butanol aqueous butanol solution. The solution was degassed by N_2 to remove O_2. CuSO4•5H2O was reduced to Cu(I) by sodium ascorbate. The mixture was stirred at 90 ºC for 36 hours. The final product was washed with CH_2Cl_2 and CH_3OH to give the final product (**3**) with a 38.12% yield.

5.2.2 Electrochemical studies

After getting **3**, we tried many solvents to dissolve it. However, none of them was able to solubilize it very well. With a relatively low concentration of **3** in H_2O with $TBAPF_6$ (tetrabutylammonium hexafluorophosphate) as the buffer, we did some electrochemistry to study its supramolecular properties. It showed some binding abilities towards a group of guest molecules, such as viologen with aliphatic

groups of different lengths (some of them have different aliphatic groups attached at the two sides of 4,4'-bipyridinium) (Figure 5-4 A), ferrocene with aliphatic groups (Figure 5-4 B), etc. We expected **3** would be able to encapsulate several guest molecules, considering its cavity size. It did show it was able to accommodate several guest molecules inside its cavity in electrochemistry. However, the electrochemical behaviors were not so easy to explain.

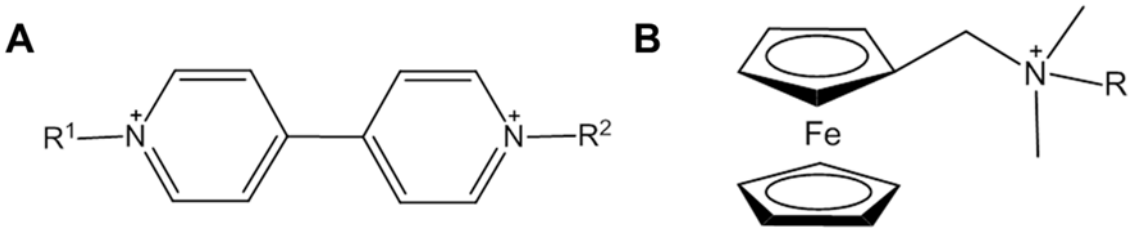

Figure 5-4. Guest molecules used.

5.3 Experimental section

5.3.1 Synthesis of 3

2c (4.332mmol, 1.878g) and **1f** (1.083mmol, 0.867g) were suspended in a 2:1 mixture (150mL) of H_2O and *t*-BuOH. The solution was degassed with N_2. $CuSO_4 \cdot 5H_2O$ (0.2166 mmol, 0.05409 g) was dissolved in a small amount of H_2O, and then degassed with nitrogen. Sodium ascorbate (0.8664 mmol, 0.1716g) was dissolved in a small amount of H_2O and then degassed with Nitrogen. The degassed CuSO4 solution and sodium ascorbate solution were added to the H_2O and t-BuOH mixture. Then the solution was stirred at 90 ºC for 36 hours. The

final product was washed with CH_2Cl_2 and MeOH to the grid of the starting materials. Then dried under vacuum to give 1.05 g product (Yield: 38.12%).

5.3.2 Spectra

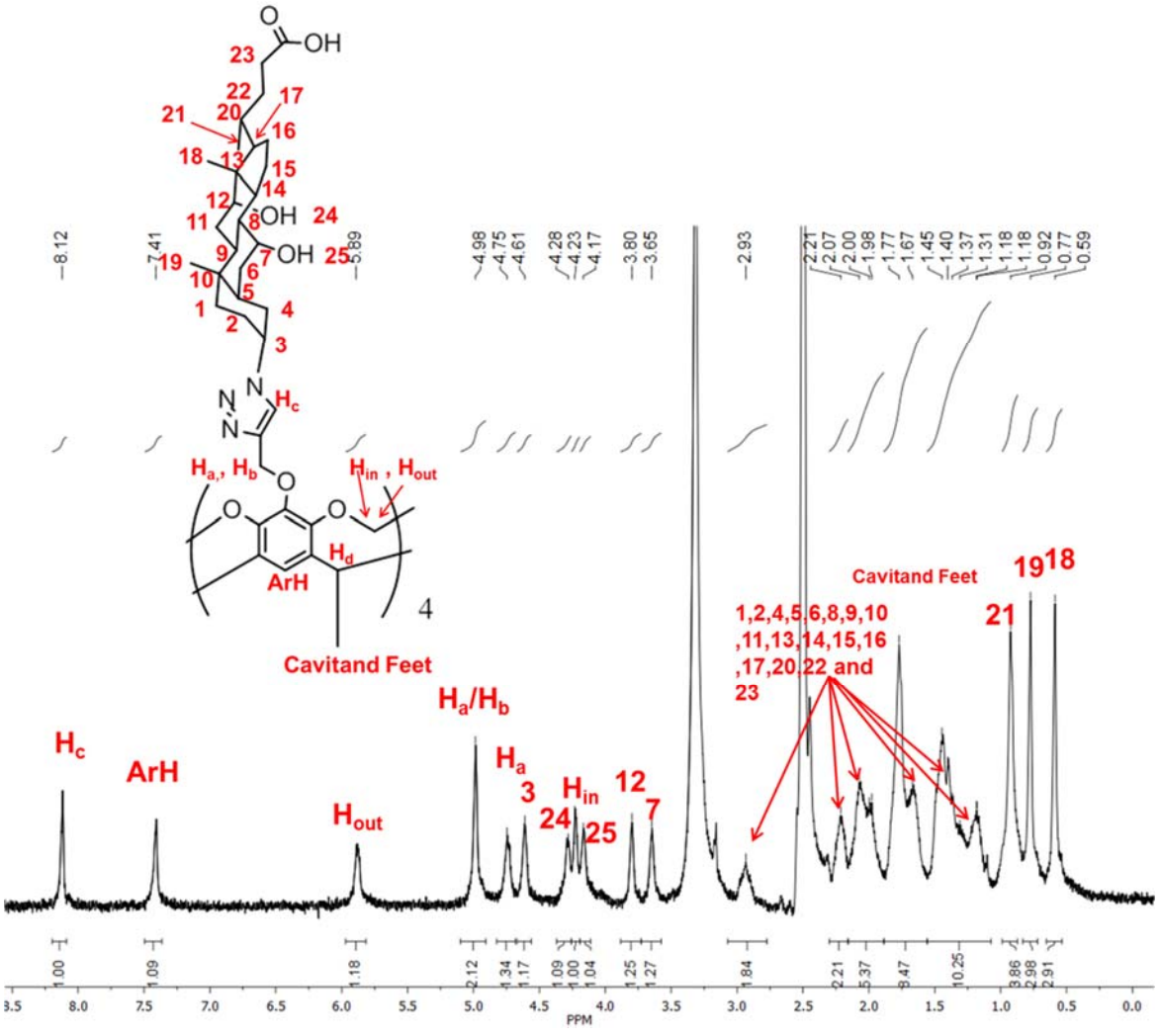

Figure 5-5. ^{1}H NMR of tetra-cholic acid cavitand (DMSO-d_6, 400 MHz).

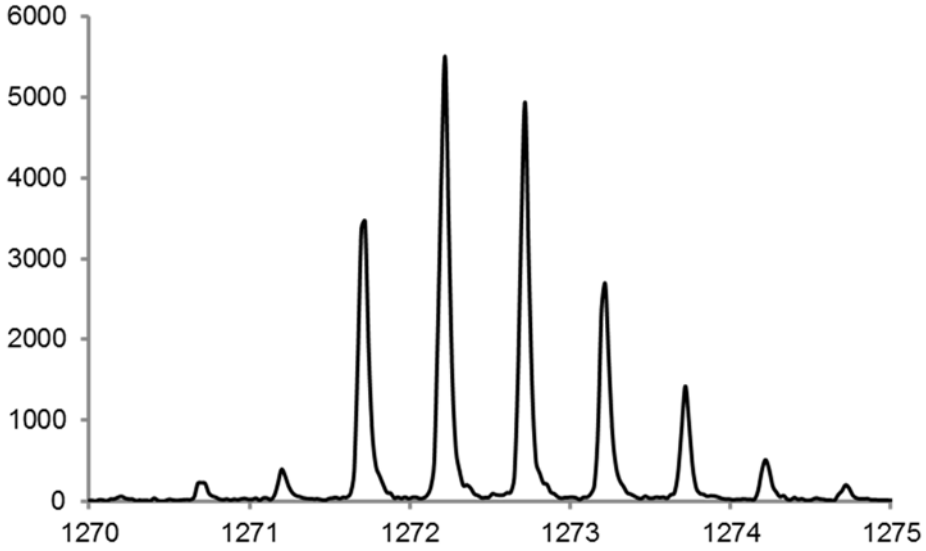

Figure 5-6. Experimental High Resolution ESI-MS Spectrum of Tetracholic Acid Cavitand. ($C_{144}H_{196}N_{12}O_{28}$+2H)/2: 1272.2162.

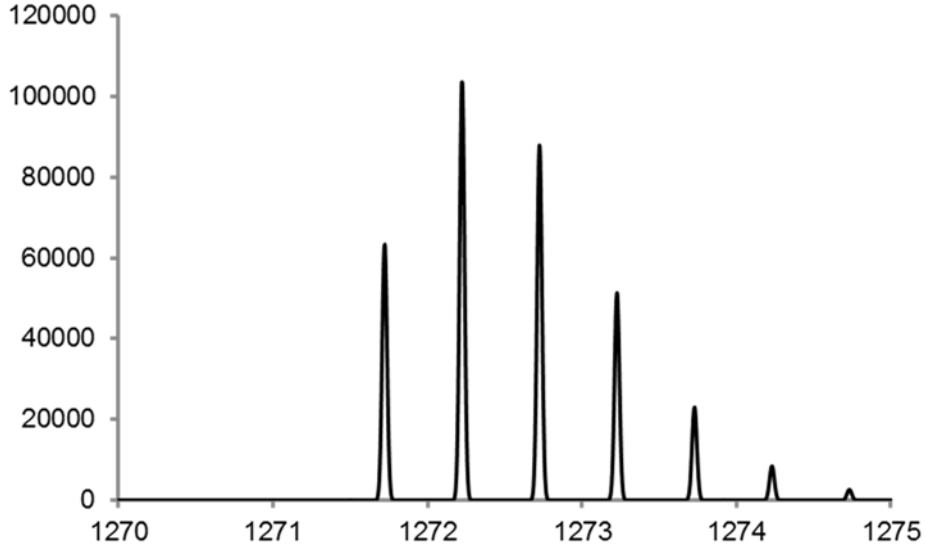

Figure 5-7. Theoretical High Resolution ESI-MS Spectrum of Tetracholic Acid.

References

1. (a) Curtis, N. F.; House, D. A., *Chemistry and Industry--London*. 1961; p 1708; (b) Jager, E. G., Ein neues Nickelchelat mit allseitig geschlossenem Ring-system. *Z. Chem.* **1964,** *4*, 437; (c) Curry, J. D.; Busch, D. H., The reactions of coordinated ligands. VII. Metal ion control in the synthesis of chelate compounds containing pentadentate and sexadentate macrocyclic ligands. *Journal of the American Chemical Society* **1964,** *86* (4), 592-594.

2. Pedersen, C. J., Cyclic polyethers and their complexes with metal salts. *Journal of the American Chemical Society* **1967,** *89* (26), 7017-7036.

3. Lehn, J.-M.; Montavon, F., CRYPTATES XIX. Ligands polyaza-polyoxa-macrobicycliques: synthèse et complexes métalliques. *Helvetica Chimica Acta* **1976,** *59* (5), 1566-1583.

4. Cram, D. J.; Karbach, S.; Kim, H. E.; Knobler, C. B.; Maverick, E. F.; Ericson, J. L.; Helgeson, R. C., Host-guest complexation. 46. Cavitands as open molecular vessels form solvates. *Journal of the American Chemical Society* **1988,** *110* (7), 2229-2237.

5. Isaacs, L., Cucurbit[n]urils: from mechanism to structure and function. *Chemical Communications* **2009,** (6), 619-629.

6. Cheng, X.-J.; Liang, L.-L.; Chen, K.; Ji, N.-N.; Xiao, X.; Zhang, J.-X.; Zhang, Y.-Q.; Xue, S.-F.; Zhu, Q.-J.; Ni, X.-L.; Tao, Z., Twisted cucurbit[14]uril. *Angewandte Chemie International Edition* **2013,** *52* (28), 7252-7255.

7. Freeman, W. A.; Mock, W. L.; Shih, N. Y., Cucurbituril. *Journal of the American Chemical Society* **1981,** *103* (24), 7367-7368.

8. Kim, J.; Jung, I.-S.; Kim, S.-Y.; Lee, E.; Kang, J.-K.; Sakamoto, S.; Yamaguchi, K.; Kim, K., New cucurbituril homologues: syntheses, isolation, characterization, and X-ray crystal structures of cucurbit[n]uril (n = 5, 7, and 8). *Journal of the American Chemical Society* **2000,** *122* (3), 540-541.

9. Day, A. I.; Blanch, R. J.; Arnold, A. P.; Lorenzo, S.; Lewis, G. R.; Dance, I., A cucurbituril-based gyroscane: a new supramolecular form. *Angewandte Chemie International Edition* **2002,** *41* (2), 275-277.

10. Liu, S.; Zavalij, P. Y.; Isaacs, L., Cucurbit[10]uril. *Journal of the American Chemical Society* **2005,** *127* (48), 16798-16799.

11. Lee, J. W.; Samal, S.; Selvapalam, N.; Kim, H.-J.; Kim, K., Cucurbituril homologues and derivatives: new opportunities in supramolecular chemistry. *Accounts of Chemical Research* **2003,** *36* (8), 621-630.

12. Ogoshi, T.; Ueshima, N.; Sakakibara, F.; Yamagishi, T.-a.; Haino, T., Conversion from pillar[5]arene to pillar[6–15]arenes by ring expansion and encapsulation of C60 by pillar[n]arenes with nanosize cavities. *Organic Letters* **2014,** *16* (11), 2896-2899.

13. Ogoshi, T.; Kanai, S.; Fujinami, S.; Yamagishi, T.-a.; Nakamoto, Y., Para-bridged symmetrical pillar[5]arenes: their Lewis acid catalyzed synthesis and host–guest property. *Journal of the American Chemical Society* **2008,** *130* (15), 5022-5023.

14. Ogoshi, T.; Ueshima, N.; Akutsu, T.; Yamafuji, D.; Furuta, T.; Sakakibara, F.; Yamagishi, T.-a., The template effect of solvents on high yield synthesis, co-cyclization of pillar[6]arenes and interconversion between pillar[5]- and pillar[6]arenes. *Chemical Communications* **2014,** *50* (43), 5774-5777.

15. Chen, Y.; He, M.; Li, B.; Wang, L.; Meier, H.; Cao, D., A monophosphoryl copillar[5]arene: synthesis and host-guest complexation with alkanols. *RSC Advances* **2013,** *3* (44), 21405-21408.

16. Yan, X.; Wei, P.; Li, Z.; Zheng, B.; Dong, S.; Huang, F.; Zhou, Q., A dynamic [1]catenane with pH-responsiveness formed via threading-followed-by-complexation. *Chemical Communications* **2013,** *49* (25), 2512-2514.

17. Yao, Y.; Xue, M.; Chen, J.; Zhang, M.; Huang, F., An amphiphilic pillar[5]arene: synthesis, controllable self-assembly in water, and application in calcein release and TNT adsorption. *Journal of the American Chemical Society* **2012,** *134* (38), 15712-15715.

18. Bissell, R. A.; Cordova, E.; Kaifer, A. E.; Stoddart, J. F., A chemically and electrochemically switchable molecular shuttle. *Nature* **1994,** *369* (6476), 133-137.

19. Philip, I. E.; Kaifer, A. E., Electrochemically driven formation of a molecular capsule around the ferrocenium ion. *Journal of the American Chemical Society* **2002,** *124* (43), 12678-12679.

20. (a) Ong, W.; Gómez-Kaifer, M.; Kaifer, A. E., Cucurbit[7]uril: a very effective host for viologens and their cation radicals. *Organic Letters* **2002,** *4* (10), 1791-1794; (b) Kim, H.-J.; Jeon, W. S.; Ko, Y. H.; Kim, K., Inclusion of methylviologen in cucurbit[7]uril. *Proceedings of the National Academy of Sciences* **2002,** *99* (8), 5007-5011.

21. Small, D. M.; Penkett, S. A.; Chapman, D., Studies on simple and mixed bile salt micelles by nuclear magnetic resonance spectroscopy. *Biochimica et Biophysica Acta (BBA) - Lipids and Lipid Metabolism* **1969,** *176* (1), 178-189.

22. (a) Kolehmainen, E., Solubilization of aromatics in aqueous bile salts: II. benzene and some substituted benzenes in sodium deoxycholate and cholate: ^{1}H and ^{19}F NMR studies. *Journal of Colloid and Interface Science* **1989,** *127* (2), 301-309; (b) Mukerjee, P.; Cardinal, J. R., Solubilization as a method for studying self-association: solubility of naphthalene in the bile salt sodium cholate and the complex pattern of its aggregation. *Journal of Pharmaceutical Sciences* **1976,** *65* (6), 882-886.

23. (a) Briganti, G.; D'Archivio, A. A.; Galantini, L.; Giglio, E., Structural study of the micellar aggregates of sodium and rubidium glyco- and taurodeoxycholate. *Langmuir* **1996,** *12* (5), 1180-1187; (b) Campanelli, A. R.; Candeloro de Sanctis, S.; Chiessi, E.; D'Alagni, M.; Giglio, E.; Scaramuzza, L., Sodium glyco- and taurodeoxycholate: possible helical models for conjugated bile salt micelles. *The Journal of Physical Chemistry* **1989,** *93* (4), 1536-1542.

24. Matsuoka, K.; Moroi, Y., Micelle formation of sodium deoxycholate and sodium ursodeoxycholate (Part 1). *Biochimica et Biophysica Acta (BBA) - Molecular and Cell Biology of Lipids* **2002,** *1580* (2–3), 189-199.

25. Funasaki, N.; Fukuba, M.; Kitagawa, T.; Nomura, M.; Ishikawa, S.; Hirota, S.; Neya, S., Two-dimensional NMR study on the structures of micelles of sodium taurocholate. *The Journal of Physical Chemistry B* **2004,** *108* (1), 438-443.

26. (a) Rinco, O.; Kleinman, M. H.; Bohne, C., Reactivity of benzophones in the different binding sites of sodium cholate aggregates. *Langmuir* **2001,** *17* (19), 5781-5790; (b) Rinco, O.; Nolet, M.-C.; Ovans, R.; Bohne, C., Probing the binding dynamics to sodium cholate aggregates using naphthalene derivatives as guests. *Photochemical & Photobiological Sciences* **2003,** *2* (11), 1140-1151; (c) Yihwa, C.; Quina, F. H.; Bohne, C., Modulation with acetonitrile of the dynamics of guest binding to the two distinct binding sites of cholate aggregates. *Langmuir* **2004,** *20* (23), 9983-9991; (d) Waissbluth, O. L.; Morales, M. C.; Bohne, C., Influence of planarity and size on guest binding with sodium cholate aggregates. *Photochemistry and Photobiology* **2006,** *82* (4), 1030-1038; (e) Amundson, L. L.; Li, R.; Bohne, C., Effect of the guest size and shape on its binding dynamics with sodium cholate aggregates. *Langmuir* **2008,** *24* (16), 8491-8500; (f) Fuentealba, D.; Thurber, K.; Bovero, E.; Pace, T. C. S.; Bohne, C., Effect of sodium chloride on the binding of polyaromatic hydrocarbon guests with sodium cholate aggregates. *Photochemical & Photobiological Sciences* **2011,** *10* (9), 1420-1430.

27. (a) Lagona, J.; Mukhopadhyay, P.; Chakrabarti, S.; Isaacs, L., The cucurbit[n]uril family. *Angewandte Chemie International Edition* **2005,** *44* (31),

4844-4870; (b) Masson, E.; Ling, X.; Joseph, R.; Kyeremeh-Mensah, L.; Lu, X., Cucurbituril chemistry: a tale of supramolecular success. *RSC Advances* **2012,** *2* (4), 1213-1247; (c) Kaifer, A. E., Toward reversible control of cucurbit[n]uril complexes. *Accounts of Chemical Research* **2014,** *47* (7), 2160-2167.

28. Kaifer, A. E.; Bard, A. J., Micellar effects on the reductive electrochemistry of methylviologen. *The Journal of Physical Chemistry* **1985,** *89* (22), 4876-4880.

29. Ong, W.; Kaifer, A. E., Salt effects on the apparent stability of the cucurbit[7]uril−methyl viologen inclusion complex. *The Journal of Organic Chemistry* **2004,** *69* (4), 1383-1385.

30. Moon, K.; Kaifer, A. E., Modes of binding Interaction between viologen guests and the cucurbit[7]uril host. *Organic Letters* **2004,** *6* (2), 185-188.
31. Quintela, P. A.; Kaifer, A. E., Electrochemistry of methylviologen in the presence of sodium decyl sulfate. *Langmuir* **1987,** *3* (5), 769-773.

32. (a) Xue, M.; Yang, Y.; Chi, X.; Zhang, Z.; Huang, F., Pillararenes, a new class of macrocycles for supramolecular chemistry. *Accounts of Chemical Research* **2012,** *45* (8), 1294-1308; (b) Ogoshi, T., Synthesis of novel pillar-shaped cavitands “pillar[5]arenes” and their application for supramolecular materials. *J Incl Phenom Macrocycl Chem* **2012,** *72* (3-4), 247-262; (c) Cragg, P. J.; Sharma, K., Pillar[5]arenes: fascinating cyclophanes with a bright future. *Chemical Society Reviews* **2012,** *41* (2), 597-607.

33. Strutt, N. L.; Zhang, H.; Schneebeli, S. T.; Stoddart, J. F., Functionalizing pillar[n]arenes. *Accounts of Chemical Research* **2014,** *47* (8), 2631-2642.
34. Lao, K.-u.; Yu, C.-h., A computational study of unique properties of pillar[n]quinones: self-assembly to tubular structures and potential applications as electron acceptors and anion recognizers. *Journal of Computational Chemistry* **2011,** *32* (12), 2716-2726.

35. (a) Cao, D.; Kou, Y.; Liang, J.; Chen, Z.; Wang, L.; Meier, H., A facile and efficient preparation of pillararenes and a pillarquinone. *Angewandte Chemie International Edition* **2009,** *48* (51), 9721-9723; (b) Shivakumar, K. I.; Sanjayan, G. J., An easy and multigram-scale synthesis of pillar[5]quinone by the hypervalent iodine oxidation of 1,4-dimethoxypillar[5]arene. *Synthesis* **2013,** *45*.

36. (a) Han, C.; Zhang, Z.; Yu, G.; Huang, F., Syntheses of a pillar[4]arene[1]quinone and a difunctionalized pillar[5]arene by partial oxidation. *Chemical Communications* **2012,** *48* (79), 9876-9878; (b) Pan, M.; Xue, M., Selective preparation of isomeric tetrahydroxypillar[5]arenes and pillar[3]arene[2]quinones. *European Journal of Organic Chemistry* **2013,** *2013* (22), 4787-4793.
37. (a) Gomez-Kaifer, M.; Reddy, P. A.; Gutsche, C. D.; Echegoyen, L., Electroactive calixarenes. 1. Redox and cation binding properties of

calixquinones. *Journal of the American Chemical Society* **1994,** *116* (8), 3580-3587; (b) Webber, P. R. A.; Beer, P. D.; Chen, G. Z.; Felix, V.; Drew, M. G. B., Bis(calix[4]diquinone) receptors: cesium- and rubidium-selective redox-active ionophores. *Journal of the American Chemical Society* **2003,** *125* (19), 5774-5785.

38. Zhu, Z.; Hong, M.; Guo, D.; Shi, J.; Tao, Z.; Chen, J., All-solid-state lithium organic battery with composite polymer electrolyte and pillar[5]quinone cathode. *Journal of the American Chemical Society* **2014,** *136* (47), 16461-16464.

39. Lehmann, M. W.; Evans, D. H., Anomalous behavior in the two-step reduction of quinones in acetonitrile. *Journal of Electroanalytical Chemistry* **2001,** *500* (1–2), 12-20.

40. Sun, H.; Chen, W.; Kaifer, A. E., A simple method based on NMR spectroscopy and ultramicroelectrode voltammetry for the determination of the number of electrons in faradaic processes. *Organometallics* **2006,** *25* (7), 1828-1830.

41. Buhleier, E.; Wehner, W.; Vogtle, F., Cascade-chain-like and nonskid-chain-like syntheses of molecular cavity topologies. *Synthesis-Stuttgart* **1978,** *2* (2), 155-158.

42. Antoni, P.; Hed, Y.; Nordberg, A.; Nyström, D.; von Holst, H.; Hult, A.; Malkoch, M., Bifunctional dendrimers: from robust synthesis and accelerated one-pot postfunctionalization strategy to potential applications. *Angewandte Chemie International Edition* **2009,** *48* (12), 2126-2130.

43. Xu, H.; Rudkevich, D. M., CO_2 in supramolecular chemistry: preparation of switchable supramolecular polymers. *Chemistry – A European Journal* **2004,** *10* (21), 5432-5442.

44. George, M.; Weiss, R. G., Chemically reversible organogels via “latent” gelators. Aliphatic amines with carbon dioxide and their ammonium carbamates†. *Langmuir* **2002,** *18* (19), 7124-7135.

45. Menger, F. M.; McCreery, M. J., Kinetic characterization of bile salt micelles. *Journal of the American Chemical Society* **1974,** *96* (1), 121-126.

46. Davis, A. P., Cholaphanes et al.; Steroids as structural components in molecular engineering. *Chemical Society Reviews* **1993,** *22* (4), 243-253.

47. A. Brady, P.; K. M. Sanders, J., Thermodynamically-controlled cyclisation and interconversion of oligocholates: metal ion templated 'living' macrolactonisation. *Journal of the Chemical Society, Perkin Transactions 1* **1997,** (21), 3237-3254.

48. Bhattarai, K. M.; Davis, A. P.; Perry, J. J.; Walter, C. J.; Menzer, S.; Williams, D. J., A new generation of “cholaphanes”: steroid-derived macrocyclic hosts with enhanced solubility and controlled flexibility. *The Journal of Organic Chemistry* **1997,** *62* (24), 8463-8473.

49. Maitra, U.; D'Souza, L. J.; Kumar, P. V., Synthesis and cation binding properties of new bile acid-based crown ethers. *Supramolecular Chemistry* **1998,** *10* (1), 97-106.

50. Kohmoto, S.; Sakayori, K.; Kishikawa, K.; Yamamoto, M., Molecular cleft possessing a cholic acid moiety as a podant and its conformation. *Journal of the Chemical Society, Perkin Transactions 2* **1999,** (4), 833-836.

51. Rao, P.; Maitra, U., A new bile acid-based ditopic adenine/biotin receptor with convergent carboxyl groups. *Supramolecular Chemistry* **1998,** *9* (4), 325-328.

52. Luo, J. C., Y; Zhu, X. X., Highly efficient synthesis and inclusion properties of star-shaped amphiphilic derivatives of cholic acid. *Synlett* **2007,** *14*, 2201-2204.

53. Sherman, J. C.; Knobler, C. B.; Cram, D. J., Host-guest complexation. 56. Syntheses and properties of soluble carceplexes. *Journal of the American Chemical Society* **1991,** *113* (6), 2194-2204.

54. Román, E.; Peinador, C.; Mendoza, S.; Kaifer, A. E., Improved synthesis of cavitands. *The Journal of Organic Chemistry* **1999,** *64* (7), 2577-2578.

55. Wess, G.; Kramer, W.; Bartmann, W.; Enhsen, A.; Glombik, H.; Müllner, S.; Bock, K.; Dries, A.; Kleine, H.; Schmitt, W., Modified bile acids: preparation of 7α,12α-dihydroxy-3β- and 7α,12α-dihydroxy-3α-(2-hydroxyethoxy)-5β-cholanic acid and their biological activity. *Tetrahedron Letters* **1992,** *33* (2), 195-198.

56. Cram, D. J.; Jaeger, R.; Deshayes, K., Host-guest complexation. 65. Hemicarcerands that encapsulate hydrocarbons with molecular weights greater than two hundred. *Journal of the American Chemical Society* **1993,** *115* (22), 10111-10116.